UNIVERSITY OF CALIFORNIA

Los Angeles

Electric Vehicle Smart Charging Infrastructure

A dissertation submitted in partial satisfaction of the

requirements for the degree Doctor of Philosophy

in Mechanical Engineering

by

Ching-Yen Chung

2014

ABSTRACT OF THE DISSERTATION

Electric Vehicle Smart Charging Infrastructure

by

Ching-Yen Chung

Doctor of Philosophy in Mechanical Engineering

University of California, Los Angeles, 2014

Professor Rajit Gadh, Chair

The increased number of plug-in electric vehicles (PEVs) on the road is making the PEV charging infrastructure gain an ever-more important role in simultaneously meeting the needs of drivers and those of the local distribution grid. When PEVs are charging, they currently only have the option to charge at a selected current or not charge at all. However, during a power shortage, the charging infrastructure should have the option to either shut off the power to the charging stations or lower the power to the PEVs in order to satisfy the needs of the grid. The current approach to charging is not well suited to scaling with the PEV market. If PEV adoption is to continue, the charging infrastructure must provide a seamless and configurable interface from the vehicle to the power grid and overcome its current shortcomings, such as underutilization of circuits, unresponsiveness to grid constraints, low degree of autonomy, and high cost. In particular, there is need for technology that controls the current being disbursed to these PEVs.

The WINSmartEV^{TM} smart charging infrastructure is proposed and is currently being developed to meet the growing demand for charging from an ever increasing population of PEV owners. It has five major components: smart charging stations, a server-based control system, systematic safety integration, an authentication and authorization system, and smart charging algorithms. This software-based technology is capable of providing power to several PEVs using scare charging resources by multiplexing or current sharing. Collaboration between the server-based central controller and the local controllers inside the charging stations facilitates the management of the charging sessions and control of the current to the PEVs. This technology provides PEV chargers that simultaneously connect to multiple PEVs and a system that takes into account external factors, such as grid capacity when scheduling smart charging sessions. It not only incorporates intelligence at every level so that charge scheduling can avoid grid bottlenecks, it also multiplies the number of PEVs that can be plugged into a single circuit.

The dissertation of Ching-Yen Chung is approved.

Daniel Yang

Richard Wirz

Puneet Gupta

Rajit Gadh, Committee Chair

University of California, Los Angeles

2014

A supportive family is significant during my PhD studies.

I can't show my wife and daughter enough appreciation.

Thanks for being with me.

I love you!

TABLE OF CONTENTS

LIST OF FIGURES

List of Tables

ACKNOWLEDGMENTS

This dissertation represents the hard work of many people. First of all, I would like to acknowledge the members of my dissertation committee: Prof. Rajit Gadh, Prof. Daniel Yang, Prof. Richard Wirz, and Prof. Puneet Gupta, for their insightful comments. Prof. Gadh, while I will always be thankful for all the time and energy you put in mentoring me over the past five years. Without question, your guidance has inspired me during my time at UCLA and will continue to influence me throughout my career. Next, I want to recognize the help of other magnificent individuals. I owe special thanks to Arturo Diaz. I appreciate your effort for this dissertation. Special thanks also go to my colleagues: Joshua Chynoweth, Charlie Qiu, Peter Chu and Jeff Angcanan. Thanks for your help and friendship.

I would like to thank my family, for their unconditional love and patience along the way. Finally, I could not have completed this dissertation without the encouragement and unfailing support of my wife, Ching-Yi Wang. This dissertation is dedicated to them.

This work has been sponsored in part by a grant from the LADWP/DOE fund 20699 & 20686, (Smart Grid Regional Demonstration Project). This material is based upon work supported by the United States Department of Energy under Award Number DE-OE000012 and the Los Angeles Department of Water and Power. Neither the United States Government nor any agency thereof, the Los Angeles Department of Water and Power, nor any of their employees make any warranty, express or implied, or assumes any legal liability or responsibility for the accuracy, completeness, or usefulness of any information, apparatus, product, or process disclosed, or represents that its use would not infringe privately owned rights. Reference herein to any specific commercial product, process, or service by trade name, trademark, manufacturer, or otherwise does not necessarily constitute or imply its endorsement, recommendation, or

favoring by the United States Government or any agency thereof. The views and opinions of authors expressed herein do not necessarily state or reflect those of the United States government or any agency thereof.

VITA

2002	B.S. (Mechanical Engineering), National Taiwan University, Taiwan.
2004	M.S. (Mechanical Engineering), National Taiwan University, Taiwan.
2004-2007	Engineer, Advanced Research Department, Lite-On IT Corp., Hsin-Chu, Taiwan.
2007-2009	Senior Engineer, Product Design Division 1, Lite-On IT Corp., Hsin-Chu, Taiwan.
2012	M.S. (Mechanical Engineering), UCLA, Los Angeles, California.
2009-2014	Research Assistant, Mechanical Engineering Department, UCLA.

PUBLICATIONS

[1] C. Chung, J. Chynoweth, P. Chu and R. Gadh, "Master-Slave Control Scheme in Electric Vehicle Smart Charging Infrastructure", *The Scientific World Journal special issue for Power, Control, and Optimization*, Mar. 18, 2014.

[2] C. Chung, P. Chu, and R. Gadh, "Design of Smart Charging Infrastructure---Hardware and Firmware Design of the Various Current Multiplexing Charging System," *The Seventh Global Conference on Power Control and Optimization, PCO 2013,* Prague, Czech, Aug. 25-27, 2013.

[3] C. Chung, A. Shepelev, C. Qiu, C. Chu, and R. Gadh, "Design of RFID Mesh Network for Electric Vehicle Smart Charging Infrastructure", *2013 IEEE International Conference on RFID Technologies and Applications, 2013 IEEE RFID TA,* Johor Bahru, Malaysia, Sep. 4-5, 2013. (The Bronze Best Paper Award)

[4] C. Chung, J. Chynoweth, C. Qiu, C. Chu, and R. Gadh, "Design of Fair Charging Algorithm for Smart Electrical Vehicle Charging Infrastructure", *International Conference on ICT Convergence 2013, ICTC 2013*, Jeju, Korea, Oct. 14-16, 2013.

[5] C. Chung, E. Youn, J. Chynoweth, C. Qiu, C. Chu, and R. Gadh, "Safety Design for Smart Electric Vehicle Charging with Current and Multiplexing Control", *2013 IEEE International Conference on Smart Grid Communications, 2013 IEEE SmartGridComm,* Vancouver, Canada, Oct. 21-24, 2013.

[6] C. Chung, J. Chynoweth, C. Qiu, C. Chu, and R. Gadh, "Design of Fast Response Smart Electric Charging Infrastructure", *2013 IEEE Green Energy and Systems Conference, IGESC 2013,* Long Beach, U.S.A., Nov. 25, 2013.

[7] R. Gadh, C. Chung, C. Chu, and L. Qiu, "Power Control Apparatus and Methods for Electric Vehicles", US20140062401A1, US2013/975313, Aug. 24, 2013.

[8] R. Gadh, C. Chung, L. Qiu, and C. Chu, "Network Based Management for Multiplexed Electric Vehicle Charging", US20130154561A1**,** US13/691,709**,** Nov. 30, 2011.

[9] R. Gadh, A. Chattophadhyay, C. Chung, P. Chu, B. Prabhu, O. Sheikh, and J. Chynoweth, "Intelligent Electric Vehicle Charging System", WO2013019989A2, WO2013019989A3, PCTUS2012/049393, Aug. 2, 2011.

[10] R. Gadh, S. Mal, S. Prabhu, C. Chu, J. Panchal, O. Sheikh, C. Chung, L. He, B. Xiao, and Y. Shi, "Smart Electric Vehicle (EV) Charging and Grid Integration Apparatus and Methods," US20130179061A1, WO2011156776A2, WO2011156776A3, PCT/US2011/040077, US13/693,747, Jun. 10, 2010.

CHAPTER 1 INTRODUCTION

As the world begins to lower its dependency on fossil fuels, Plug-in Electric vehicles (PEVs) are becoming a viable option for many people. The popularity of the PEV is shifting the energy burden from the direct burning of fossil fuels to the electric grid, and the grid must effectively respond in order to adequately supply this increased demand. The rising number of PEVs being used will also increase the demand for charging infrastructures of all types, from public fast chargers that will relieve range anxiety to home and garage chargers used for everyday charging. As a result, charging stations in both parking structures and private garages will become more prevalent. However, the availability of charging stations is a limiting factor for the widespread adoption of PEVS. Long-distance commuters depend on the charging infrastructure in parking lots and garages to ensure the ability to finish their round trips home. The lack of infrastructure could be caused by the underutilization of electric circuits; chargers may be connected to PEVs for much longer than necessary because the batteries are not typically empty. In addition, they will now have to charge their vehicles during on-peak hours which will stress the grid. Therefore, these charging stations will be responsible for meeting the requirements of the distribution grid, PEV owners, and parking lot operators.

The charging infrastructure must evolve into a more grid-responsive, dynamic, intelligent, and convenient system in order to meet the future needs of PEV stakeholders such as drivers, distribution grid operators, and electric utilities among others. This smart grid requires a safe and reliable infrastructure to control the current to PEVs and respond to the increase of on- and off-peak demand of electricity by increasing capacity or more intelligently using currently available resources, including generation, distribution, and infrastructure capacity.

In order to satisfy the demand of PEV charging requests and intelligently use available

resources, a PEV charging management system needs to be implemented to handle the peak demand of PEV charging, regardless whether charging takes place in a parking garage or at home. The need for a reliable infrastructure for monitoring and controlling vehicle charging is top priority. When PEVs are charging, they currently only have the option to charge at a selected current or not charge; during a power shortage, charging stations should be able to turn off the power or reduce the current to the PEVs to lower the impact on the power grid. Also, as long as the total power consumed is within the safety limit of a given circuit, smart PEV charging stations should be capable of charging several PEVs from that single circuit using different duty cycles or power levels. This charging infrastructure will require charging stations that can service multiple vehicles simultaneously by rationing the available power and intelligently scheduling charging sessions so as not to overload the circuit.

Basic, non-network, commercial charging stations, such as those provided by Schnieder, Leviton, and ClipperCreek, simply provide basic charging stations without monitoring power information and providing network features. Furthermore, neither remote nor local charging algorithms are implemented on these charging stations which also require point of sale (POS) devices to authorize and enable charging. However, these simple charging stations can be used as a platform for developers to implement their own network services for smart charging purposes. In order to connect simple commercial charging stations to the WINSmartEV^{TM} platform [1-4], four components are required: smart PEV charging infrastructure, the control system, the metering system, and the communication system. An aggregate control box containing the control system, metering system and communication system is proposed and designed for integration with simple commercial charging stations. By adding an additional controller, the commercial charging station can join the WINSmartEV^{TM} smart electric vehicle charging

infrastructure with the capability of remotely monitoring and controlling variable currents. Although safety designs have been implemented inside those basic, non-network, commercial charging stations, systematic safety integration with the local power grid is not addressed for the charging system.

There is currently a number of PEV charging networks on the market with most focusing on payment systems. Current commercial PEV charging stations, like Coulomb [5, 6] and Blink, have their own proprietary networks to control their stations through remote servers. Coulomb provides a ChargePoint application programming interface (API) and an OpenCharge protocol for the developers. The current application uses their network to locate available charging stations for users. It is possible to build the smart charging system by using the existing network with this API and protocols when they are obtained. However, these charging networks do not have the capability to charge multiple vehicles on a circuit or maximize the number of vehicles charging on the local grid. A software update will not give them this ability either, because the networks are not software based. As a result, algorithms for sharing circuits among many PEVs do not apply to them. A method for sharing an electrical circuit among charging stations is proposed by Coulomb [7], but no details of charging algorithms are provided. They are likely to have smart charging algorithms on their charging stations, but the stations are not designed for current sharing purposes because they only have one or two outlets.

Both Coulomb and Blink require a short range Radio Frequency Identification (RFID) card for authorization purposes. In both cases, the user must take extra steps to authorize charging. Mal et al [8] proposed using conventional RFID tags inside PEVs and RFID readers on parking garage access gates together with middleware and an aggregate charging controller to authorize, assign, and enable charging. However, this system still requires action from the user and is not as

flexible as may be desired.

The prevention of electrical shock is critical to any PEV charging system. A software based PEV charging system with multiplexing capabilities must have a unique safety system that integrates safety on all levels of control. It is uncertain if commercial charging stations with proprietary networks, like Coulomb and Blink, have an integrated safety design.

Based on the roles and intelligence of electric vehicle support equipment (EVSE), preliminary classifications of EVSE and related standards, such as ICE 61851, 15118, and 61850, are presented [9]. Several problems exist with today's approach to charging PEVs. Primary among these is the fact that the current laissez faire system is not responsive to grid limitations and, therefore, not well suited for large-scale use. PEVs represent non-negligible electrical loads [10], and their continued treatment as conventional loads will present problems for the power grid with further market adoption of PEVs. The impact of PEVs on existing power distribution networks have been analyzed, evaluated, and assessed using simulations of models and conditions [11-16]. Power grid impact case studies, such as those conducted in Beijing [17] and Italy [18], have been investigated and assessed. It has been presented that voltage fluctuations and increased on-peak loads caused by uncoordinated charging activities will lead to a higher blackout probability [19], among other problems. To make matters worse, no charging station is currently capable of performing demand-response by request from a utility or distribution system operator. In addition, the current approach to PEV charging lacks technical sophistication and user-convenience, which will impede market adoption if left unaddressed. Even the most sophisticated charging stations must be manually pre-programmed to perform scheduled charging, requiring user action to authenticate charging or accept a payment.

No station is currently capable of computing a vehicle-specific charging schedule that takes

the PEV's state of charge (SOC) into account. This is largely due to the fact that no standard exists to regulate the information exchange between PEVs and EVSE during the charging process. The current SAE J1772 standard [20] does not allow Vehicle ID or battery charge information to be communicated, only power availability and the ability of a PEV to accept power. Consequently, the attributes of PEVs are not available to outside third parties, including the EVSE. There are few ways to establish Vehicle to Grid (V2G) communication without substantial modifications to the vehicles, the charging interface and the charging stations currently on the market [21, 22].

Before V2G communications standards such as SAE J2836/1-6 and J2847/1-5 [23] are adopted, however, custom communication channels must be implemented in order to obtain a vehicle ID or battery state of charge (SOC) from a PEV. In addition to the inability to receive charge information from a PEV, current charging stations are unable to remotely recognize incoming client vehicles and authorize charging without additional user interaction.

The UCLA Smart-Grid Energy Research Center (SMERC) is developing a software-based PEV monitoring, control, and management system called WINSmartEV^{TM} [1-4, 67] which allows remote monitoring and variable current control of PEV charging. This smart charging infrastructure is capable of providing variable power to several PEVs from one circuit using multiplexing and variable current for controlled charging. WINSmartEV^{TM} can take input data from any relevant source on the internet, giving it the capability of using complex algorithms that take into account external factors and predictive models in order to balance the requirements of PEV charging and the demands of the grid.

The objectives of a smart charging infrastructure include:

(1) Reducing the overall energy cost to the society and PEV owner;

(2) Making charging simple and convenient for the PEV owner;

(3) Improving monitoring and control of the local power system by managing charging operations of the PEVs based on local grid conditions.

In order to achieve these objectives, a smart charging infrastructure should include the ability to do the following:

(1) Switch between auto and manual mode for PEV charging control;

(2) Switch between charging algorithms;

(3) Scale the entire system, including gateways, algorithm, and user accounts, from single parking structures to an entire city;

(4) Integrate station status onto commercial map systems such as Google Maps;

(5) Generate visual reports;

(6) Send email notification to users for closing charging sessions;

(7) Dynamically show available charging stations;

(8) Differentiate privileges for different levels of users and administrators;

(9) Maintain system security with features such as Secure Sockets Layer (SSL).

A smart charging infrastructure should also have a web-based application suitable for any mobile device such that PEV users can be ready to access the User Control Center on the server without downloading extra apps.

WINSmartEV^{TM} consists of a centrally controlled network of charging stations that address the inherent problems with the current approach to PEV charging and the inability of current systems to respond to grid-imposed constraints. The system's charging controller is able to schedule charging on each station under its control and switch between multiple PEVs connected to a single station. To address the lack of technical sophistication and the resulting inconvenience

for the users of existing charging stations, the system currently supports user authentication, billing, and record keeping to be performed through a smart-phone interface. This system centers on a server-based aggregated charging controller and utilizes a user database together with a smart-phone interface for charging authorization.

The current WINSmartEV^{TM} infrastructure is the first step in achieving a grid-responsive, intelligent, and convenient charging system. The following improvements represent the next steps forward. A safety design is developed and integrated at each level to achieve a safe and reliable infrastructure. In order to allow the WINSmartEV^{TM} charging controller to derive a vehicle-specific charging schedule that takes both the vehicle's SOC and the grid load into account, a solution is developed for remotely monitoring the SOC throughout the charging process by using in-vehicle monitoring devices called Vehicle Monitoring/Identification Modules (VMMs). For security and financial reasons, among the many functions these charging stations will perform are user authorization, authentication, and billing. In order to simplify user interactions and make charging more convenient, a solution for remotely authenticating and authorizing vehicles for charging is developed. No extra authorization step is required by the user, unlike traditional point of sale (POS) devices used in non-network charging stations or short range RFID cards used in networked stations [5, 6]. The VMMs, located in the PEVs, act as RFID tags for vehicle identification and charging authorization. These devices allow charging authorization to take place seamlessly at multiple charging stations within the wireless signal range. The VMMs communicate directly with the control center through a ZigBee mesh network, thus simplifying the system and eliminating the need for a layered architecture to manage a variety of automatic identification hardware as seen in [28].

The existing WINSmartEV^{TM} collects power information from meters by using a data pull

method. Because the wireless infrastructure is available and ubiquitous, the chargers are generally connected to the internet through 3G cellular networks. Local communication between and within chargers is conducted through a ZigBee mesh network. Therefore, when the data pull method sends a power information request command from the server to a charger, the signal must pass through the internet and a 3G network before it reaches the gateway of the charging station. Then the gateway relays the power information request to the specific meter for which it is meant. When the gateway receives a reply from the meter, it relays the response back to the server, traversing the routing path back in reverse order. With many meters each requiring multiple requests, the aggregated round trip time causes slow performance. In order to enhance the system's performance and shorten the response time of the system, a device is developed that will collect the power information locally in order to send it in to the server together as one packet. By decreasing the number of requests required for status reports and control operations, this Power Information Collector (PIC) will significantly decrease the delay time for switching PEV charging sessions or changing current to the PEVs. By reducing the traffic between the server and the charging stations, the improvements allow the control center to serve a larger system, which enhances the capability of the existing WINSmartEV^{TM} framework. Moreover, because the charging station's local control unit has access to the meters' power information, it can employ local charging algorithms to control charging. This will leave the control server with more computation power to handle a larger system.

A charging algorithm that relies on a smart phone interface for entering PEV data, such as arrival and departure times, and initial and final state of charge (SOC), is proposed in [8]. The schedule algorithm proposed in [29] requires the initial energy states of a PEV as the input. These approaches are not valid unless the user provides the actual SOC data. To solve this problem, the

authors of [30] propose a custom-built module, named Vehicle Monitoring/Identification Module (VMM), which reads the in-vehicle Controller Area Network (CAN) data bus and transmits SOC data via a ZigBee wireless link to a charging station and then onto the charging controller. However, without insider knowledge of the PEV manufacturers, identifying the data location on the CAN bus could present a challenge for obtaining the SOC data. The Battery Management System (BMS) can be developed with CAN communication [31] to retrieve SOC. Nevertheless, the development of the BMS system inside the PEV is beyond the topic of this thesis.

The control scheme for PEV charging can be either centralized [37] or decentralized [32, 36, 38, 41-43]. In addition, the charging algorithms can be developed based on time [32-34], energy price [35, 36], power capacity [37-40] or regulation [41-43] depending on the issues and targets. Some charging management systems for parking lots [44, 45] are also presented. The aforementioned PEV charging control scheme is summarized in Table 1.

TABLE 1. PEV CHARGING CONTROL SCHEMES

Author	Issue	Target	Parameters
[32]Ahn, U. Michigan	Manage renewable energy and EVs	Minimize generation cost and CO2 emission	Base load, EV numbers, unplug time, initial SOC
[33]Vandael, KU Leuven, Belgium	Peak load causes expensive production	Reduce peak load	Incomplete and unpredictable charge time and energy amount
[34] Lu, Penn State U.	Maintain power consumption within safety threshold	Satisfy more consumers	Charge time, priority, unevenness
[35]Mahat, Aalborg. U. Denmark	EVs have impact on the grid	Reduce charging cost	Price signal
[36] Rigas, Aristotle U. Greece	Manage EV charging	Maximize charging station and EV user's profit. Minimize the impact on their schedule	Price strategy
[37]Lopes, Porto-INESC, Portugal	Integrate EV and power grid	Illustrate impact and benefit	
[38]de Hoog,	Uncontrolled	Increase PEV	SOC voltage at

U. Melbourne, Australia	charging leads to overload	penetrations	connection
[39]Bayram, N. Carolina State U.	Stochastic charging demand threatens grid reliability	Provision power source	Stochastic process
[40]Logenthiran, U. Singapore	Manage power distribution system	Reduce charging cost and peak load	Incomplete and unpredictable charge time and energy amount
[41]Sun, U. Toronto, Canada	Provide regulation service	Align EV's interest with system's benefit	Battery degradation cost, charging/discharging inefficiency, energy gain/loss, external source cost
[42]Lin, U. Hong Kong	Provide bi-directional regulation service	Meet EVs' share of regulation demand request by grid operator	Current and past regulation profile
[43]Wang, Nanyang T. U. Singapore	Provide frequency regulation service	Minimize overall cost of PEV charging	Time slots

Unfortunately, the solutions deal with hypothetical problems rather than real systems. In [32], the plug-in times, plug-off times, and initial SOC are randomly generated, which do not correspond to real life cases. Furthermore, different PEVs' charging speeds are not taken into account. In [33], the PEV's power consumption is assumed to be a continuous distribution, which does not correspond to the J1772 specification's 6A minimum charging current. Another case that is not based on a real life scenario is [34], which assumes a triangular charging curve. For example, the battery pack in a Nissan Leaf consists of 48 modules and each module has 4 cells, totaling 192 cells [66]. A PEV's on-board charger is responsible for handling battery charging and it draws a static current from the charging station following the limitation set by the duty cycle of the pilot signal; thus the triangle charging curve assumption is not correct.

A smart charging infrastructure needs to interweave the control scheme, the platform, and the infrastructure as shown in Figure 1.

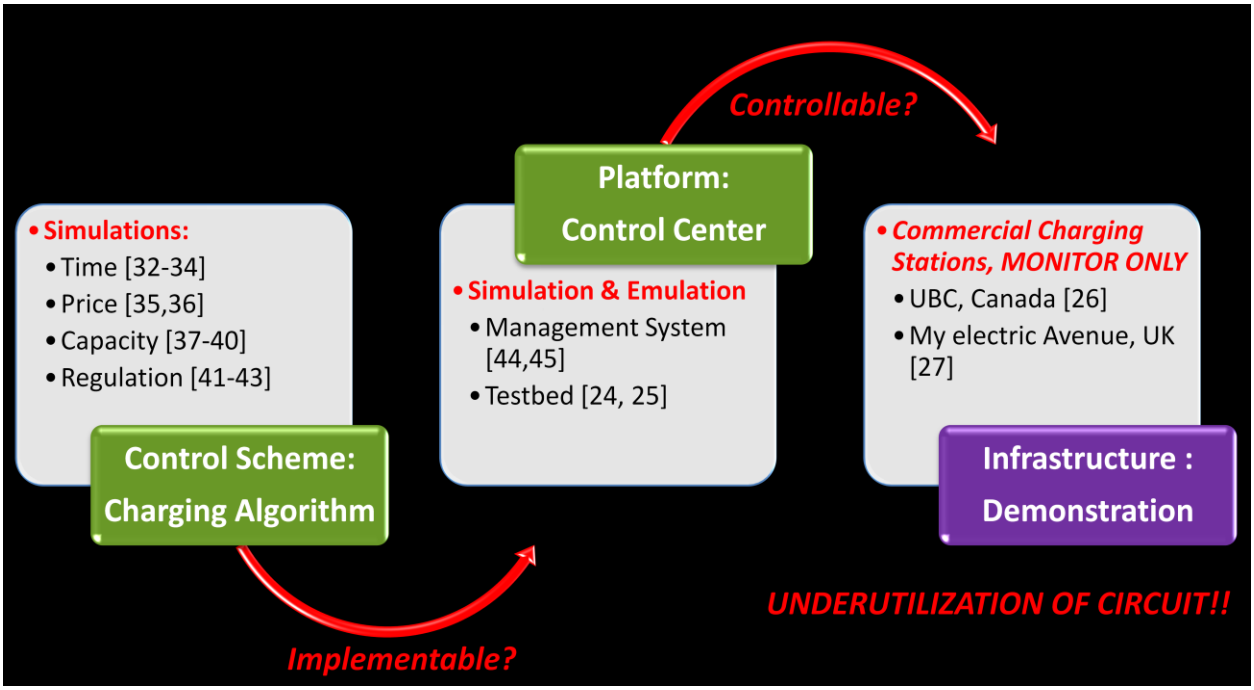

Figure 1. Interweaving of the components in smart charging infrastructure

Published charging algorithms, intended for publishing papers, are not implementable because the initial conditions and assumptions of these algorithms do not correspond to real world cases. Testbeds [24] and platforms [25] have been developed for emulation or simulation, but these systems are not valid unless they work with real PEVs. Certain scale PEV demonstrations, - like those conducted by Powertech EV Services at University of British Columbia (UBC), Canada [26] and My Electric Avenue in United Kingdom (UK) [27] – could only provide limited functions, such as power usage monitoring and grid impact assessment, and did not include control of the charging stations. In addition, none of the aforementioned literatures address how to achieve variable current and multiplexing control. There is no mention of the collaboration between the control center and the charging stations, let alone the unique safety requirements of a software based charging system with variable current and multiplexing control. Moreover, none of them discuss how to improve the performance of the smart charging system.

Instead of an on-site EV charging approach, a strategy for battery replacement is presented [46]. The scheduling and inventory management problems [47, 48] of battery replacement services have also been studied. However, this business model is not practical because the current PEVs' batteries on the road are not designed for replacement.

The main contribution of this thesis is to devise a smart charging system to solve the issue of circuit underutilization. Table 2 shows some facts of Level 1 and Level 2 charging stations.

TABLE 2. FACTS OF LEVEL 1 AND LEVEL 2 CHARGING STATIONS

Station	**Level 1**	**Level 2**
Voltage (V)	110	208
Current (A)	12	30
Power (kW)	1.32	6.24
Miles per hour charging	Focus: 5 Leaf: 5.4	Focus: 23.7 Leaf: 13.5
Charging Hours (from Empty to Full)	Focus: 16 Leaf: 16	Focus: 4 Leaf: 8
PEV	**Ford Focus**	**Nissan Leaf**
On board charger (kW)	6.6	3.3
Miles/kWhr	3.8	4.1
Battery Size (KWhr)	23	24
Rating Range (Miles)	75	75

The table shows that a Ford Focus is fully charged in four hours, while a Nissan Leaf fully charges in eight on a Level 2 station. The underutilization of a circuit occurs when a charger remains connected to a PEV for much longer than necessary. In the case of people who work eight hours a day, the Nissan Leaf fully utilizes the circuit but the Ford Focus under utilizes it for at least four hours.

WINSmartEV^{TM} has been developed to maximize the charging capacity for a given electrical infrastructure. This system is software based with the control system located on a central server that maximizes feature flexibility. The charging devices control the current to multiple vehicles at

once, allowing many PEVs to charge from a single circuit. Furthermore, the central server can control the aggregated power to any cluster of chargers in order to keep the total power consumption within the required parameters while maximizing the number of vehicles that can be charged on the local network. In order for the system to work optimally, sophisticated algorithms need to be implemented that maximize the use of available electrical grid and circuit capacity. Currently, a round-robin algorithm is used to schedule charging in the multiplex charging system of WINSmartEV^{TM} in order to fairly distribute energy to PEVs. In order for PEV charge multiplexing to become more appealing to users, fairness in the allocation of charge time should be maximized when energy is free. Charge time fairness is defined and an algorithm to maximize this fairness is developed. The algorithm, which optimizes fairness in allocating charge time and energy distribution, can help this technology become more readily accepted by consumers.

The processes including the smart charging algorithm [49], safety requirement [50], and the RFID authentication and authorization [51] involve collaboration between the server and the charging stations. These special features are developed based on the existing hardware and software. In order to maximally utilize the power resource on the local grid and improve the performance of the PEV charging infrastructure for managing charging sessions or current control, collaboration between the master (server) and the slave (local controller) is required. Therefore, a master-slave control scheme for the PEV smart charging infrastructure is developed to enhance the performance of the features including smart charging algorithms, safety requirements, and RFID authentication and authorization. The control scheme involves a server-based central controller and local controllers inside the charging stations.

To encourage electrical power sharing, a four-outlet smart charging station connected to a

single circuit is designed and implemented. The standard charging stations for this system are connected to a single circuit and provide four points for PEV charging. There are two types of charging stations, Level 1 stations that connect to standard 120V household circuits, and Level 2 stations that connect to 208V or 240V circuits for faster charging. The Level 1 station, known as EVSmartPlug™ controls four standard outlets. The PEV user plugs the PEV's trickle charging cable into the outlet on the charging station in order to charge the PEV. Because the control system only controls the 120V power to the EVSmartPlug™, all control happens by switching the outlets on and off. Therefore, all communication between the pilot signal and PEV takes place within the PEV's trickle charge cable. The schematic of a 4-channel EVSmartPlug™ station is shown in Figure 2.

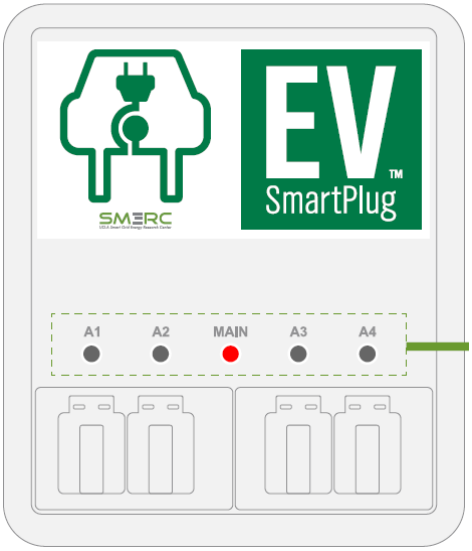

Figure 2. Schematic of a 4-outlet SmartPlug™ station

With this control scheme, an authorized user is able to start or stop PEV charging via a mobile device and the central control server can intelligently schedule charging. The PEV user can also use a web app to check other information such as available charging stations, charging status, monthly charging records, and the user account. A screen shot of the mobile app is shown in Figure 3.

Figure 3. Screen Shots of User Control Center

By running charging or scheduling algorithms, an EVSmartPlug^{TM} station can share the power of a single 120V power source with four EVs. A standard 15A 120V outlet can only handle 12A continuously and a 120V trickle charge for a PEV is always 12A; therefore, the station can only turn on one channel and charge one PEV at a time. Because of this constraint, the charging algorithm is the central component of the charging operation. Currently, the station runs a round-robin charging algorithm for multiple PEVs.

The EVSmartPlug^{TM} station can be viewed as a simplified version of the smart Level 2 charging station introduced below. Because the smart plug has no pilot signal to control its activation, only switching the type of algorithm can affect the function of these stations. Figure 4 shows the installation of the Level 1 SmartPlug^{TM} station in a UCLA parking lot.

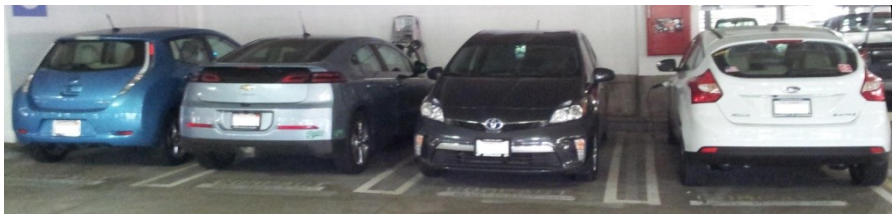

Figure 4. Installation of a 4-outlet SmartPlug^{TM} Station

As of this date, there are five Level 1 charging stations and five Level 2 charging stations installed on the UCLA campus. Figure 5 shows the first installation of the J1772 Level 2 four-outlet smart charging station in a UCLA parking lot.

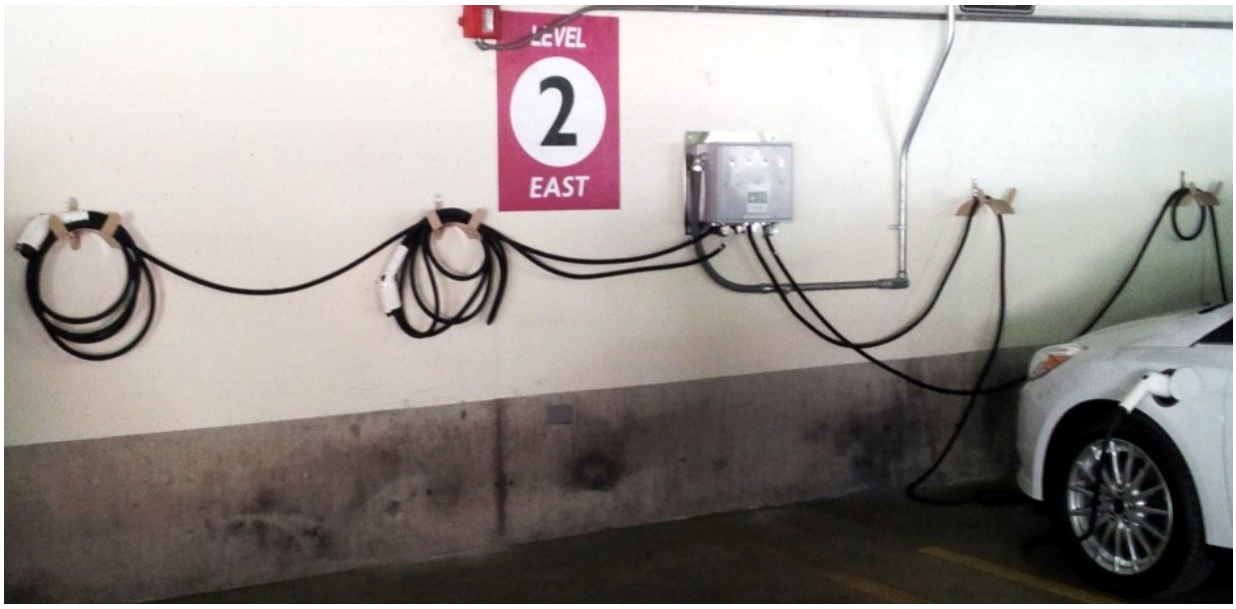

Figure 5. Installation of a J1772 Level 2 4-outlet Smart Charging Station

The charging station supports variable-current charging of multiple EVs at one time. Currently, an authorized user is able to check available charging stations, start or stop PEV charging, check the charging status, view monthly charging records, and manage the user account via a mobile device. Refer back Figure 3 for a screen shot of the mobile app.

This thesis is structured using the following order. First, the communication system over the entire infrastructure is outlined in chapter 2. Then the master-slave control system of the WINSmartEV^{TM} smart charging infrastructure is described in chapter 3. Next, the smart charging algorithms and the safety requirements for all levels are described in chapters 4 and 5. Last, the system performance is evaluated with experiments and discussed in chapter 6. By using this smart charging infrastructure to manage PEV charge scheduling and current flow, energy shortage in local grids can be prevented.

CHAPTER 2 COMMUNICATION SYSTEM

The communication system is the backbone of the smart charging infrastructure, which allows the charging stations to exchange information with the control center. The network architecture for smart charging infrastructure at UCLA is devised with existing standards and technologies for non-proprietary network purposes. In addition to the network architecture, the local communication system inside the charging station for both local controllers and meters also needs to be implemented. Later, based on existing hardware, a novel mesh network RFID Authentication and Authorization Scheme is developed without user involvement. This chapter is structured in the following way: First, the UCLA EV Network Architecture is introduced in section 2.1. Next, the details of the hardware and firmware of the local communication system inside the charging station are described in section 2.2. Finally, the RFID Authentication Scheme is described, and experimental results of RFID response time and RSSI tests are presented in section 2.3.

2.1 Network Architecture

Figure 6 illustrates the network architecture of the WINSmartEV^{TM} smart charging infrastructure.

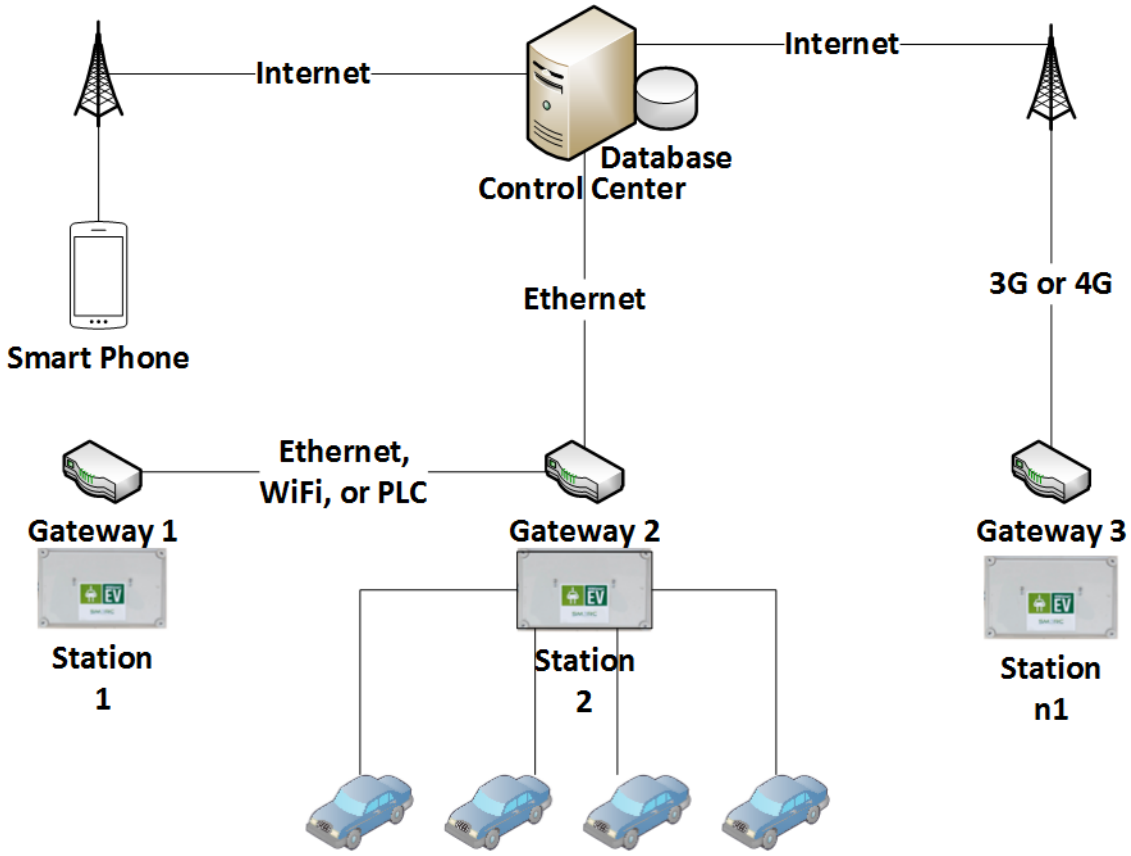

Figure 6. Network Architecture of WINSmartEV™

A server-based control system with aggregate charging controls all charging stations using multiple protocol gateways that connect via Ethernet, WiFi, or 3G connection; 3G is necessary due to its applicability anywhere a cellular signal exists, especially where wired or WiFi communication is unavailable. For internet access via Ethernet, a DHCP router assigns static or dynamic IP addresses to a gateway; a gateway can also use a power-line communication (PLC) module on its Ethernet port for internet access when Ethernet wiring is not available. For WiFi communication, the gateway is configured as a client to another gateway or router within WiFi range; port forwarding is used on the host gateway or router so that the control server can access the client gateway. The connection between the charging stations is for relaying commands from the server to the charging stations. Figure 7 shows a WiFi port forwarding setup in a UCLA parking lot.

Figure 7. WiFi Port Forwarding Setup

In this setup, the Level 2 charger's gateway serves as a master while the Level 1 charger's gateway acts as a client. Both gateways must have auto channel selection enabled to broadcast their SSID on different channels, thereby avoiding collisions.

2.2 Communication inside the charging station

Since the National Institute of Standards and Technology (NIST) has announced the first draft of the framework and roadmap to coordinate the interoperability and standards for the smart grid [52], specifying ZigBee [53-55] for its low power and mesh network capabilities, ZigBee is adopted for our system. The control system's efficiency may possibly improve, based on user preference and local power capacity, by sending commands to charging stations through a gateway supporting multiple communication protocols.

The communication scheme for the metering and control systems are now described. The metering system in the Level 1 and 2 charging stations consists of a gateway and four meters with relays; an embedded relay inside the Level 1 charger distinguishes the two types of stations. The Level 1 station's meter can be directly controlled by the server through the gateway; the server can relay a retrieval command for power information – voltage, current, frequency, power

factor, and energy consumption – which the meter returns through the ZigBee network. A ZigBee coordinator embedded in the gateway creates a mesh network to which the meters must join. The metering system needs to associate the meters' IDs and their physical outlet numbers. The schematics of a four-outlet metering system are shown in Figure 8.

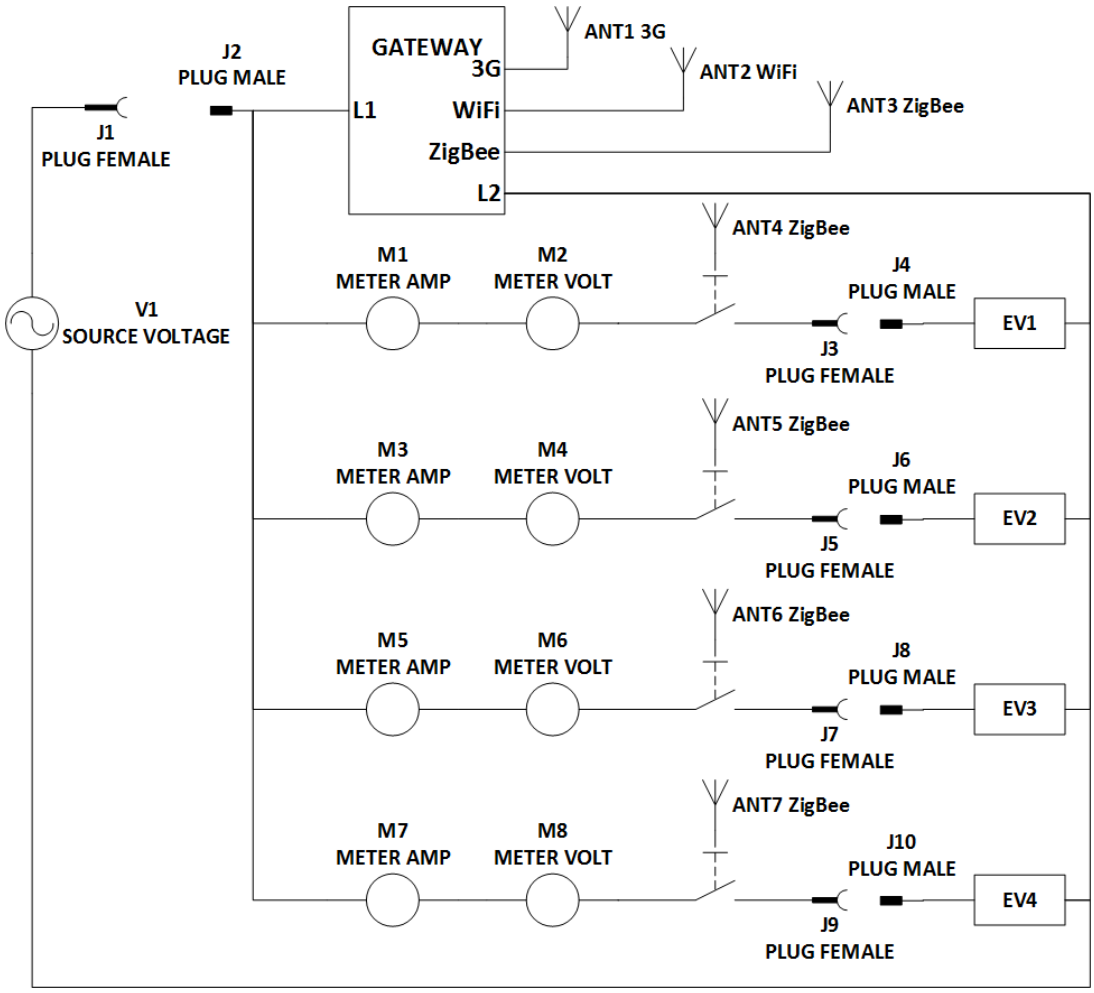

Figure 8. Schematics of Metering System

The ZigBee mesh network facilitates communication among many control devices – gateway, meters, and the local controller; as a consequence, charging stations can communicate with each other as well. Therefore, only one gateway is required in each localized area to service multiple charging stations and their PEVs. The details of the communication blocks in Level 2 charging stations are shown in Figure 9.

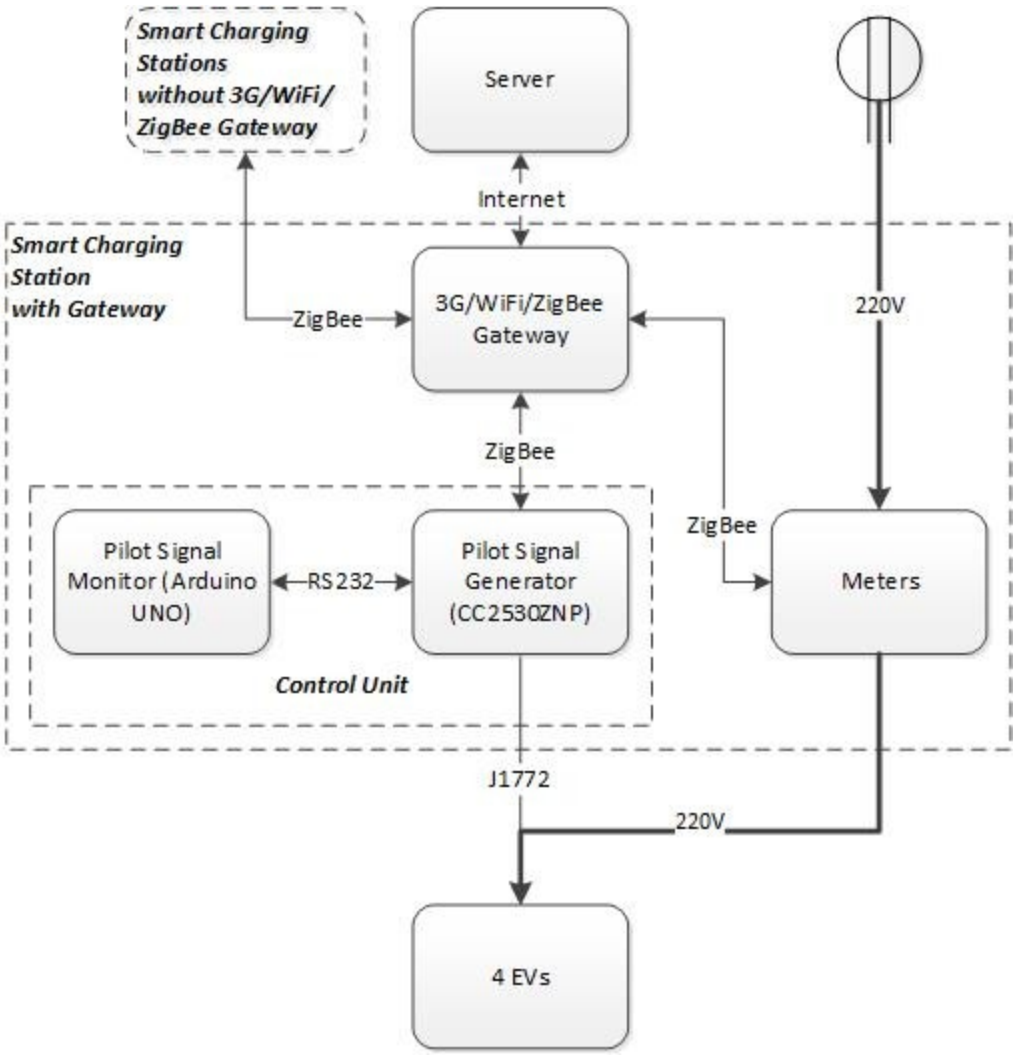

Figure 9. Details of Level 2 Smart Charging Station [51]

The ZigBee coordinator in the gateway handles the messages between the gateway and end devices or routers, including meters, local controllers, and the PEVs' Vehicle Monitoring/Identification Modules (VMMs). Whenever a ZigBee end device or router joins the mesh network, a 16 bit dynamic address is assigned by the coordinator; the coordinator must also recognize and register the MAC addresses of the devices to dispatch commands and parameters to them. The prototype for a ZigBee coordinator [56] is implemented using CC2530ZNP [57, 58] with MAX3232 as shown in Figure 10.

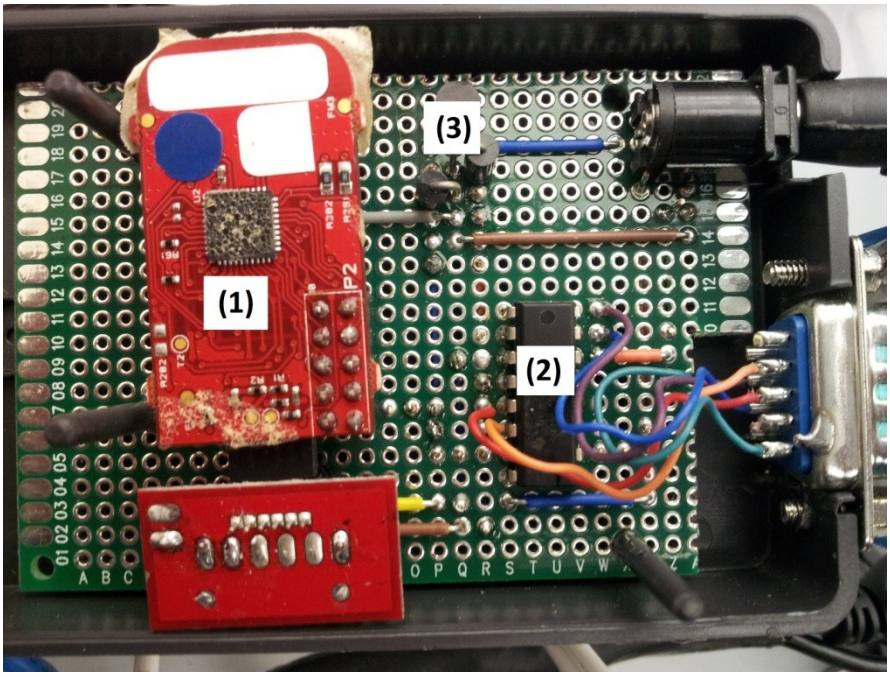

Figure 10. Prototype of ZigBee Coordinator Implementation [56]

The print circuit board (PCB) version of the ZigBee coordinator with surface mount devices (SMD) [51] is implemented for mass production purposes as shown in Figure 11.

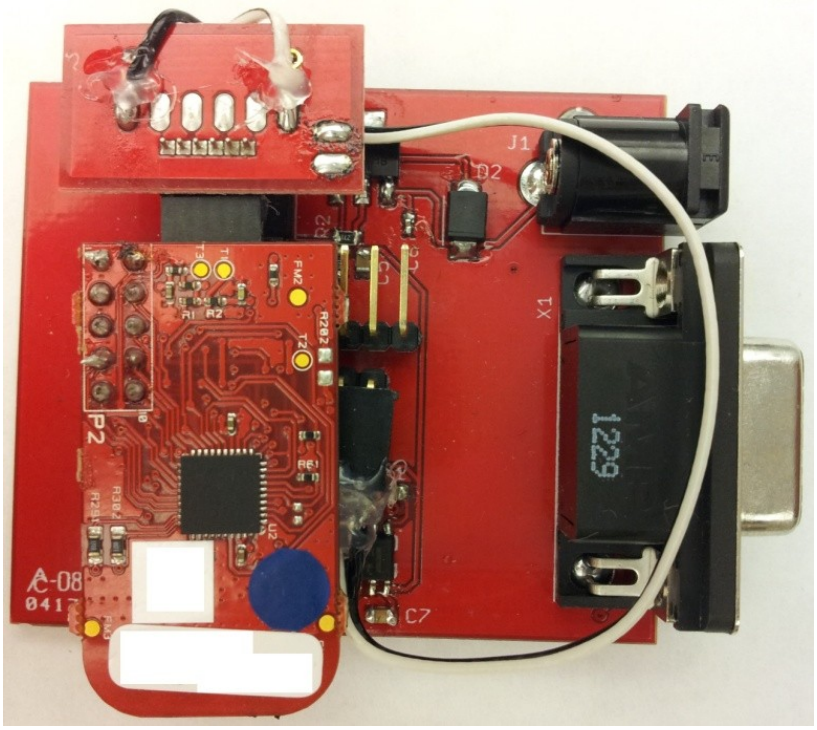

Figure 11. PCB Version of ZigBee Coordinator [51]

The firmware flow of our ZigBee coordinator is shown in Figure 12.

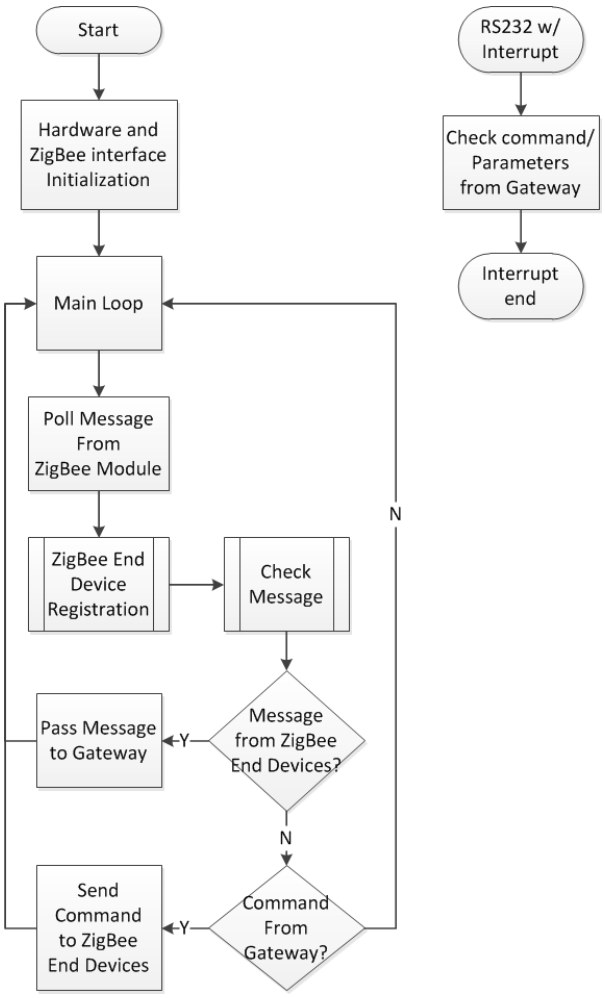

Figure 12. ZigBee Coordinator Firmware Flow [56]

The current system has two types of controllers: the first supports ZigBee communication and the second does not. The controller without a ZigBee module talks to the gateway through a USB port with the RS232 standard. The controller with ZigBee communication consists of a ZigBee coordinator and ZigBee end-device; the gateway uses the coordinator to dispatch or receive responses from the end-device. Both types of controllers connect to the gateway using a RS232-USB adapter cable, which must be compatible with the gateway to ensure proper functionality. When a 3G USB dongle is used for communication, both the dongle and RS232-USB cable are assigned a USB port and only assigned ports should be used.

2.3 RFID Authentication and Authorization Scheme

A decentralized authorization and authentication mechanism in multi-server environments has been proposed [59]. Users are able to authenticate themselves through a mobile app [1, 3, 4] in the current WINSmartEV^{TM} system, while a short range RFID authorization system is developed in [2]. Beyond these traditional identification methods, an innovative charging authorization system reads RFID tags over the mesh network, facilitating the authentication process at a charging station without user involvement; at the moment of the PEV's arrival, authorization takes place [51]. Adding this authorization capability does not involve hardware changes and only requires updating the firmware and software of the system. Aside from the ease of implementation, another benefit of the authorization scheme is the robust connection made between PEVs and charging stations in a real-world environment, subject to signal blocking conditions; data can traverse any available path in the mesh network. The authorization concept of the ZigBee-based Mesh Network RFID is shown in Figure 13.

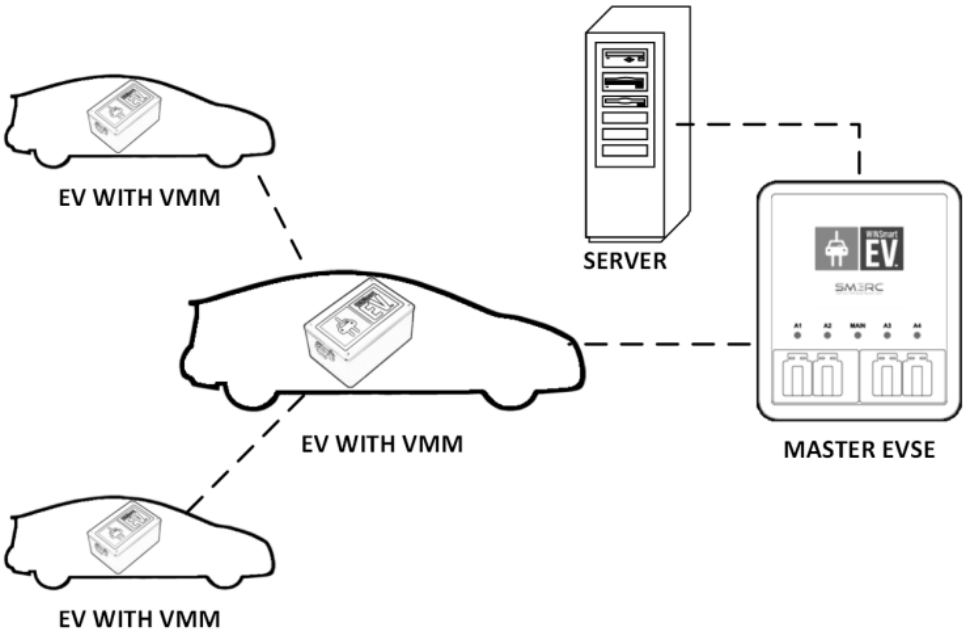

Figure 13. Mesh Network RFID with PEV Smart Charging Infrastructure [51]

The wireless mesh network consists of a ZigBee coordinator, located in a central charging station, and ZigBee routers, located in each of the custom-made PEV-mounted VMMs. The ZigBee routers in the VMMs serve as RFID tags, which use the unique 64-bit MAC address of each ZigBee device. The ZigBee coordinator, attached to the Gateway in the charging station, serves as the RFID reader; the architecture allows only one ZigBee coordinator to be used for multiple charging stations. Thus, the Mesh Network RFID has the advantage of using existing hardware without additional cost and provides traditional RFID benefits – unique ID and wireless communication – while adding mesh-networking capability. The mesh network provides robust connections between PEVs and charging stations, as previously mentioned. The reduced cost is due to each PEV transmitting its data to a single master station, allowing other stations to be simplified, lower cost versions.

The server periodically handles authentication and authorization. The charging authentication process includes retrieving the ZigBee MAC address, authorizing users, and detecting the PEV plug-in status. When the charging station detects a PEV at a distance, the Received Signal Strength Indication (RSSI) of the handshake serves as the metric for identifying a PEV approaching a charging station. The PEV plug-in status is used to identify the presence of a PEV at a charging station and to associate the vehicle's ID with a particular outlet. Figure 14 shows the charging authentication process on the ZigBee RFID mesh network.

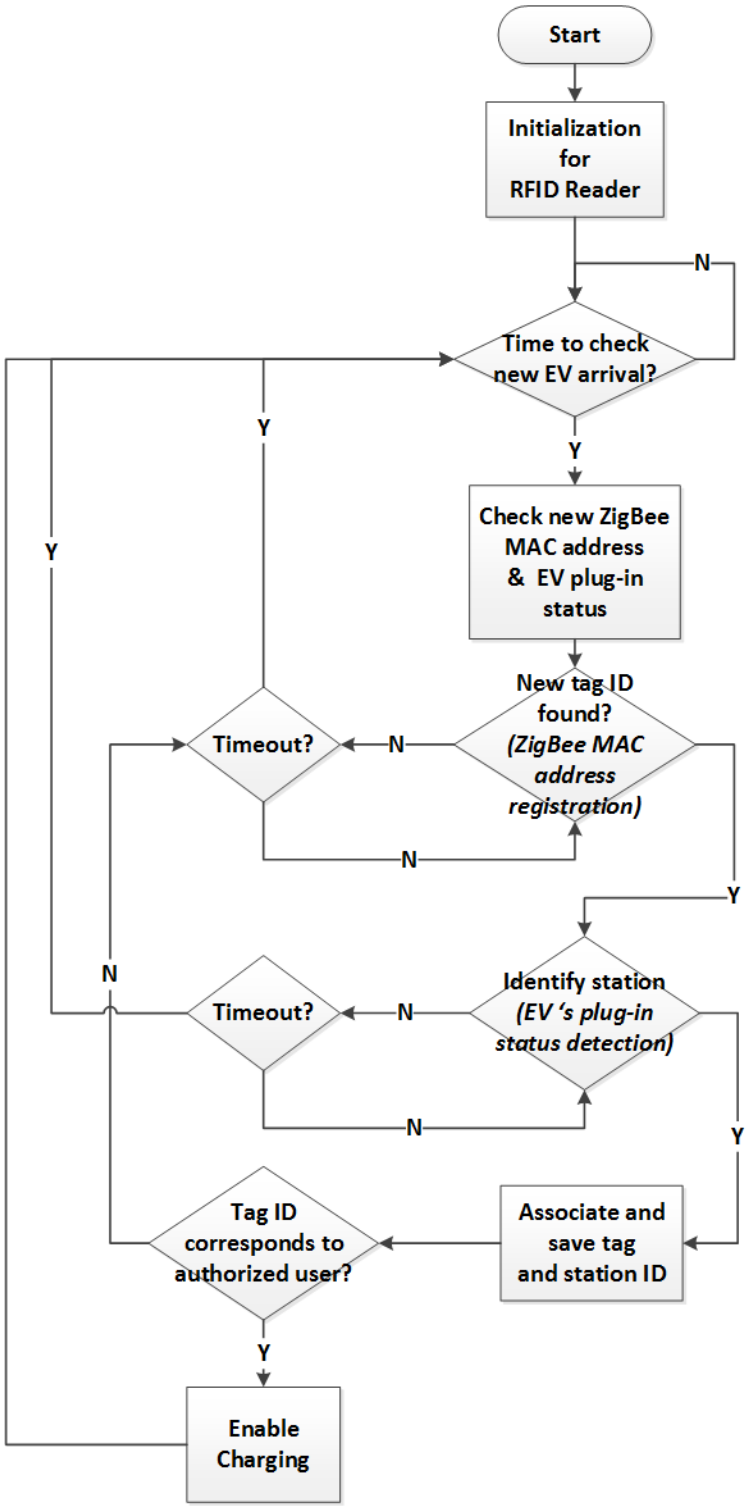

Figure 14. Charging Authentication Process Using RFID [51]

The charging authentication process checks for new PEV arrivals on a specific interval by transmitting commands. After RFID reader initialization, the server sends the "rgst" command to

check if new ZigBee MAC addresses (tag IDs) have been registered. The “stat” command is also sent out to identify into which charging station a newly arrived PEV is plugged. The aggregate charging server uses the PEV plug-in status to identify the presence of a PEV at a charging station and to associate the vehicle’s ID with a particular charge point. If the tag ID corresponds to an authorized user account stored in the database, the server sends the enable charging command to start PEV charging. The server commands to the charging stations are in the format: **comd[command] [channel] [parameter]**. The description of the commands and return values are summarized in Table 3.

TABLE 3. COMMANDS OF THE CHARGING STATION [51]

Command	Description and Example
Rgst	Return all registered ZigBee MAC address
	comdrgst0000 [return]: rgst01[MAC address][approach/leave/stay] rgst02[MAC address][approach/leave/stay]
Stat	Charging station status request
	comdstat0100 request channel 1 status [return]: duty0150rely0101plug0101stat0100

The ZigBee coordinator serves as the RFID reader and handles messages between the gateway and the end devices/routers. When a ZigBee router joins the mesh network, the coordinator assigns it a 16 bit dynamic address and associates the address with the unique MAC address of the ZigBee device. The ZigBee coordinator recognizes an approaching or departing PEV by the RSSI from the ZigBee router or ZigBee End Device. To ensure a stable connection with each Zigbee device on the network, a handshake protocol is implemented. The handshake between the RFID reader (ZigBee Coordinator) and an RFID tag (ZigBee router) is summarized in Table 4.

TABLE 4. ZIGBEE HANDSHAKE COMMANDS

Command	Initiating Device	Format
Request	ZigBee router	“comdtest[MAC address]”
Response	ZigBee coordinator	“comdresp[MAC address]”

To add authorization/identification capability, the firmware of the ZigBee coordinator inside the charging station and the software on the server need to be re-designed. The ZigBee coordinator firmware flow is shown in Figure 15.

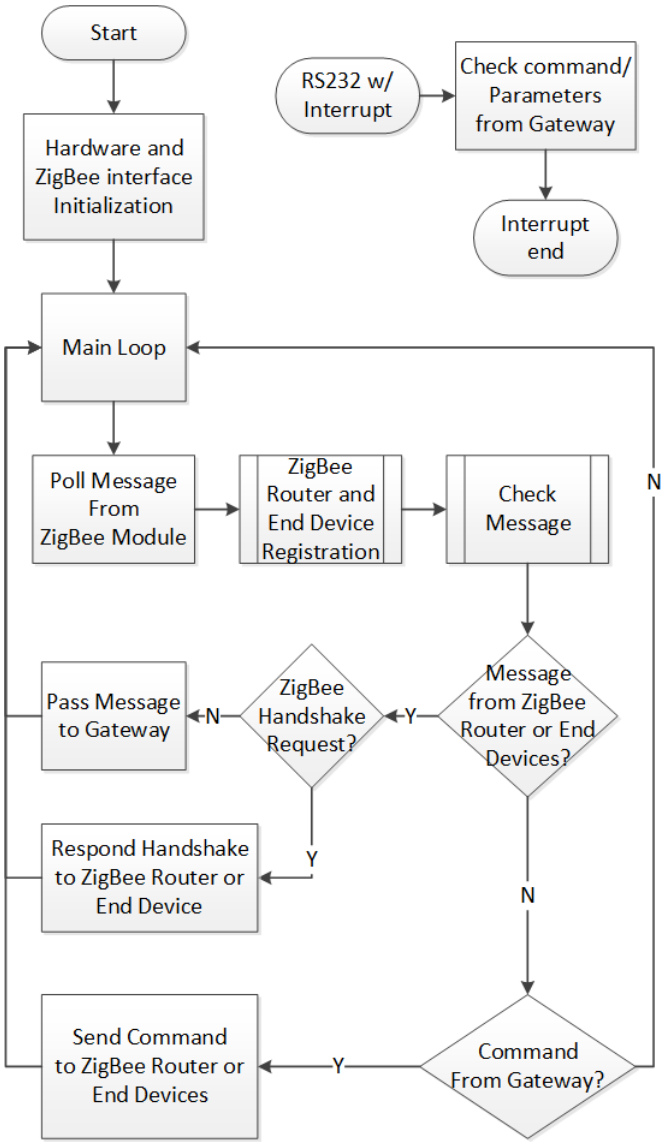

Figure 15. ZigBee Coordinator Firmware Flow [51]

The RFID tag is handled by a ZigBee-enabled remote monitoring module, located in the PEV, known as the VMM. The module has the ability of identifying each PEV, like a conventional RFID chip, with the ZigBee MAC address serving as the unique identifier. In addition, the module adds the ability to monitor PEV states through the vehicle's CAN bus; this ability turns the VMM into a remote sensor as well as an RFID tag. Figure 16 shows a schematic and cutaway view of the VMM.

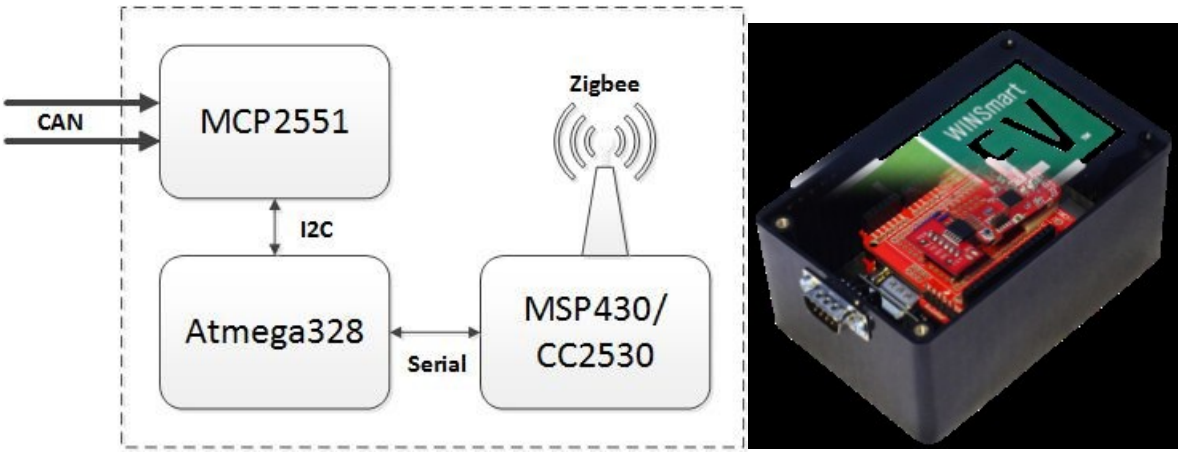

Figure 16. Schematic and Cutaway View of VMM [51]

The VMM employs a Texas Instruments ZigBee board equipped with an MSP430 microcontroller and a CC2530 RF transceiver for communicating with the network coordinator node. To monitor the PEV's CAN bus, the device uses an MCP2551 CAN transceiver chip and an ATMega328 microprocessor. Figure 17 shows the firmware flow on the VMM's MSP430 microprocessor.

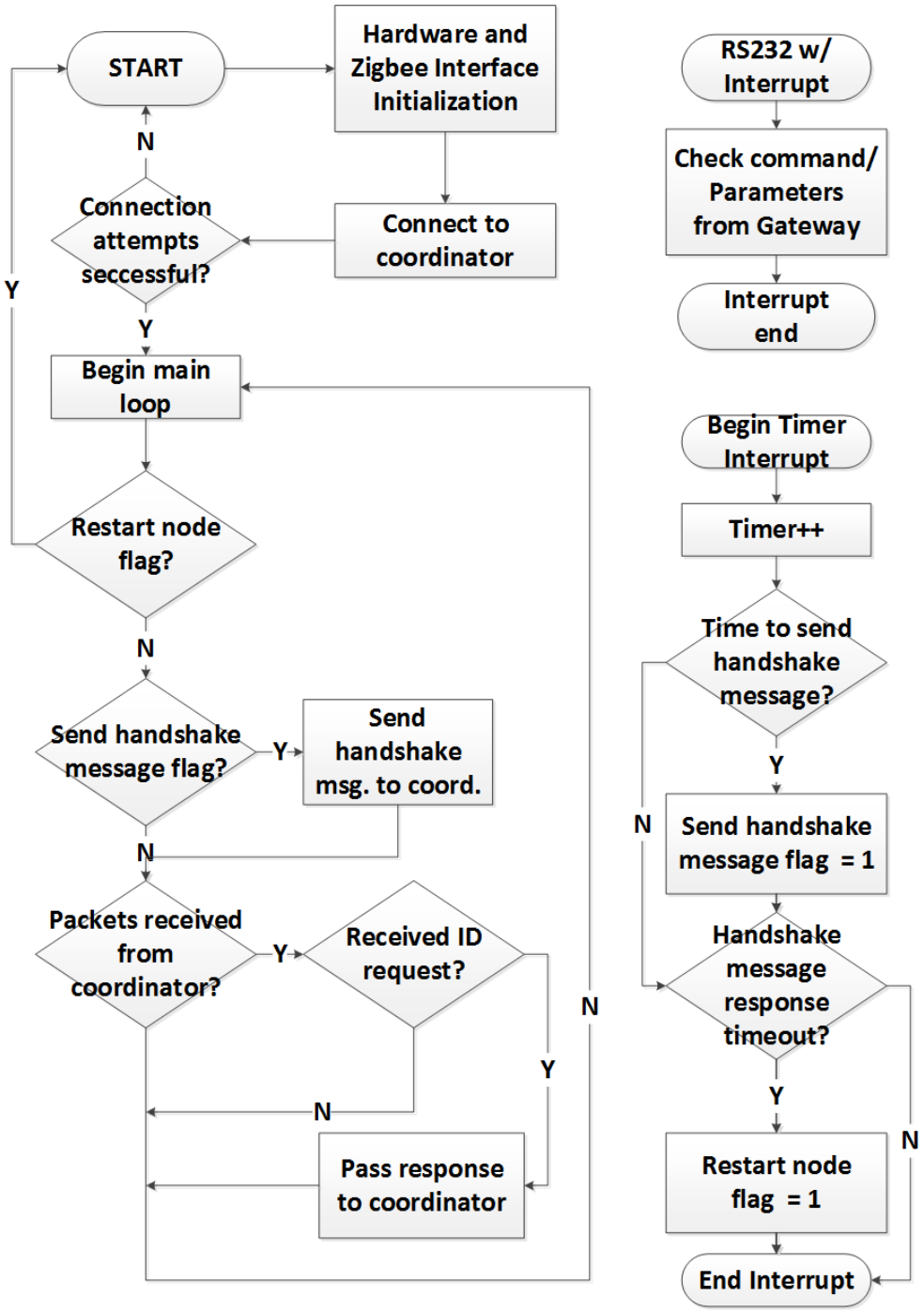

Figure 17. ZigBee Node Firmware in the VMM [51]

The firmware is responsible for establishing a connection with the Zigbee coordinator, responding to ID requests, and maintaining the wireless connection by transmitting periodic handshake messages and restarting the node if no response is received for the handshake. The

flowchart in the top right corner of Figure 17 shows the logic of the MSP430 processor's timer interrupt which is used primarily as a helper method for ensuring connectivity with the coordinator node; to this end, the interrupt keeps a running time count which it uses to set flags that are later used in the main loop to transmit handshake messages or restart the node.

Rough processes are discussed in PEV charging authentication via RFID, including ZigBee MAC address retrieval, user authorization, and detection of PEV plug-in status. The RFID authentication and authorization control scheme involves collaboration between a master controller (server) and a local controller (ZigBee coordinator). In order to accelerate the performance of the system, the local controller needs to be modified to push data to the master controller. Instead of the server periodically sending "rgst" commands to retrieve new tag IDs from the ZigBee coordinator, the coordinator pushes newly detected tag IDs to the database. The local controller inside the charging station is the trigger signal for the PEV plug-in status. Once the PEV plug-in status is detected, the local controller pushes the status and tag ID to the database. If the tag ID corresponds to an authorized user account in the database, the command to begin PEV charging is sent .

Experimental results of RFID response time and an RSSI tests are presented as follows. The setup of experiments is shown in Figure 18.

Figure 18. ZigBee-based RFID Experiments Setup [51]

There are two major time delays in the system: the ZigBee request and response delay, and the CAN-bus monitoring delay. The local controller has to wait T_{wait} to get the response to a data query in (2-1).

$$\begin{aligned} T_{wait} &\geq T_{ZigBee} + T_{CAN\_read} \\ &= \left(T_{ZigBee\_Forward} + T_{ZigBee\_Reverse}\right) + T_{CAN\_read} \end{aligned} \tag{2-1}$$

The ZigBee router response times and CAN-bus reading times are presented in the next three figures. The distribution of response times for one-hop communication between a coordinator and a router is shown in Figure 19.

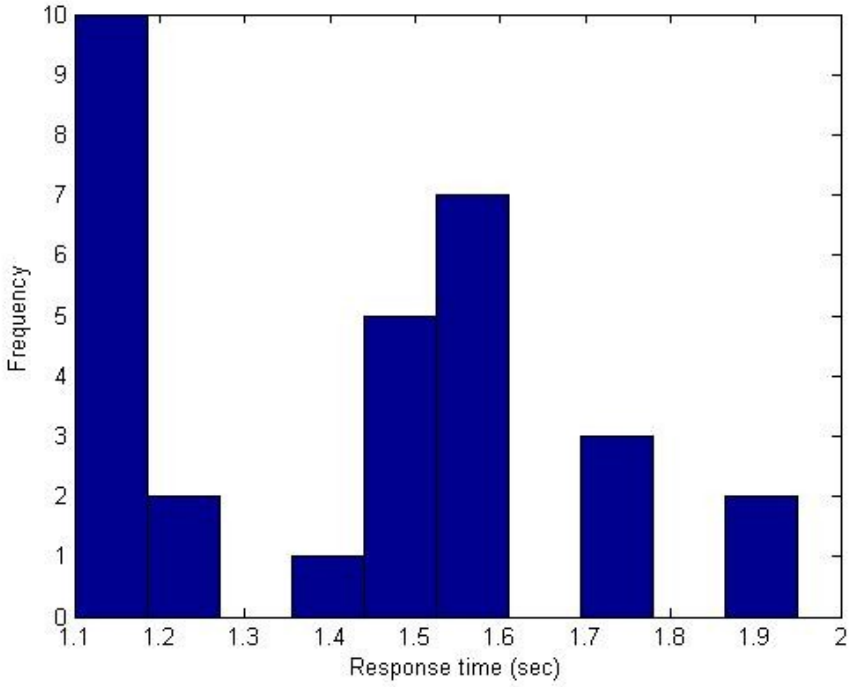

Figure 19. ZigBee Router Response Times in 30 Trial Runs [51]

The result shows a considerable variation in router response times with an average delay around 1.4 seconds. In this case, a two second minimum interval must be incorporated to allow for message response. However, it is likely that more than one hop will be required to transfer

data because a mesh network is involved. The distribution of response time for two-hop communication between a coordinator and a router through a router/repeater is presented in Figure 20.

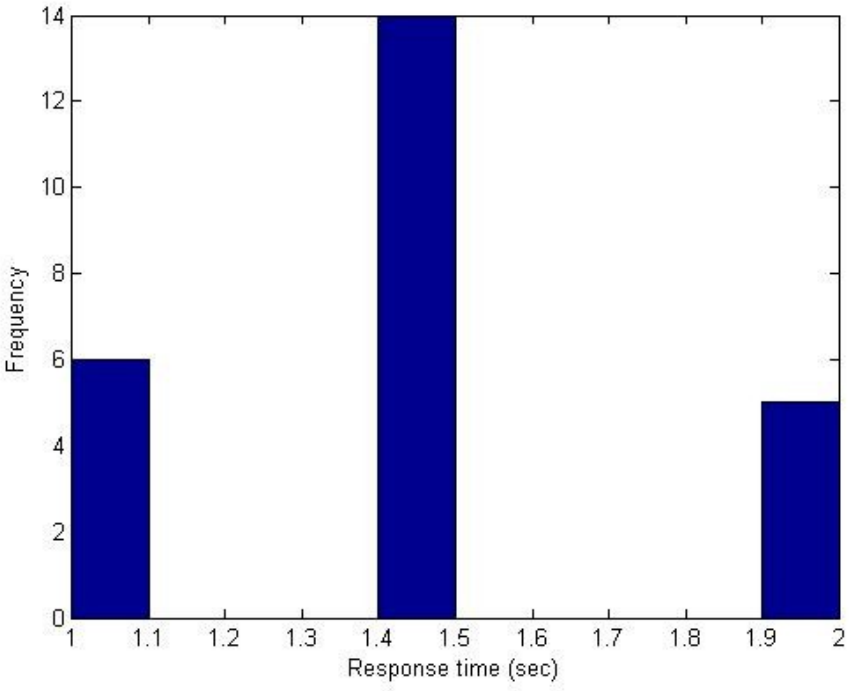

Figure 20. Two-hop ZigBee Router Response Times in 30 Trial Runs. [30]

The distribution of two-hop communication again varies between 1 and 2 seconds with an average of 1.5 seconds. Note that the response times are all multiples of 0.5 seconds, which is likely due to a delay in the intermediate router.

Because the CAN standard includes automatic message arbitration that forces non-critical messages to wait until messages with higher priority have been transmitted, the CAN-bus read delay is not a constant, but varies in time from vehicle to vehicle and between specific messages. In practice, messages with different priorities result in variable transmission rates. The distribution of times to read the SOC message on a Nissan Leaf CAN bus is shown in Figure 21.

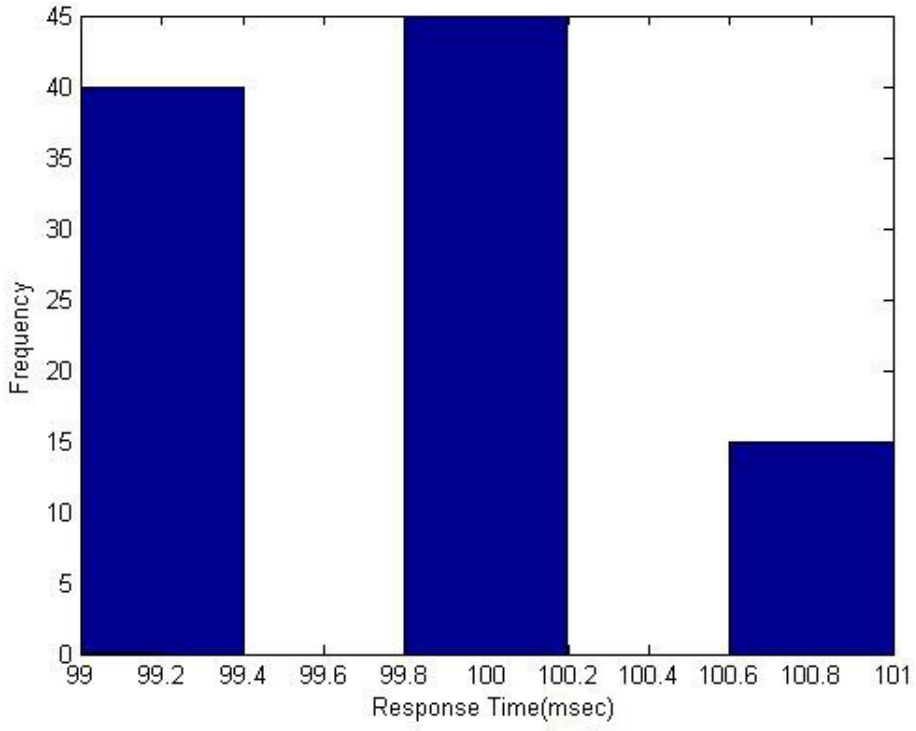

Figure 21. Nissan Leaf CAN Bus Reading Times for 100 Trial Runs [30]

The maximum time for a two-hop response is 2 seconds, which means T_{ZigBee} has a maximum value of 2 seconds. Considering T_{CAN_read} has a maximum value of 0.1 second, T_{wait} will have to be greater than 2.1 seconds per equation (2-1). As a result, a 2.1 second minimum waiting interval must be incorporated on the local controller. However, we find that an interval much larger than 2.1 seconds needs to be incorporated for detecting an approaching PEV. Accounting for the 3G communication delay presented in [55], the maximum round trip time of 3G is around 5 seconds, which means the server will need to wait 7.1 seconds to receive a response to a data request.

The RSSI is utilized to identify whether a PEV is approaching or departing a charging station. The results of RSSI vs. distance between charging station and PEV are shown in Figure 22.

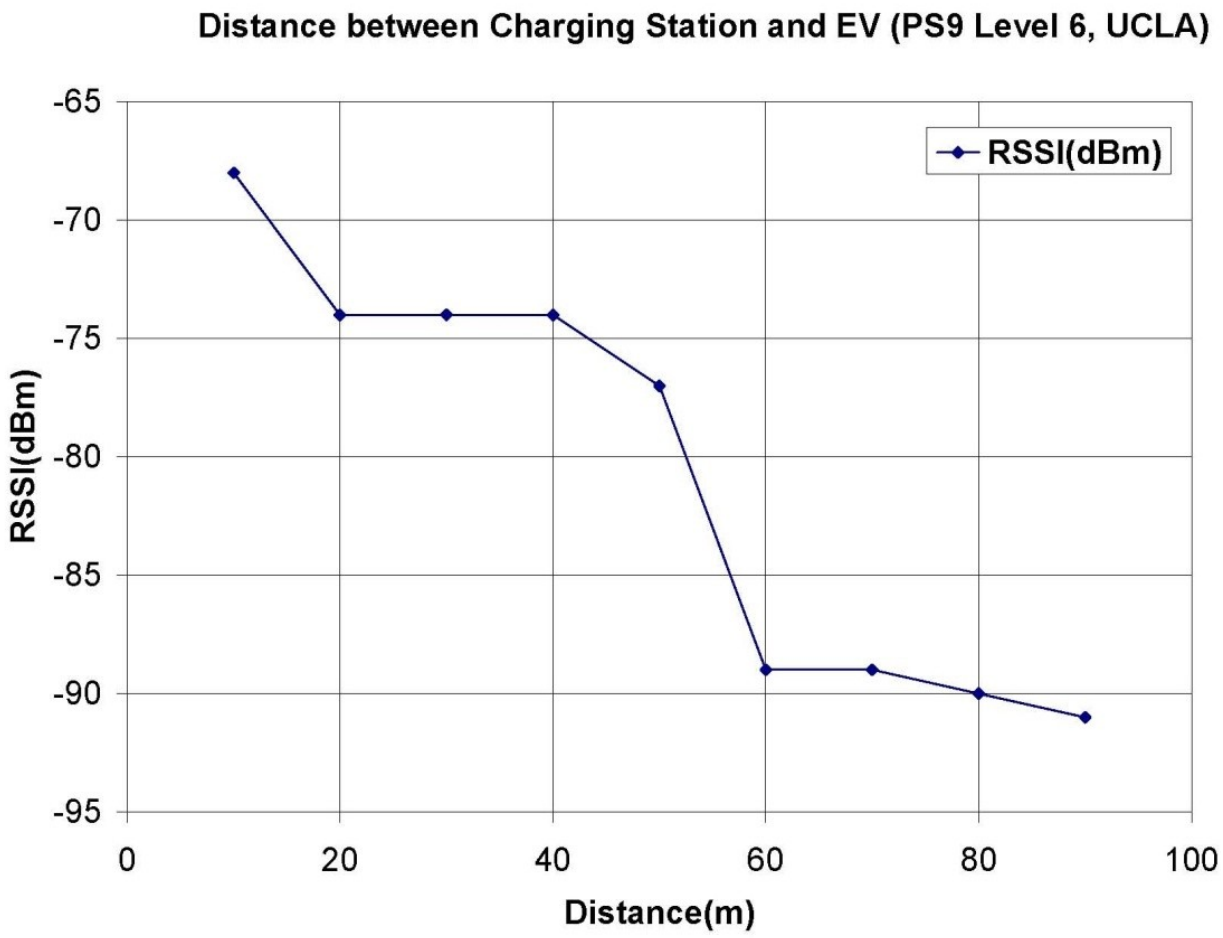

Figure 22. RSSI vs. Distance between Charging Station and PEV [51]

The experiment shows that when the PEV is within 50 meters of the charging station, the RSSI has a sudden jump from -89 dBm to -77 dBm. Although the theoretical range for ZigBee communication is 75 meters, in the real world, the charging station will detect the PEV at 50 meters. Note that the RSSI has another jump when the PEV approaches within 20 meters, which implies that RSSI would be an appropriate metric for identifying a PEV approaching a charging station. As for determining the PEV's rate of approach or departure, in most cases, the accepted speed limit in a parking lot is 5 mph, which means a vehicle approaches a charging station 4.5 meters every 2 seconds. Assuming that the PEV parks 5 meters away from the charging station, after a PEV is detected at a distance of 50 meters, the station will have a maximum of 10

handshakes to determine whether the PEV is approaching or leaving.

We now turn our attention to the collaboration between master and slave controllers in the RFID mesh network, and discuss exception condition handling. A server needs an exception handling process to manage charging stations when more than two PEVs come to the same charging station around the same time, because the charging station might not have a way to associate the IDs with the corresponding outlets. The charging station is only able to associate IDs with outlets if there are different currents when charging; this is the case when the PEVs have on-board chargers of different sizes. However, if the on-board chargers are the same size, the server cannot associate IDs with the outlets. In this case, the server can later associate the charging sessions with IDs and outlets when the PEVs leave by detecting the PEVs' RSSI; the server can also associate the IDs and outlets by SOC when PEVs are fully charged before they leave. In the case of PEVs with similar on board chargers, if they arrive and leave around the same time without being fully charged, there is no need to distinguish the charging session because the drivers will be billed for the same energy consumption.

2.4 Summary

In this chapter, the communication systems including the network architecture and local communication system inside the charging station are constructed for the smart charging infrastructure. Based on existing hardware, this charging system demonstrates how an intelligent RFID Authentication and Authorization Scheme functions without user involvement. This improvement advances an extra step in smart charging tasks.

CHAPTER 3 CONTROL SYSTEM

As ever more PEVs are purchased, a sufficient charging infrastructure becomes even more important. The lack of infrastructure investment, which is one of the issues facing PEV adoption, could be due to underutilization because a single dedicated PEV charger may be connected to a single PEV for much more time than required to charge the battery as it is typically not empty. In order to maximally utilize the power source on the local grid, a Level 2 PEV charging station with one-circuit-to-four-outlet is designed based on the 30A limitation of a normal continuous circuit installation and the minimum PEV charging current (6A) as defined in the J1772 standard to manage charging sessions and control the current to vehicles. Theoretically, the number of outlets could be 5 in order to fully utilize the maximum capacity of the circuit; however, in real practice, using 5 outlets could easily trip the circuit breaker if any PEV draws more than the specified current.

The PEV charging control scheme can be either centralized or decentralized. No matter what type of control scheme is applied, the collaboration between the master controller on the server and the slave controllers inside the charging stations is required to manage the charging sessions or control the current to the PEVs. This management involves collaboration between a master controller (server) and slave controllers (charging stations) to perform the features of RFID authentication and authorization, smart charging algorithms, and safety requirements; these topics are described in chapters 2, 4, and 5. The following sub-sections discuss the master controller, slave controller, and overall control scheme.

3.1 Master Controller: Server-based Controller

As described in chapter two, a server-based control system for aggregate charging controls

all charging stations though multiple protocol gateways using 3G, Ethernet, or WiFi. The control system monitors and controls charging activities using four main software components: 1) Database, 2) Station Controller and Data Collector, 3) System Monitoring and Control Center, and 4) User Control Center. Figure 23 shows the relation among these components.

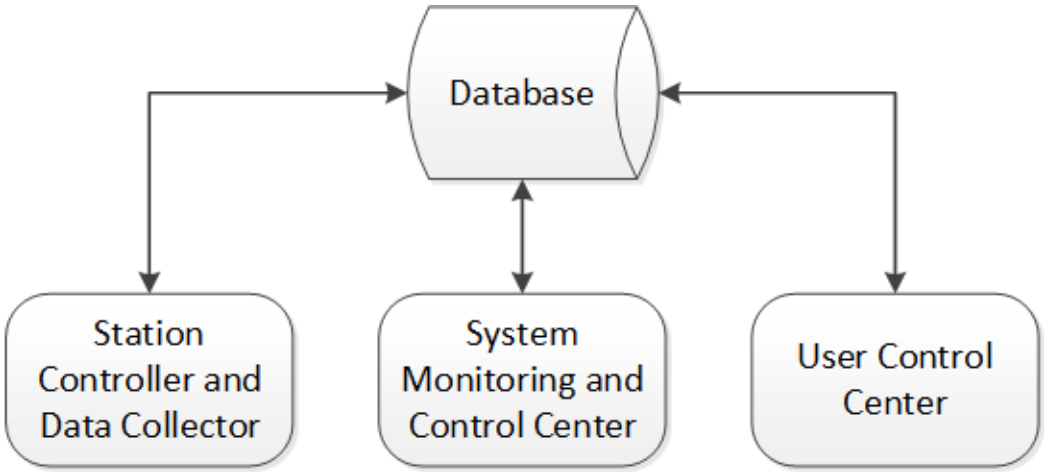

Figure 23. Four Major Components in Smart Charging Infrastructure [49]

The Database stores all data from gateways, stations, charging algorithms, PEV users, parking lots, and cities, including charging status, user charging records and other management information.

The Station Controller and Data Collector send commands to charging stations to control charging operations while accumulating power information. The Station Controller automatically controls the stations using selected charging algorithms, which can be modified and updated to change the controller's functions. While the station controller controls the stations, the data collector periodically collects each station's status.

The System Monitoring and Control Center is designed with multiple purposes as shown in Figure 24. Charging stations can be manually controlled using this interface and monitored by the system administrator, who can also setup and manage the parameters of the stations – the IP address, selection of charging algorithm, power source, etc. – and manage user accounts. The

Monitoring and Control Center also generates reports of power usage and charging records.

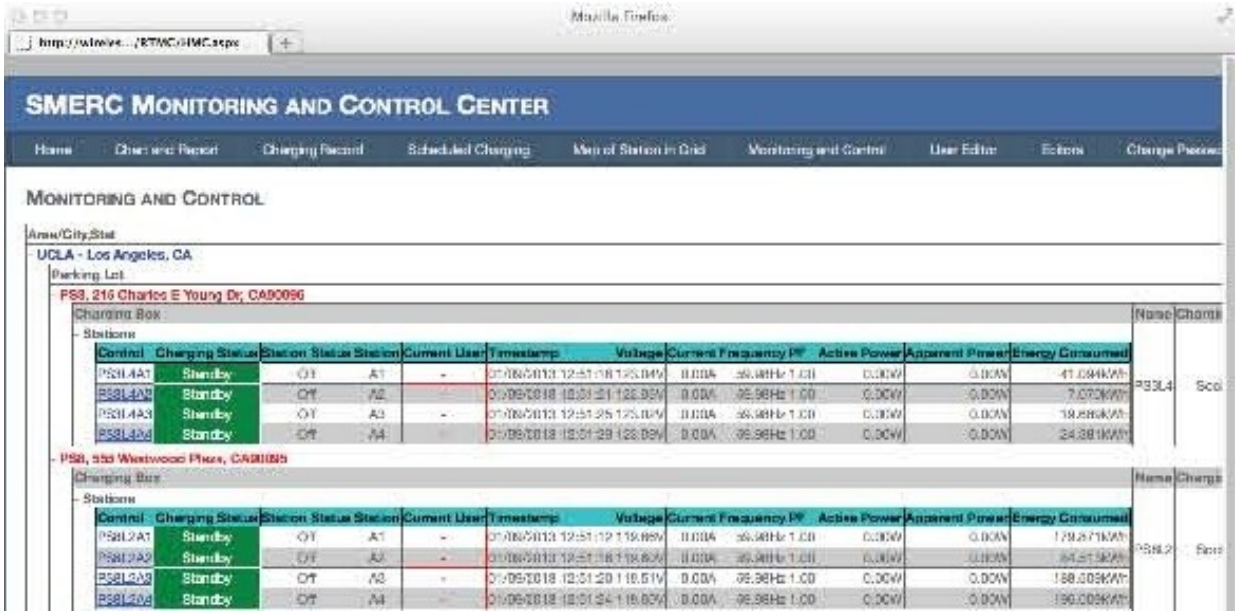

Figure 24. Screen Shot of Monitor and Control Center [49]

The User Control Center allows authorized users to check available charging stations in selected parking lots and cities, start or stop charging, check charging status, view monthly charging records, and manage account information via a mobile device.

3.2 Slave Controller: Local Controller in Level 2 EVSE.

According to charging interface standard SAE J1772 [20], the pilot signal of a Level 2 charging station uses the Pulse Width Modulation (PWM) format. Based on the pilot signal's duty cycle provided by the charging station, a PEV adjusts its load to meet the limitation; thus, using this characteristic of adjustment, a charging station is able to control the charging speed by changing the duty cycle of the pilot signal. We can use the control scheme between the pilot signals and PEV to create a current-sharing algorithm for the Level 2 charging station. Figure 25 shows the relation between the current being supplied and the pilot signal's duty cycle.

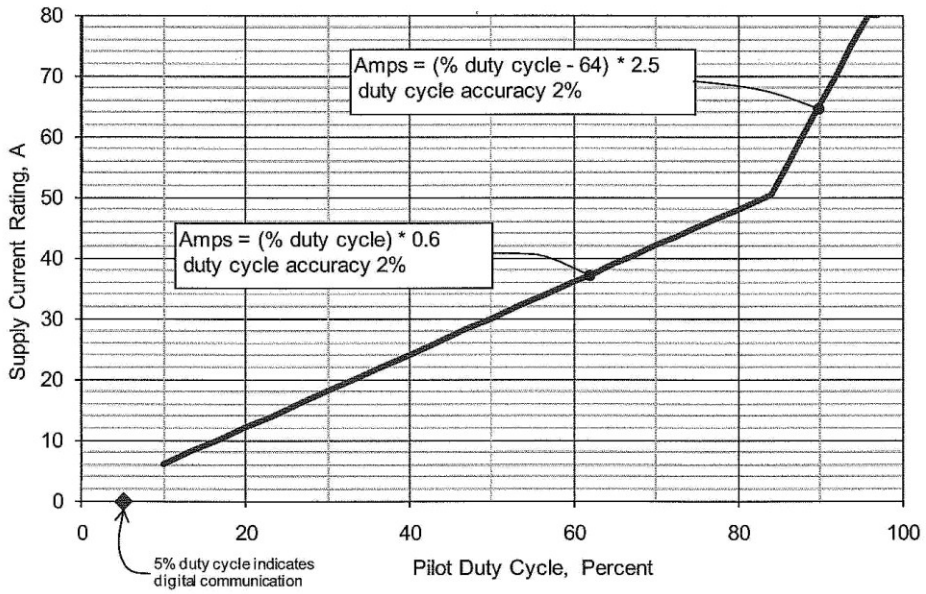

Figure 25. Supply Current vs. Pilot Duty Cycle [20]

The smart Level 2 charging station consists of a charge box with four J1772 plugs that can simultaneously connect to four PEVs. The charging station turns power to the PEV on and off, by controlling relays, and alters the rate of power that each vehicle draws by controlling the pilot signal. The Level 2 station's hardware and firmware are designed and implemented in [56]. Figure 26 shows the first prototype of the 4-outlet smart charging station.

Figure 26. First Prototype of 4-outlet Charging Station [56]

Inside the local (slave) controller, ZigBee-based hardware provides multiple functions including pilot signal generator, pilot signal monitor, safety relay controller, and auto-reset function. Of these functions, the pilot signal generator and monitor play key roles in the charging station's control unit, which uses three microprocessors to fulfill functionality. A prototype control unit, using the CC2530ZNP and Arduino UNO microprocessors, is shown in Figure 27.

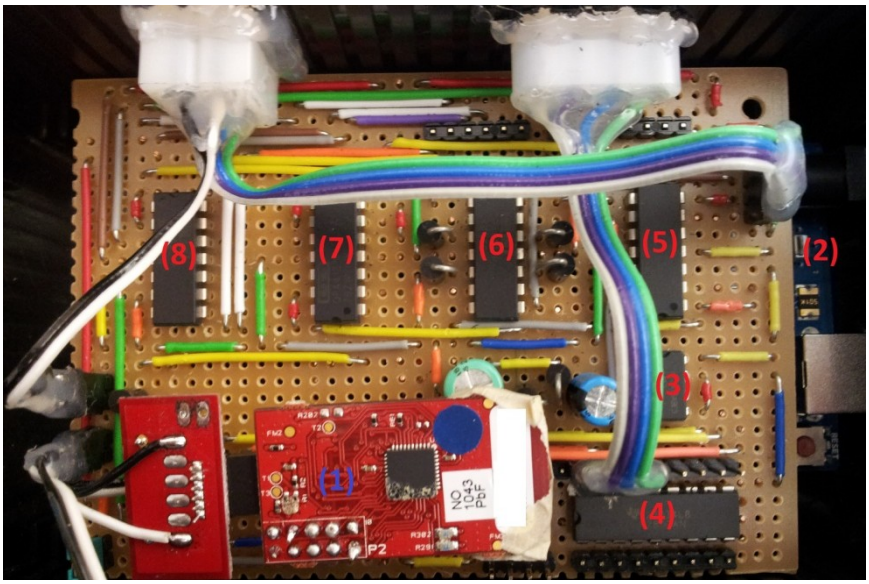

Figure 27. Prototype Controller: (1)Pilot Signal Generator (2)Pilot Signal Monitor (3)555 Counter (4)Relay Driver (5)Schmitt Trigger (6)Unit Gain (7)Inverting Amplifier (8)Inverting LPF [56]

Figure 28 shows the print circuit board (PCB) version of the local controller with surface mount devices (SMD) that is used for mass production purposes.

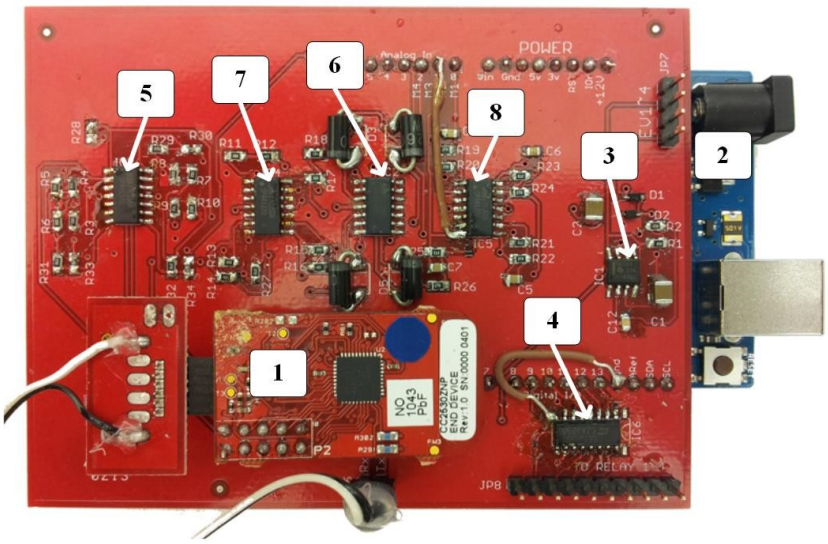

Figure 28. PCB Version Controller: (1)Pilot Signal Generator (2)Pilot Signal Monitor (3)555 Counter (4)Relay Driver (5)Schmitt Trigger (6)Unit Gain (7)Inverting Amplifier (8) Inverting LPF [51]

Figure 29 shows the schematic of the peripheral circuit designed to generate pilot signals with variable duty cycles.

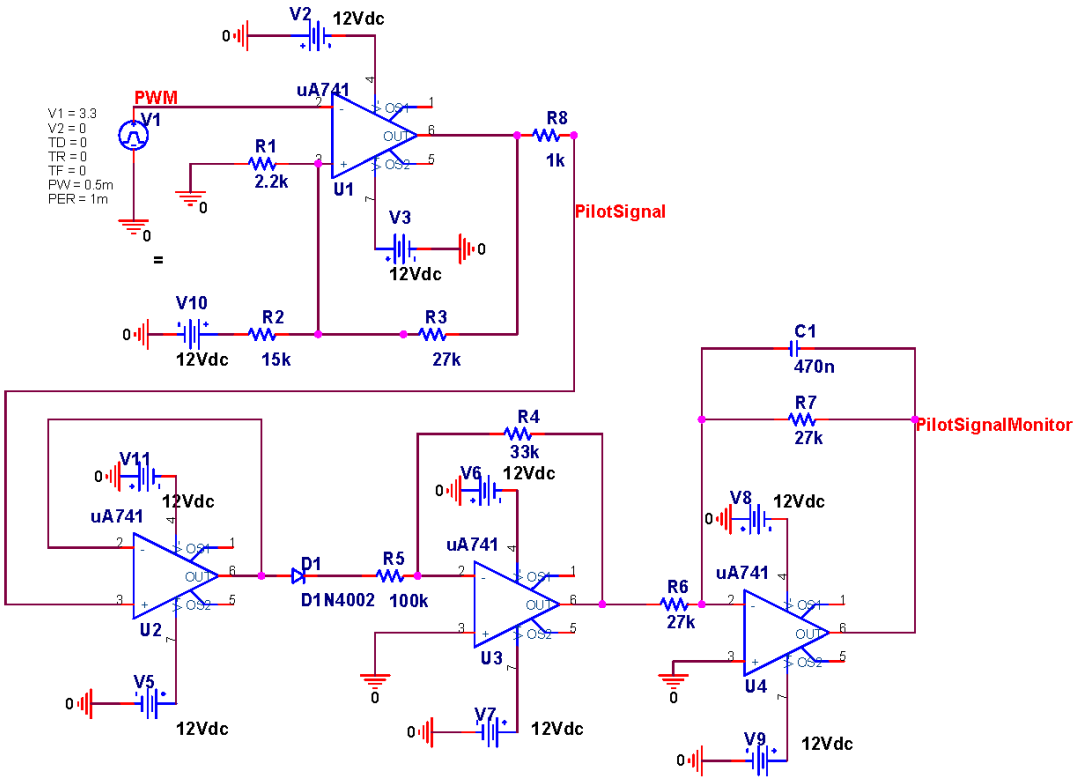

Figure 29. Peripheral Circuit of Pilot Signal Monitor [56]

As seen in Figure 29, the pilot signal generator produces a PWM signal that is amplified, when fed to the PEV, from 3.3V/GND to +/-12V by a Schmitt trigger. Following the Schmitt trigger is the unit gain which isolates the circuit in order to avoid a load effect on the monitoring circuit; note that a Schottky diode is inserted after the unit gain because only the positive part of the signal is monitored. For monitoring purposes, the pilot signal is de-amplified to fall within the A/D converter's range and fed through a low pass filter to produce a DC voltage. We do not use the peak value detection method because it tends to be affected by unexpected spikes producing unreliable measurements. The peripheral circuits are simulated by PSpice as shown in Figure 30.

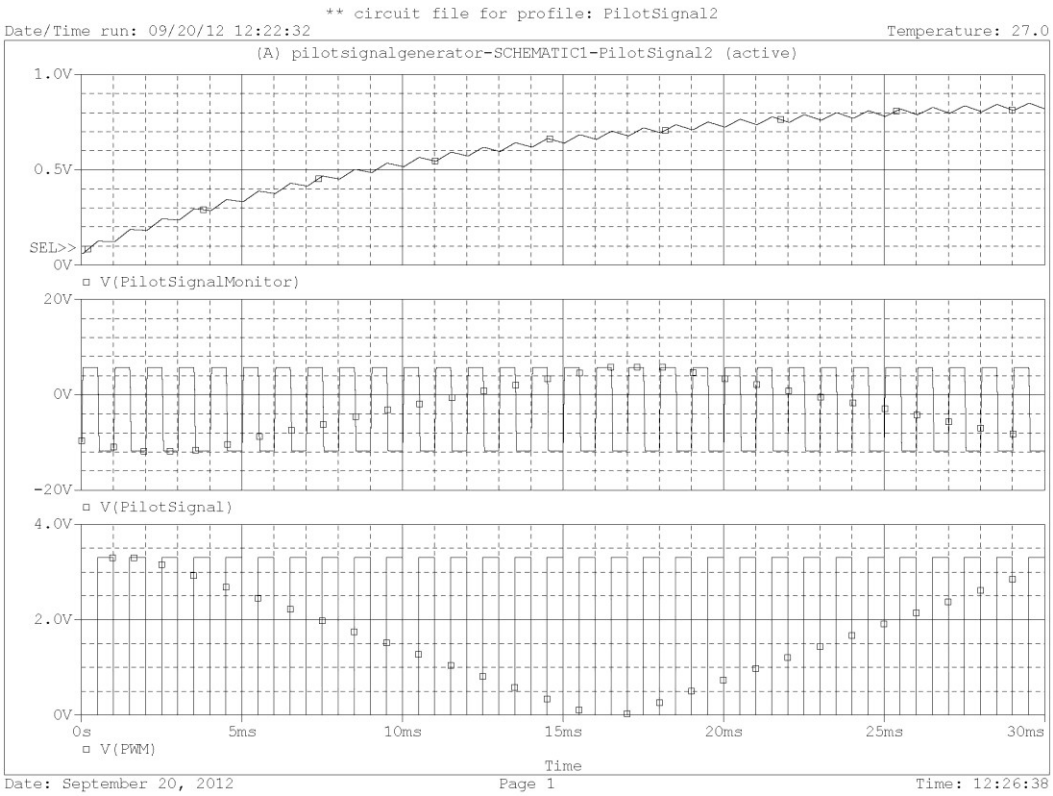

Figure 30. Peripheral Circuit Simulation of Pilot Signal: (From Bottom to Top: (1)PWM from MSP430 (2)Pilot Signal (3)Signal at Monitor End) [56]

The peripheral circuit simulation indicates that to reach a steady state requires a 30 ms duration, which needs to be compensated in the firmware of the pilot signal monitor. The pilot signal generator, which generates four PWM signals, is implemented as a ZigBee end device in the MSP430 of CC2530ZNP. The firmware flow of the MSP430 is shown in Figure 31.

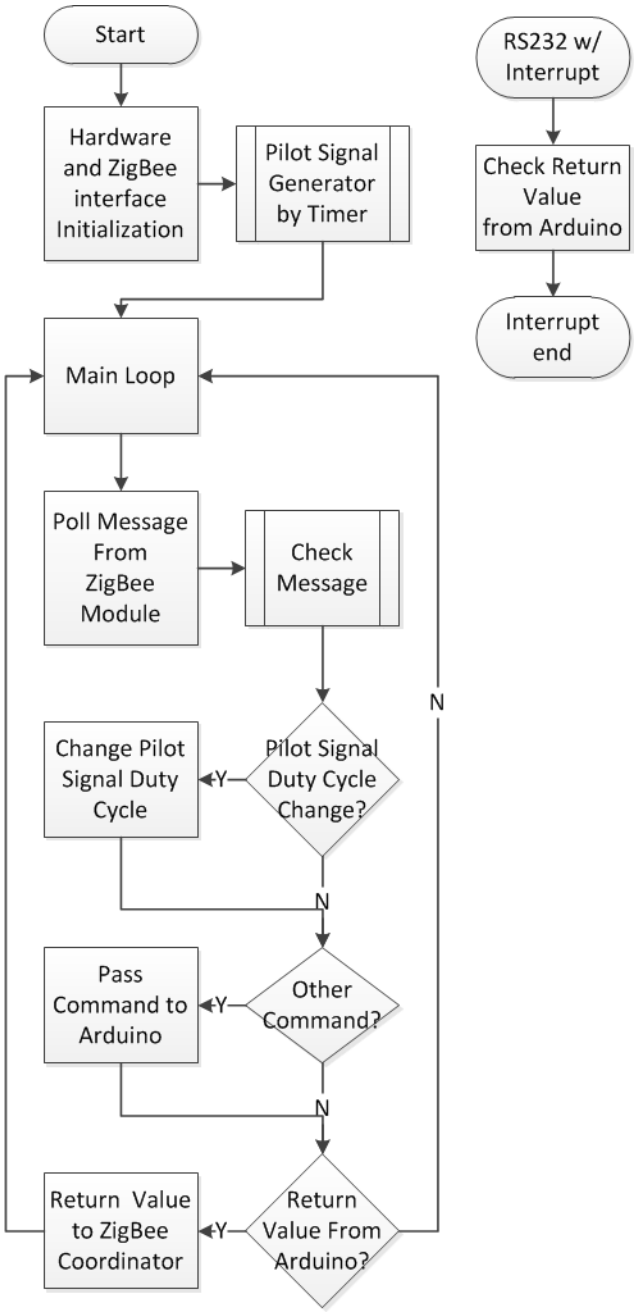

Figure 31. Firmware Flow of MSP430 of CC2530ZNP at the ZigBee End Device (Pilot Signal Generator) [51]

As seen in the firmware flow chart, after the initialization of the hardware and ZigBee interface, two internal timers generate four PWM signals during the startup process. Messages from the CC2530 ZigBee chip are then checked in the main loop. The duty cycle of the PWM changes when receiving the command from the server. Other commands are passed to the Arduino UNO processor.

The aggregate charging server must identify the presence of a PEV at a charging station and associate the vehicle's ID with a specific charge point using the PEV plug-in status. This status is monitored by a pilot signal circuit by detecting pilot signal voltage levels set by the PEV. According to J1772 specification [20], a charging station detects the PEV plug-in status using a generated pilot signal with a duty cycle based on the power capacity of the station. The voltage of the pilot signal pin varies depending on the presence of a PEV; when there is no PEV connected, the voltage should be DC +12V; a connected PEV changes the voltage to +9V or +6V, depending on whether the PEV is ready to accept energy or not. When the PEV is fully charged, the positive part of the pilot signal varies from +6V to +9V; the voltage changes from +6V to +12V when the PEV is unplugged. Figure 32 shows the firmware of the pilot signal monitor.

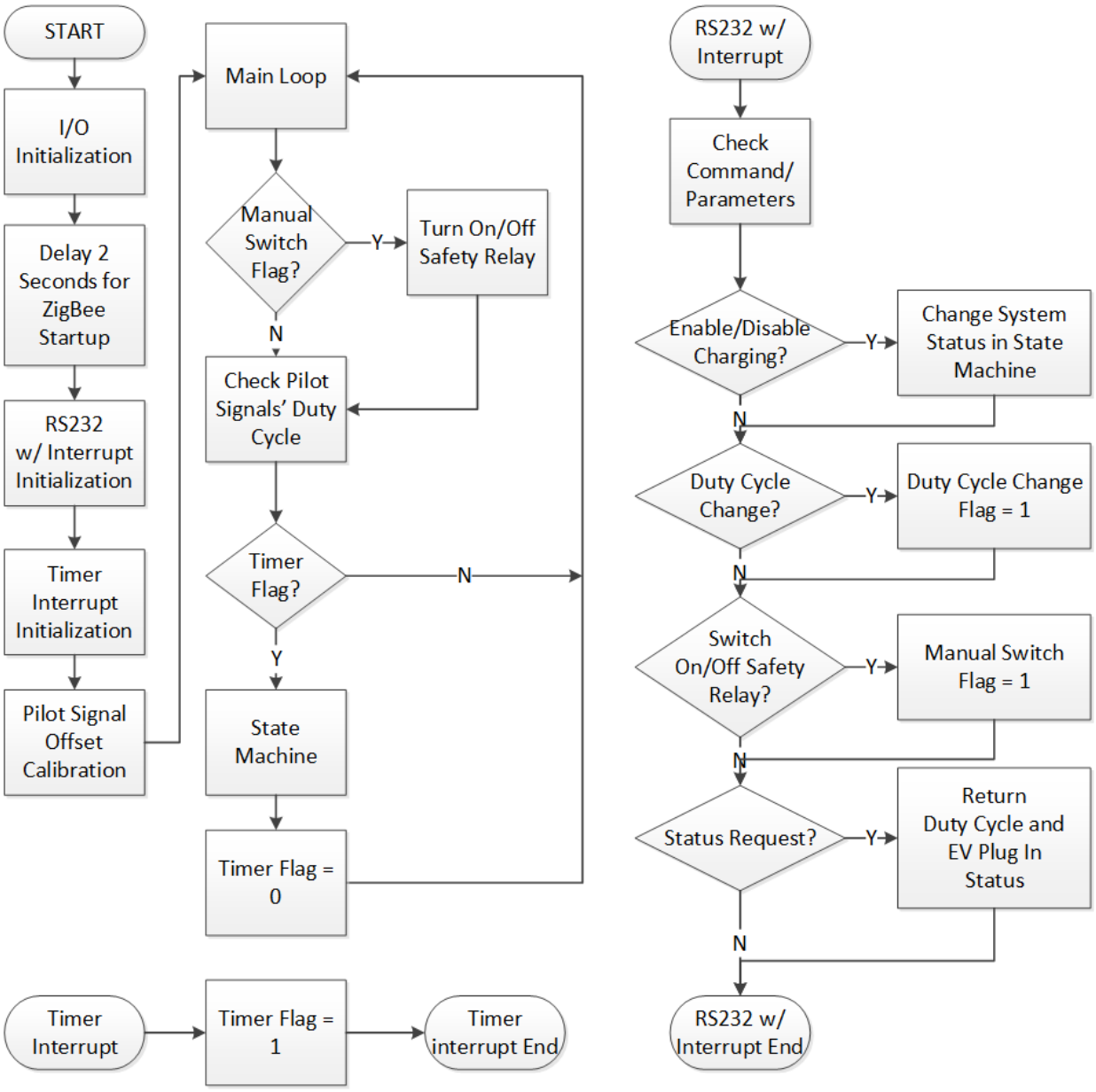

Figure 32. Firmware Flow Chart of Pilot Signal Monitor [56]

The pilot signal monitor features two interrupt loops, RS232 and a timer interrupt. The interrupt loop of the RS232 handles messages from the MSP430, so they are not missed while executing other processes in the main loop. Actions such as commands are also handled by the RS232 routine including check, flag set, and message return; however, most actions are processed in the main loop according to flags. The timer interrupt ensures that routine services, such as checking for PEV existence and turning the safety relay on/off, have exact intervals;

moreover, the service's interval can be changed remotely without re-flashing the firmware, which makes the service more flexible. The timer interrupt's only function is to set the timer flag; handling services in this routine would increase the loop's processing time which may break the timer interrupt if an RS232 command arrives at the same time. Most errors are caused by this unexpected firmware flow, so the time of the timer interrupt routine should be kept as small as possible. This kind of event-triggered firmware structure adds flexibility to services, because the firmware handles services according to the flags in the main loop.

Before the aggregate server is notified of the PEV status change, the firmware-based state machine in the pilot signal monitor executes detection of PEV plug-in status. Detection of plug-in status is handled with the Timer Flag, which is set to 1 in the timer interrupt loop; the flag is set to 0 after the detection process finishes. Currently, the interval of the timer interrupt is 1 second in the firmware, which means the detection process is handled every 1 second; note that the detection process time needs to be less than the interval of the timer interrupt so the detection process can be handled correctly. The RS232 internal interrupt and timer interrupt are initialized at the startup process. Afterward, the pilot signal offset is calibrated before the PEV detection. During startup, a delay of two seconds before the initialization of a serial connection is required to wait for the CC2530 startup. Figure 33 shows the firmware flow of the state machine.

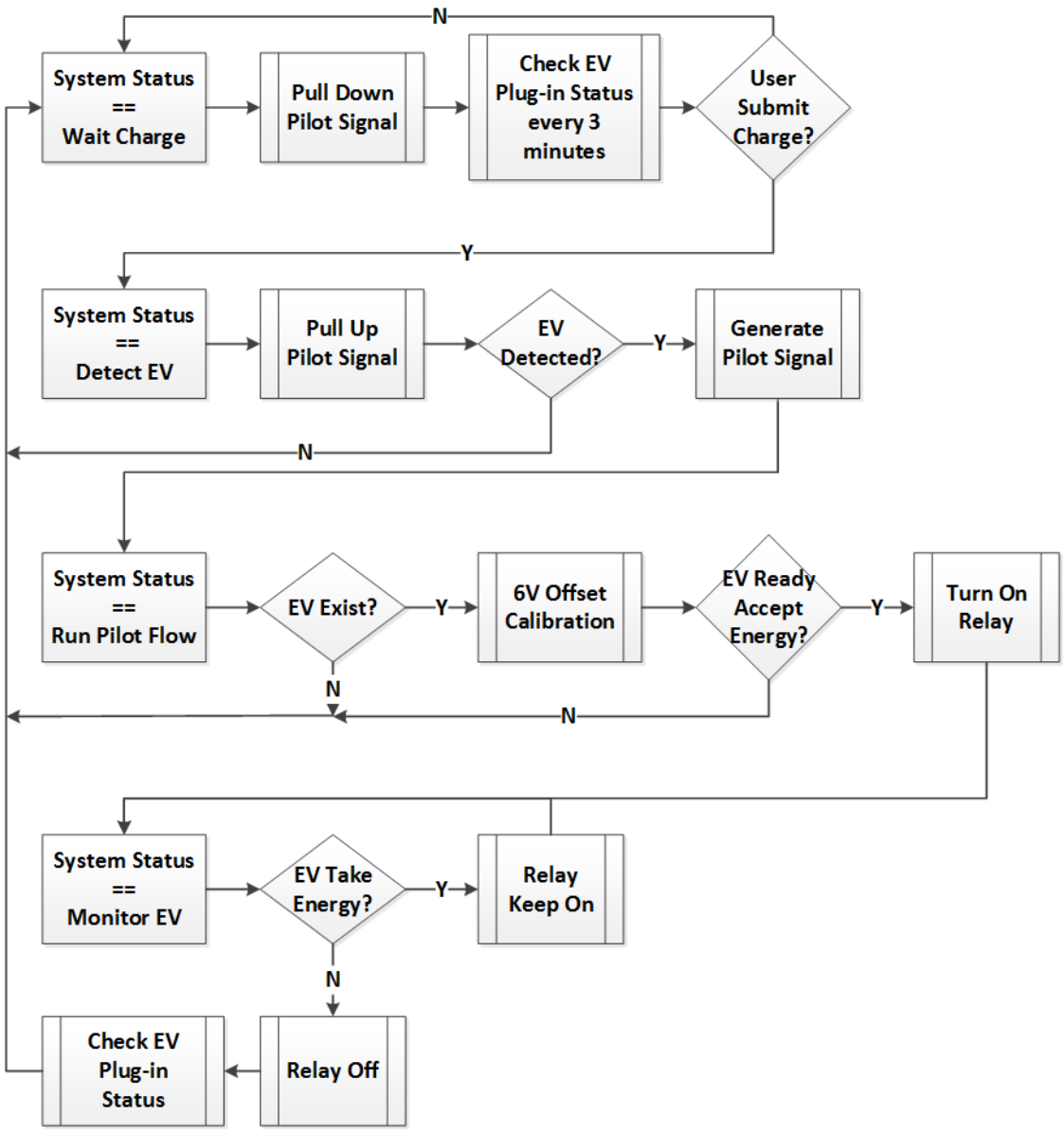

Figure 33. State Machine Flow Chart [56]

In current practice, the ZigBee function on the local controller is a redundant communication channel between charging stations except for communicating with VMMs. Each charging station has a gateway supporting multiple protocols, so information exchange between stations can be fulfilled by WiFi or Ethernet. A simplified design with enhanced features and functionalities requires a more powerful microprocessor; the ATMega2560 microprocessor has more input and output pins (I/Os), as shown in Figure 34.

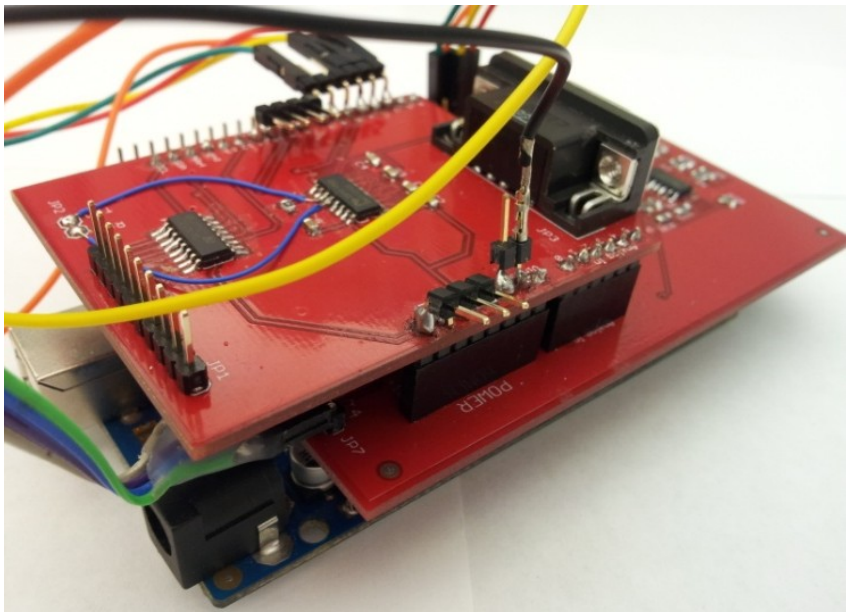

Figure 34. Simplified J1772 EVSE Controller without ZigBee Function

Pilot signals are generated by the internal timer and monitored by the analog input pins of the ATMega2560. Only one microprocessor is used in this design to fulfill the aforementioned functionalities, except ZigBee communication. In addition to monitoring capabilities, the circuit shown in Figure 34 generates a pilot signal with variable duty cycles that indicates available current to the PEV, per the J1772 specification.

To involve smart charging algorithms at the server level, the server can select or disable local charging algorithms embedded in the local controller's firmware. Three major operational flows at the server level need to be engaged regardless of where the charging algorithm resides: Enable Charging, Disable Charging, and Pilot Signal Duty Cycle Change. As shown in Figure 35, each operational flow has three sub-processes: Read Meter On/Off Status, Read Meter's Power Information, and Read Outlet's Status. The power information includes the voltage, current, and active power; the outlet's status includes pilot signal's duty cycle, safety relay on/off status, PEV plug-in status, and firmware-based state machine's stage.

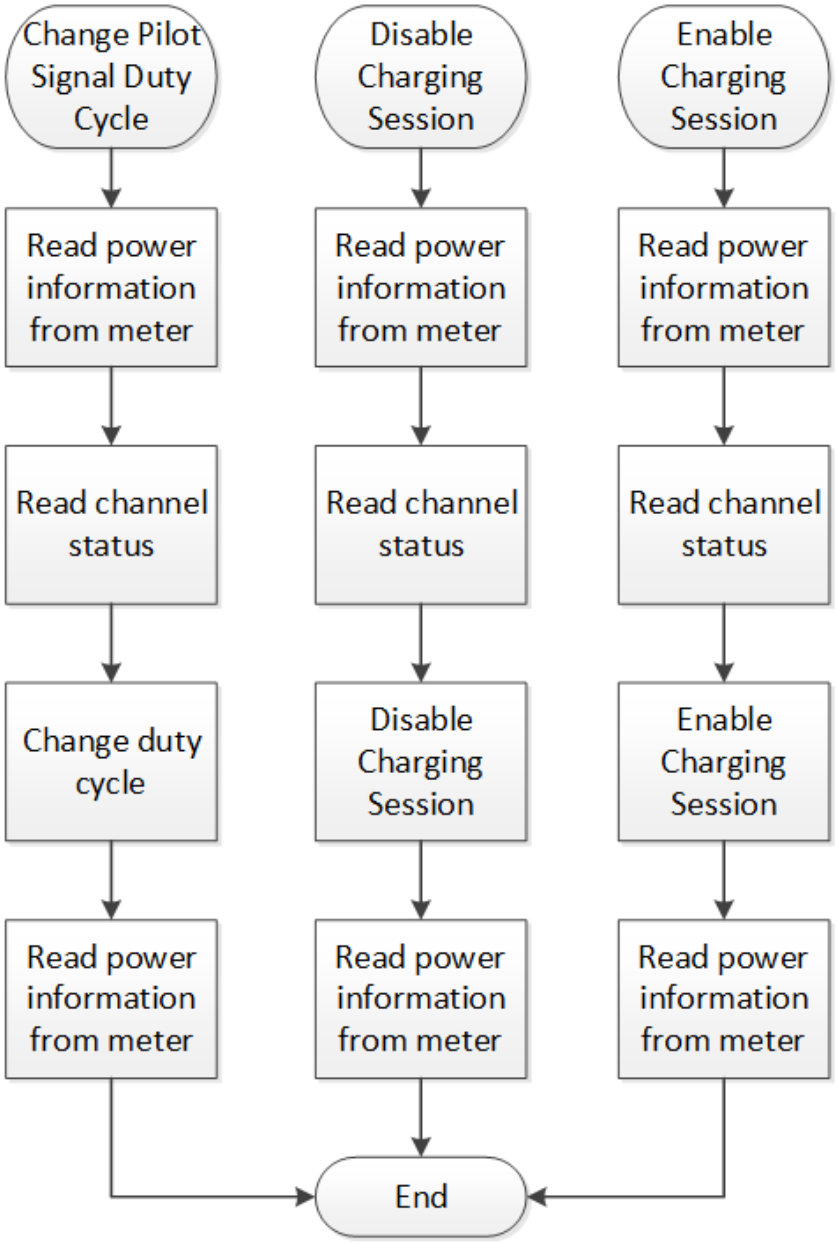

Figure 35. Server Operation Flow [56]

In the Enable Charging routine of the server operation flow, the server sends a command to change the pilot signal duty cycle and turn on the safety relay and meter. Afterward, the server waits $T_{waiting}$ seconds and sends a command to read power information. In the Disable Charging routine, the server resets the pilot signal duty cycle after turning off the meter and the safety relay. For the routine Change Pilot Signal Duty during Charging, the server changes the duty

cycle of the pilot signal and reads power information after waiting $T_{waiting}$ seconds. Commands sent to the charging station use the following format: **comd [command] [channel] [parameter]**

The description of the commands and return values of the charging station are summarized in **TABLE** 5.

TABLE 5. COMMAND AND RETURN VALUES OF THE CHARGING STATION

Command	Description	Example
atrs	Auto-reset the whole system, including gateway, meters, relays, and control unit	comdatrs0000 [return]: N/A
duty	Change the duty cycle	comdduty0150 [describe]:change channel 1 duty cycle to 50% *duty cycle: 10~85 (6A~51A) [current=duty cycle*0.6] 86~96 (55A~80A) [current=(duty cycle-64)*2.5] [return]: duty0150rely0100plug0101stat0100
enab	Enable PEV charging	comdenab0100 [describe]: enable channel 1 [return]: duty0125rely0100plug0101stat0100
rely	Turn on/off the relay manually	Ex1: comdrely0101 [describe]: turn on relay at channel 1 [return]: duty0150rely0101plug0101stat0100 Ex2: comdrely0100 [describe]: turn off relay at channel 1 [return]: duty0150rely0100plug0101stat0100
Rest	Disable PEV charging	comdrest0100 [describe]: disable channel 1 [return]: duty0100rely0100plug0101stat0100
Stat	System statue request	Ex1: comdstat0100 [describe]: request channel 1 status [return]: duty0150rely0101plug0101stat0100 Ex2: comdstat9900 [describe]: request all channels status [return]: duty0050rely0000plug0000stat0000 duty0150rely0100plug0100stat0100 duty0250rely0200plug0200stat0200 duty0350rely0300plug0300stat0300

Because the control scheme is server-based, the server will need to wait $T_{waiting}$ to account for the communication delay and response time of the charging station and PEV.

3.3 Slave Controller: Solutions for Simple Commercial Level 2 EVSE

The smart charging infrastructure can be achieved by installing the metering system on simple charging stations, like those from Leviton, ClipperCreek, and Schneider, so they can be directly controlled by switching type algorithms – such as round-robin and fair charging algorithm – run on the server.

There are two types of simple, off-the-shelf, commercial charging stations with or without dedicated current switching options: Dedicated Current Switching and Variable Current Controlling. In the current switching method, the commercial charging station provides terminals inside the charging station for the installer to throttle the current. Stations without the switching current option can be added to the WINSmartEV^{TM} infrastructure using a controller with Variable Current Control. Details of these two types of controllers are described in the following subsections.

3.3.1 Current Switching Method

As previously mentioned in the Current Switching case, the installer can use terminals inside commercial charging stations to throttle the current. For example, the output current of ClipperCreek CS-40 model can be changed based on terminal connections as described in [64]. Changing connections between terminals permit selecting three stages of current: 30A, 6A, and 0A. Switching current on multiple charging stations in a locale has a communication cost, which can be reduced using a ZigBee mesh network solution with relays implemented. Figure 36 and Figure 37 show the implementation of these two types of controllers using Texas Instrument CC2530ZNP.

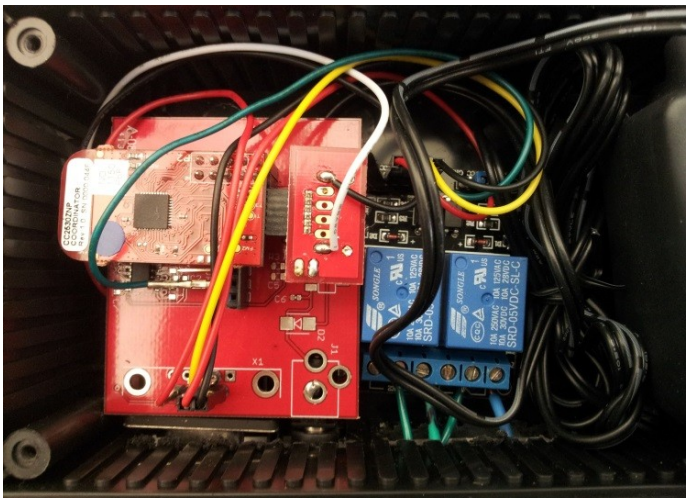

Figure 36. ZigBee Coordinator Type Controller

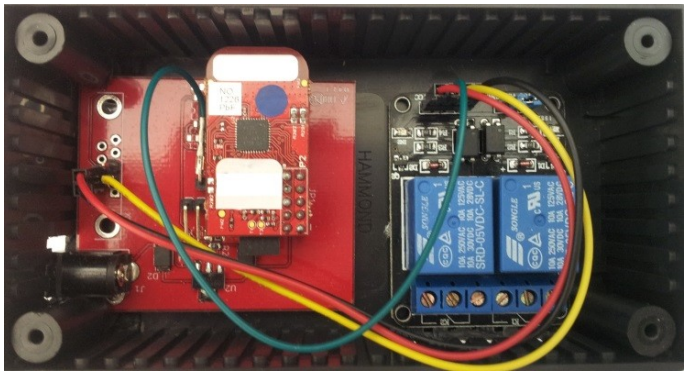

Figure 37. ZigBee Router Type Controller

Both controllers switch relays on and off to control the connection of the terminals inside the charging stations upon receiving the command from the server to change the output current.

In order to send commands to the corresponding controllers, the ZigBee coordinator must associate the routers' unique MAC addresses and their dynamic IDs. The MAC addresses on server commands are used by the coordinator to look up corresponding dynamic IDs on the joining list of routers to pass commands to the appropriate routers. To ensure a robust network connection with each ZigBee device, the coordinator and routers use a handshake protocol. Figure 38 and Figure 39 show the firmware flow of the ZigBee coordinator and the ZigBee router in the MSP430 of CC2530ZNP.

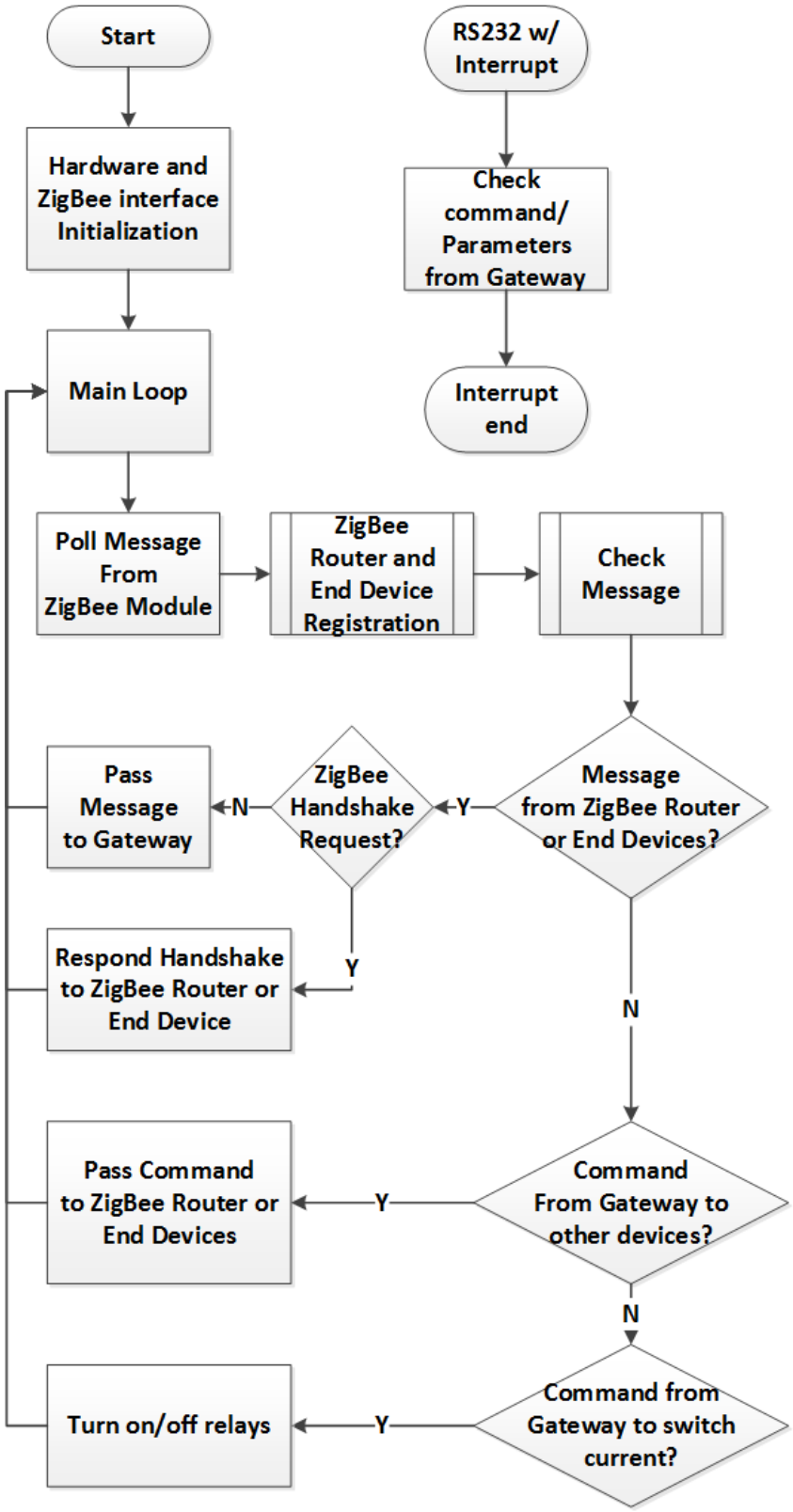

Figure 38. ZigBee Coordinator's Firmware Flow [51]

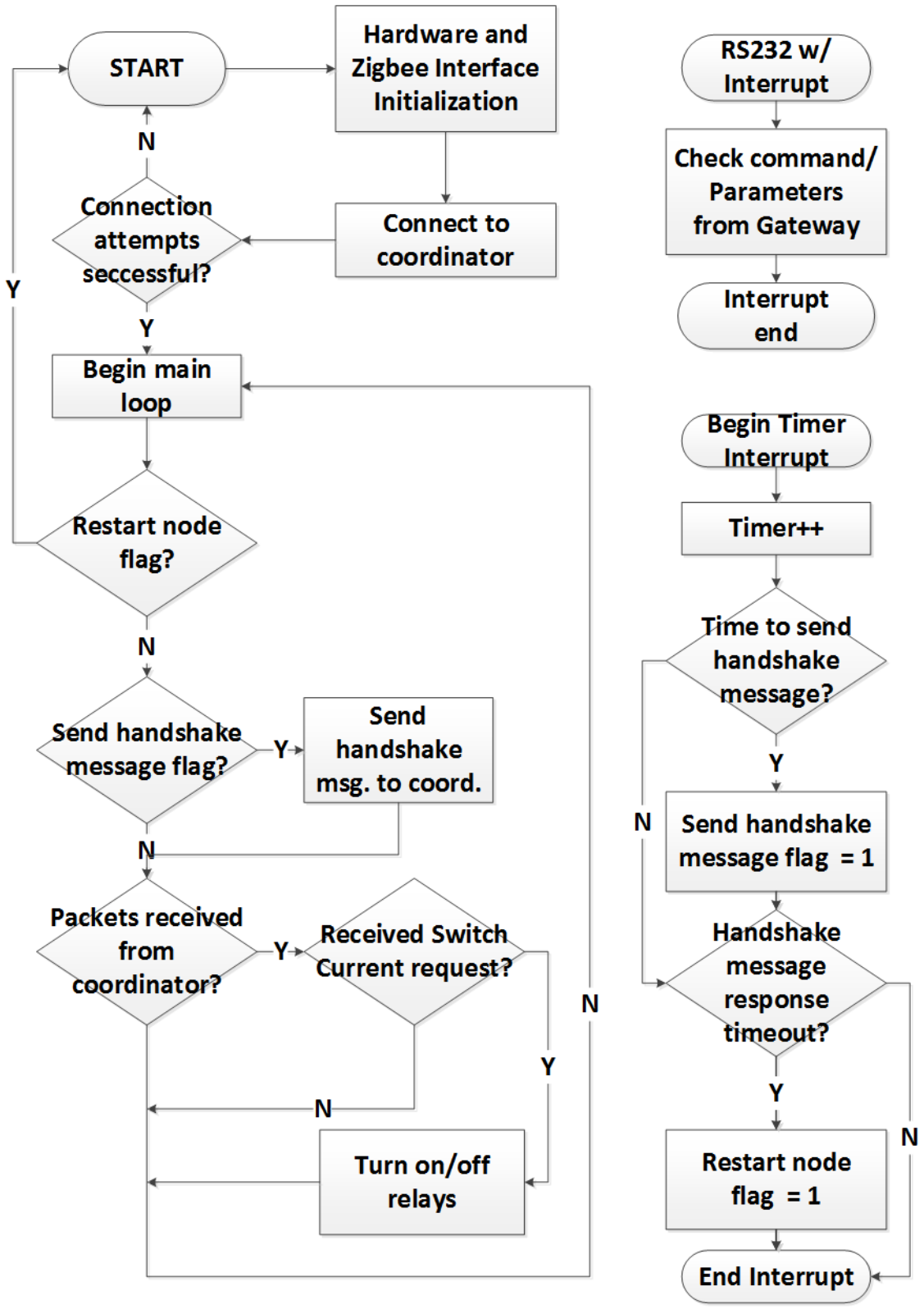

Figure 39. ZigBee Router's Firmware Flow [51]

The control box houses a gateway, meter, and controller as shown in Figure 40.

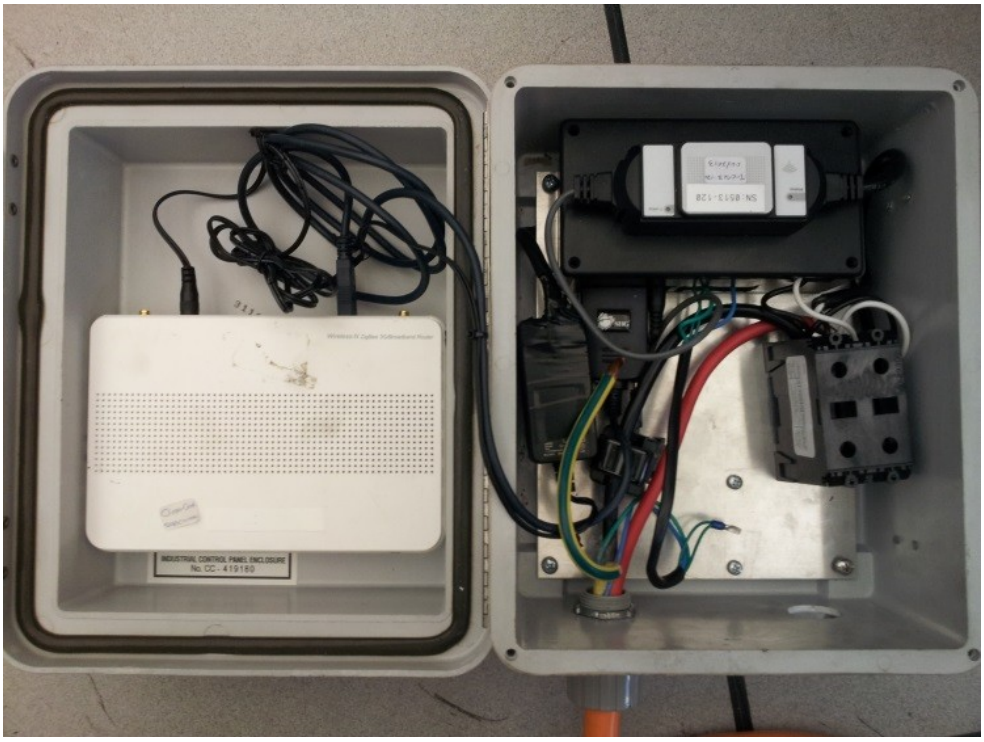

Figure 40. Control Box for ClipperCreek Charging Station

Figure 41 shows a controller box installed on a ClipperCreek charging station.

Figure 41. Installation of a smart ClipperCreek Charging station

3.3.2 Variable Current Control Method

Simple commercial charging stations without the switching current option can join the WINSmartEV^{TM} infrastructure using a controller with Variable Current Control. To implement a variable current control on these stations, without violating GFCI safety requirements, requires an extra circuit because simple charging stations incorporate the J1772 standard, which requires them to control relays and the duty cycle of the pilot signal when connected to a PEV; the relays are used to turn the PEV on and off and the duty cycle rates the power that the PEV draws. Therefore, to respond to server commands, the circuit must emulate the behavior of a PEV and generate a pilot signal with variable duty cycle, as shown in Figure 42.

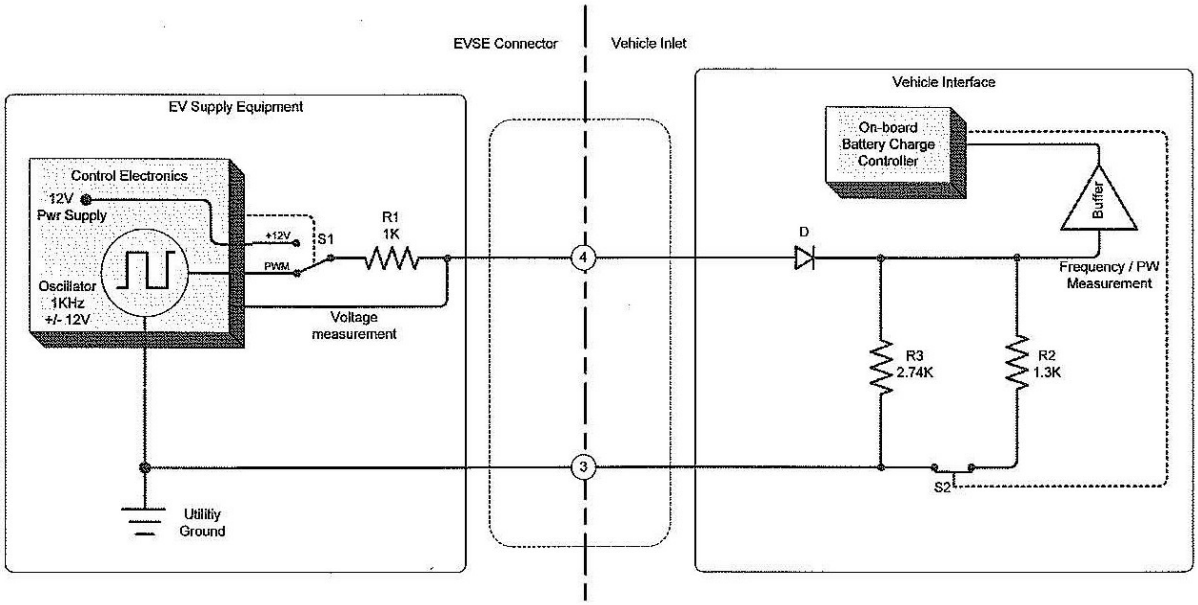

Figure 42. Pilot Signal Connection in J1772 Standard [20]

Figure 43 shows the implementation of the Variable Current Control type of controller.

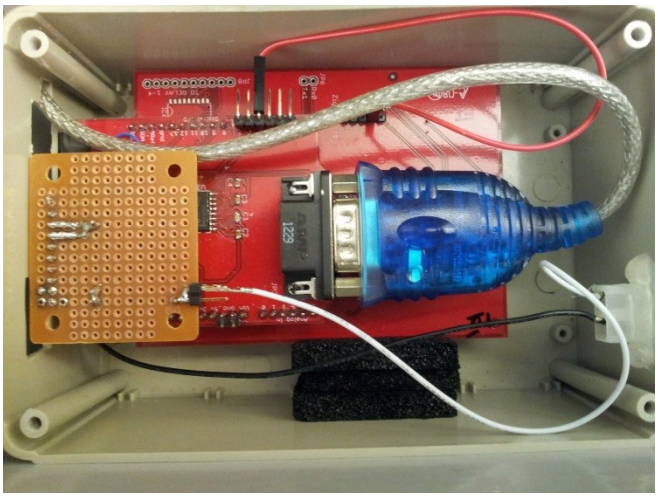

Figure 43. Variable Current Control Type of Controller

Unlike the Current Switching Method, the interface between the charging station and the PEV is the controller, which consists of two components: Pilot Signal Generator/Monitor and PEV emulator. The Pilot Signal Generator/Monitor generates the pilot signal for the PEV, while the PEV Emulator emulates the PEV's response to the original pilot signal generated by the commercial charging station; the emulator consists of a diode, two resistors, and two Darlington transistors acting as the switch. Figure 44 shows the schematic of the PEV emulator and Figure 45 shows the state machine flow.

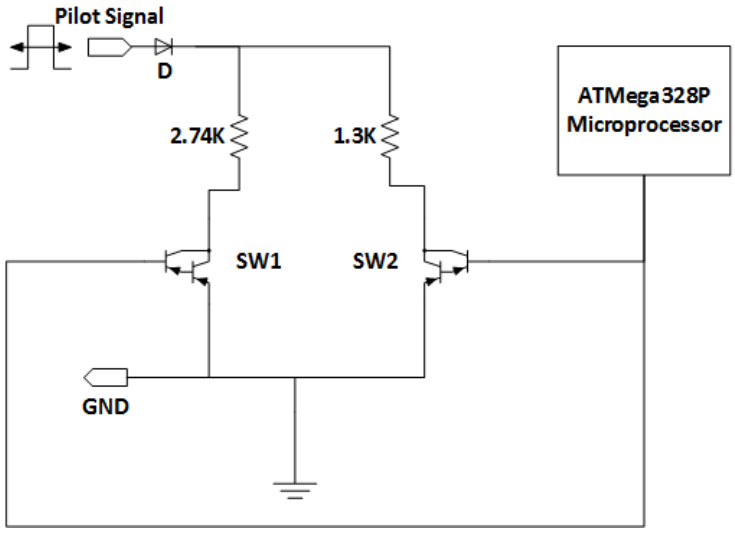

Figure 44. Schematics of PEV Emulator

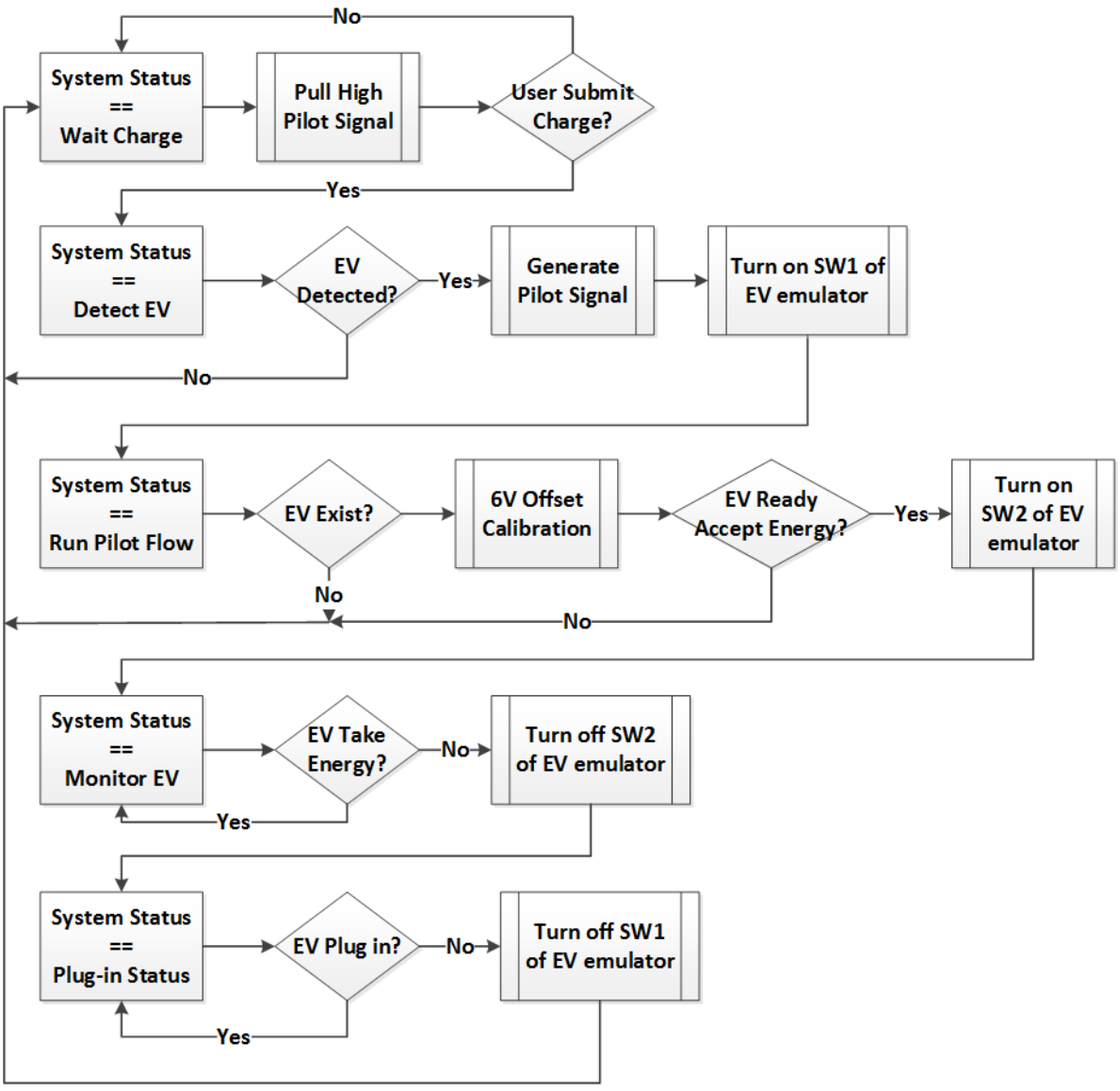

Figure 45. State Machine Flow in the Firmware

Similarly to the previous Current Switching controller type, the Variable Current Controller also comprises a gateway, meter, and control unit as shown in Figure 46.

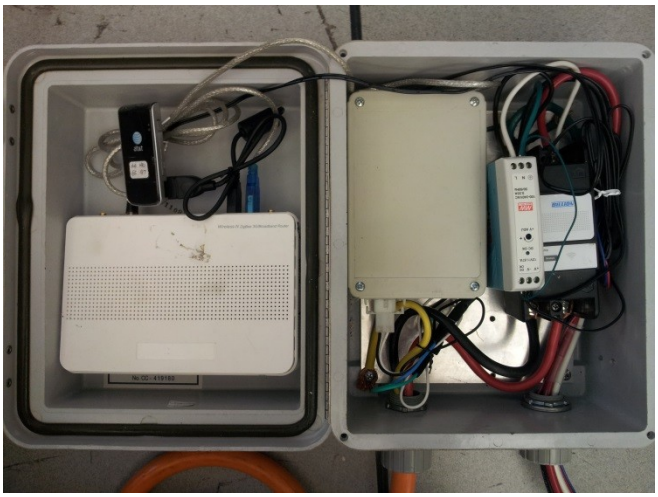

Figure 46. Control Box for Schneider Charging Station

As we see, by adding an additional controller, a commercial charging station can join the WINSmartEV^{TM} PEV charging infrastructure with the capability to remotely monitor and control variable currents. Figure 47 shows the implementation of the control box, and Figure 48 shows a demonstration with a Nissan Leaf.

Figure 47. Implementation of smart Schneider Charging Station

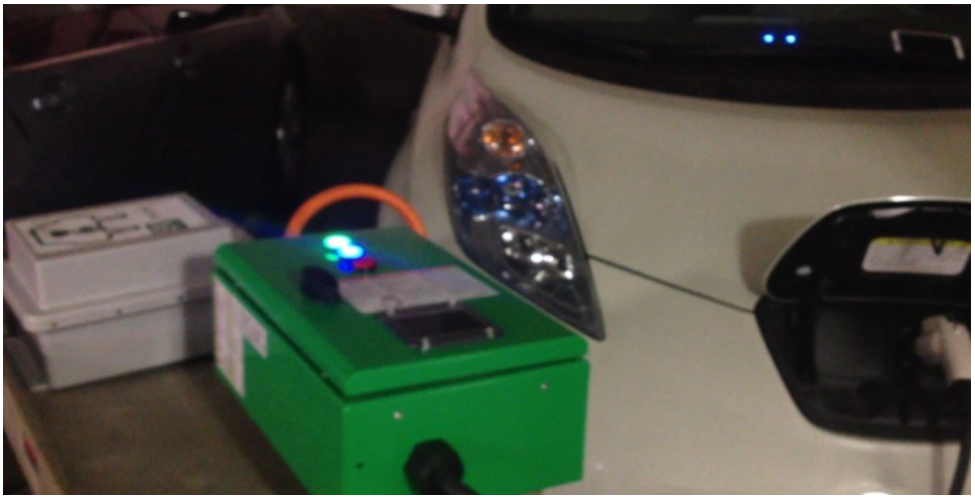

Figure 48. Demonstration with a Nissan Leaf

The metering system only requires a gateway and a meter as shown in Figure 49.

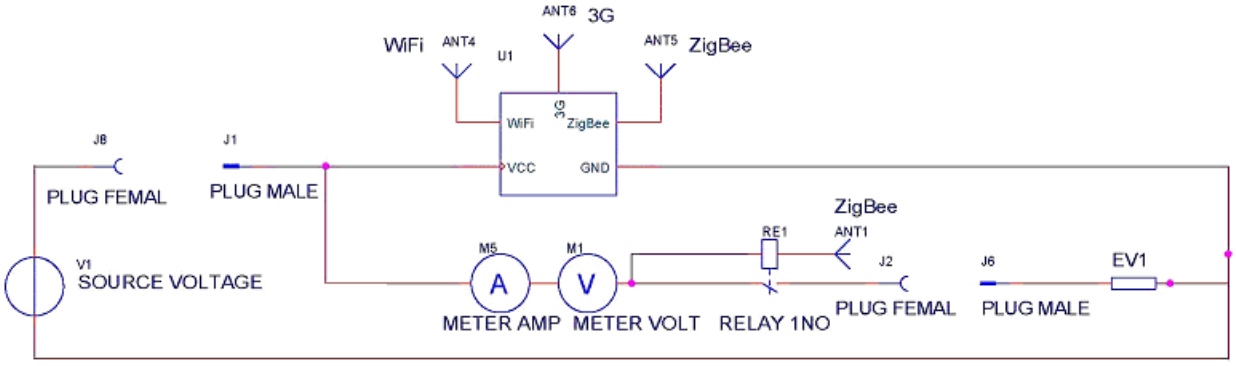

Figure 49. Schematics of the Metering System

3.4 Slave Controller: Local controller in Level 1 EVSE

The Level 1 charger controls four EVSmartPlug™ outlets to provide power to PEVs. Because a PEV's trickle charging cable is plugged into the outlet for charging, the control system only switches the outlet on and off to control the 120V power transfer. The metering system executes the relay on/off commands from the server, in current Level 1 charging practice, to turn on/off the meter and control the power to the outlet; thus, there is no actual local controller inside the charging station.

Station control occurs using smart scheduling algorithms; a round-robin algorithm allocates a

single 120V power source with four PEVs by turning on 1 outlet and charging 1 PEV at a time.

When a power information request using the data pull method is sent from the server to a charging station, the signal must pass through the Internet and 3G network before it reaches the station's gateway. The gateway relays the power information command to the specific meter, and when the gateway receives a reply from the meter, it relays the response back to the server where the information travels back in reverse order. With multiple meters requiring multiple requests each, the aggregated round trip times cause slow performance.

In order to enhance the system's performance and shorten the response time of the system, a Power Information Collector (PIC) [60] gathers power information locally and periodically sends it to the control center in one packet.

For the server to obtain data from the meters in the existing system, each request must pass through multiple stages before the information is returned. Requests begin as HTTP commands sent by the server over the Internet and through the 3G network before reaching the gateway. The gateway then relays the commands through the Zigbee mesh network to the meters; each response travels the same path in reverse direction. Because 2 sets of data, power information and ON/OFF status, are required in each meter update, two commands are needed to update each meter; with four meters in each charging station, eight HTTP commands are required to update the data for one charger.

In order to change eight requests to one request for each status update, thereby cutting the time by a factor of 8, the PIC acts as a local data collector. This PIC collects and compiles a comprehensive list of information on a 4-outlet charging station and sends it to the server upon receipt of a single request, which significantly reduces 3G traffic. Because the collector will connect directly to the gateway, the HTTP request never has to pass through the ZigBee mesh

network, which further reduces the response time; the response time for this one request is shorter than the response time for each of the eight requests through the mesh network. In addition, the data collector can cycle its updates quickly, which makes the information received by the control server always up to date. The smart charging station with PIC is shown in Figure 50.

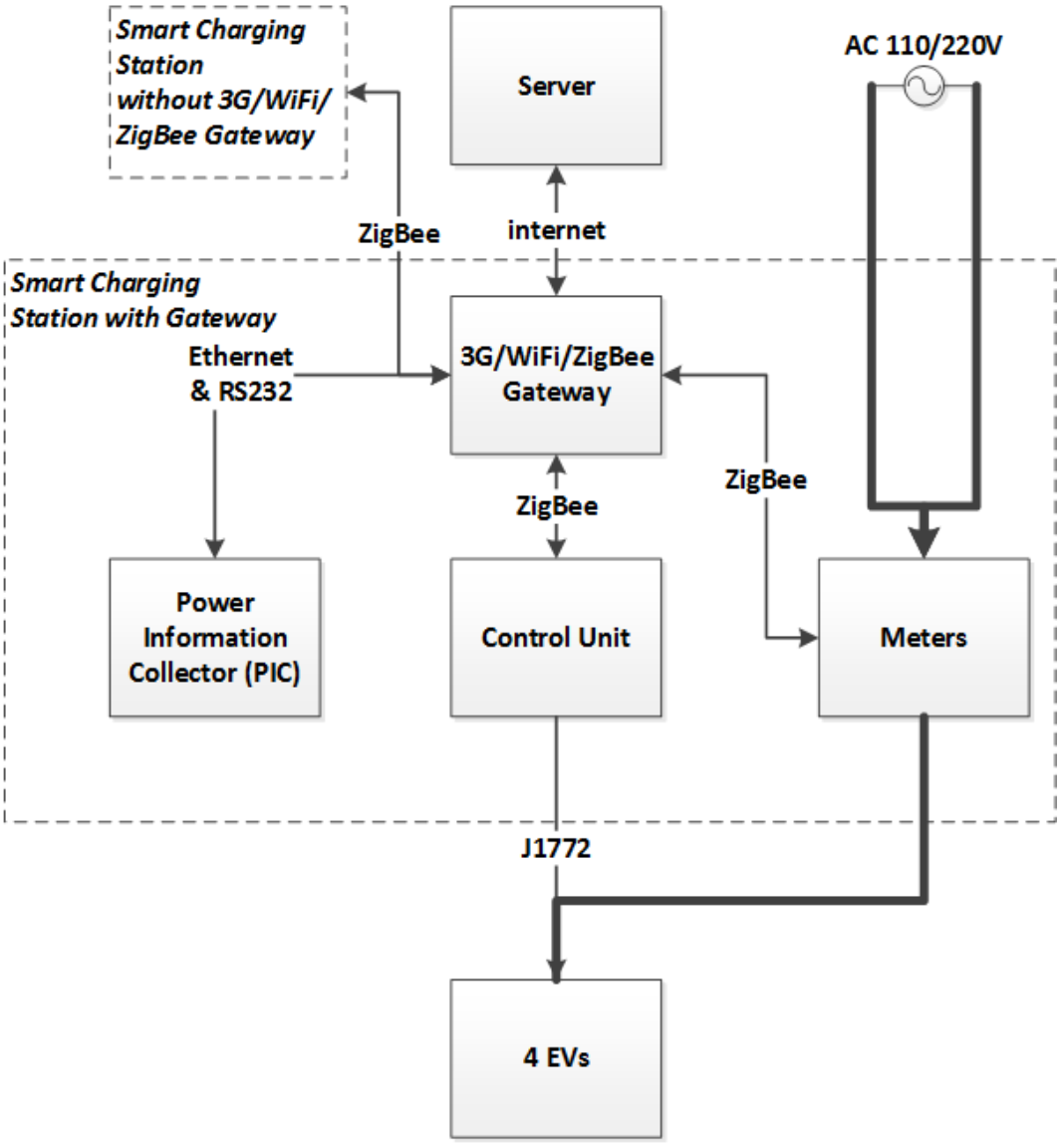

Figure 50. Smart Charging Station with PIC [60]

Figure 51 shows the schematic of the PIC and the connection between the PIC and gateway.

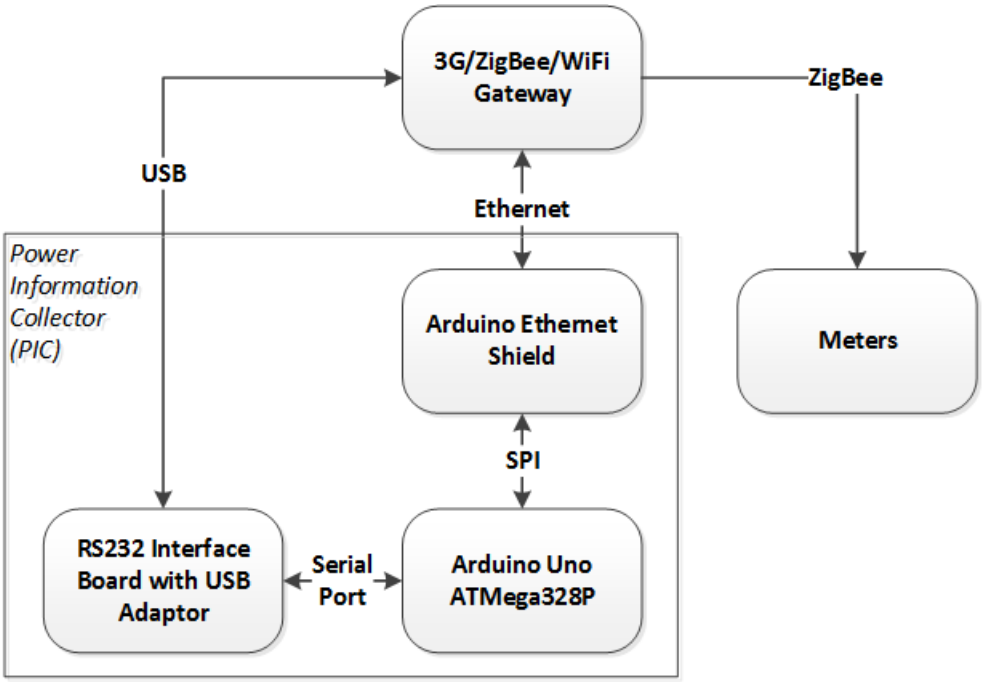

Figure 51. Schematic of PIC [60]

The PIC consists of an Arduino UNO board with an ATMega328P microprocessor, an Arduino Ethernet Shield, and a RS232 serial port interface board. The RS232 serial port interface board and the Arduino Ethernet Shield are wired to the gateway for communication. The RS232 serial port communicates between the server and the PIC, while the Ethernet port retrieves the power information and On/Off status of the meters. Figure 52 shows the firmware flow on the ATMega328P microprocessor of the PIC.

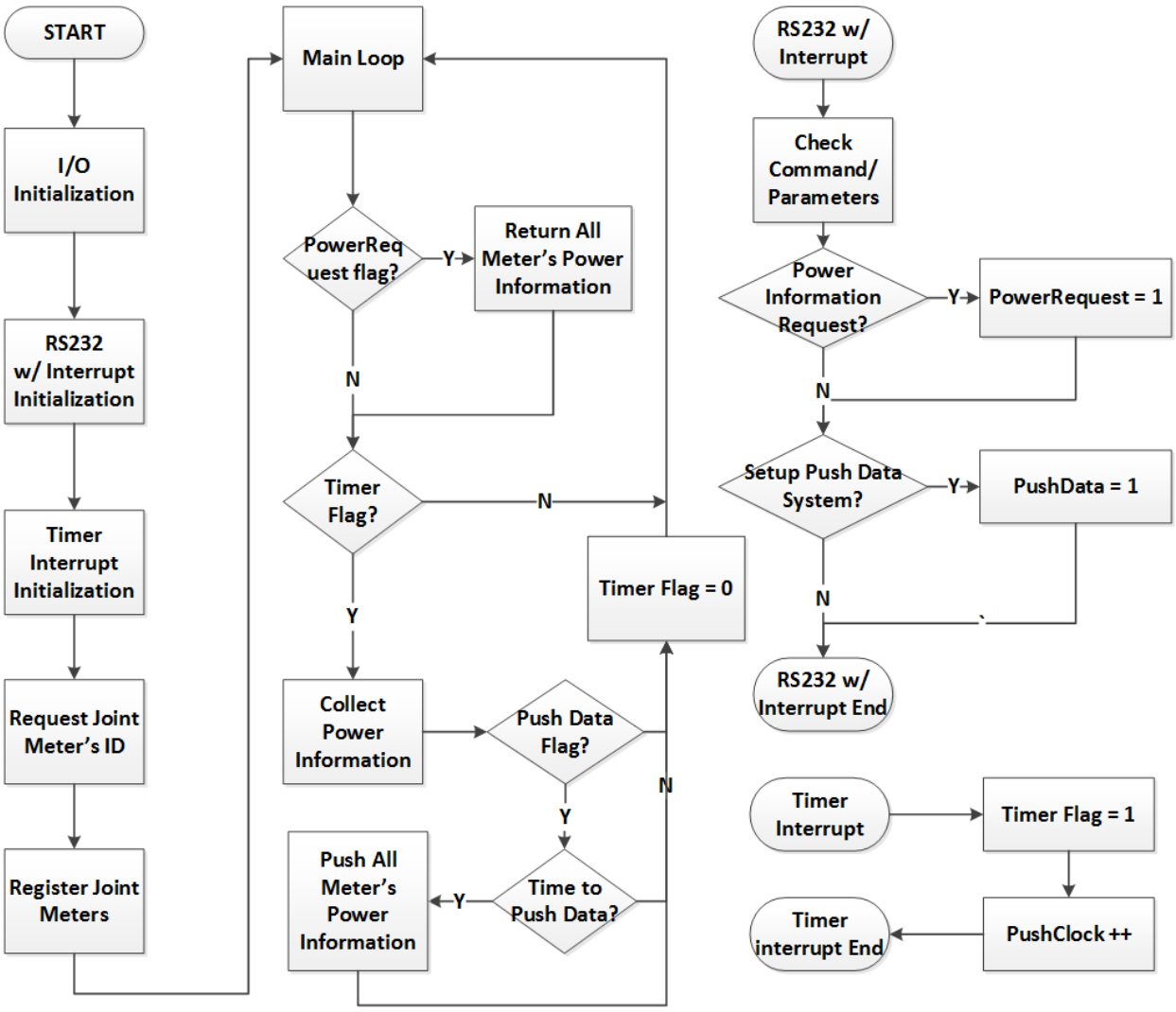

Figure 52. Firmware Flow of the PIC [60]

There are three loops in the PIC's firmware flow: the main loop, RS232 interrupt loop, and timer interrupt loop. Before the main loop, the RS232 with internal interrupt and timer interrupt are initialized at the startup process. Afterward, the meters' IDs are requested and registered for later retrieval of power information and relay status; other commands from the gateway include requesting power information and setting up the system that pushes data. These commands are handled by the RS232 within the interrupt loop which ensures that the commands will not be missed while executing other processes in the main loop. Most actions are handled in the main loop according to flags, but only command checks and flag sets are handled in the RS232

interrupt loop. With the timer interrupt, the power information and the status of the relays can be pushed to the control center periodically by setting the PushData flag. The time period of data pushing can be changed remotely, which makes the service more flexible; however, to avoid unexpected actions, the duration of the timer interrupt routine should be as small as possible. Therefore, only the timer flag is handled in the timer interrupt routine to avoid missing RS232 commands or breaking the timer interrupt loop. We should note that the time required for the power information collection and the data pushing processes should be less than the interval of the timer interrupts so these processes can be handled correctly. The hardware implementation of the PIC is shown in Figure 53.

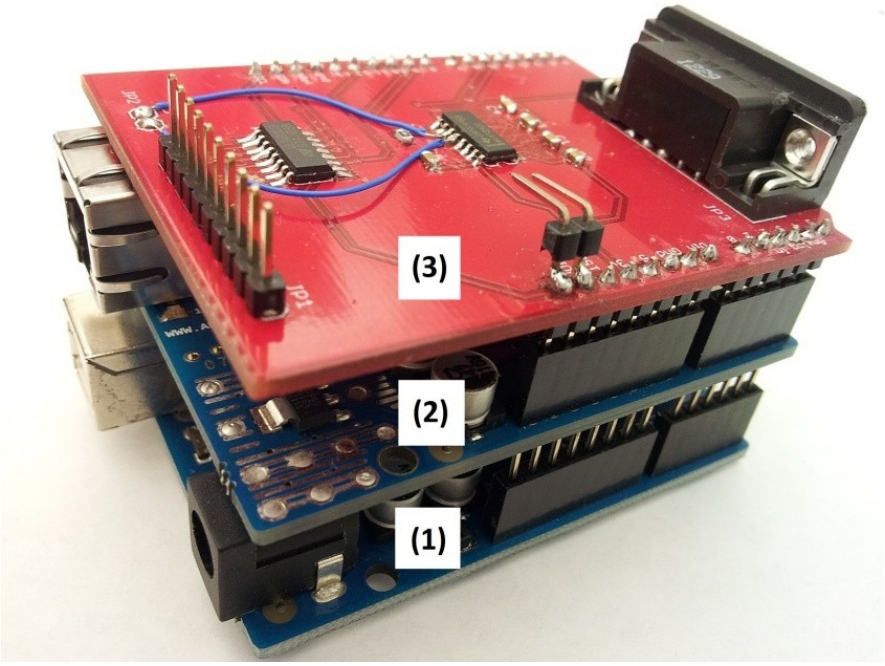

Figure 53. Implementation of PIC: (1)ATMega328P (2)Ethernet Shield, and (3)RS232 Interface with Relay Driver [60]

Figure 54 shows a PIC local controller that controls the power on the outlets; the design accelerates the charging station's response time.

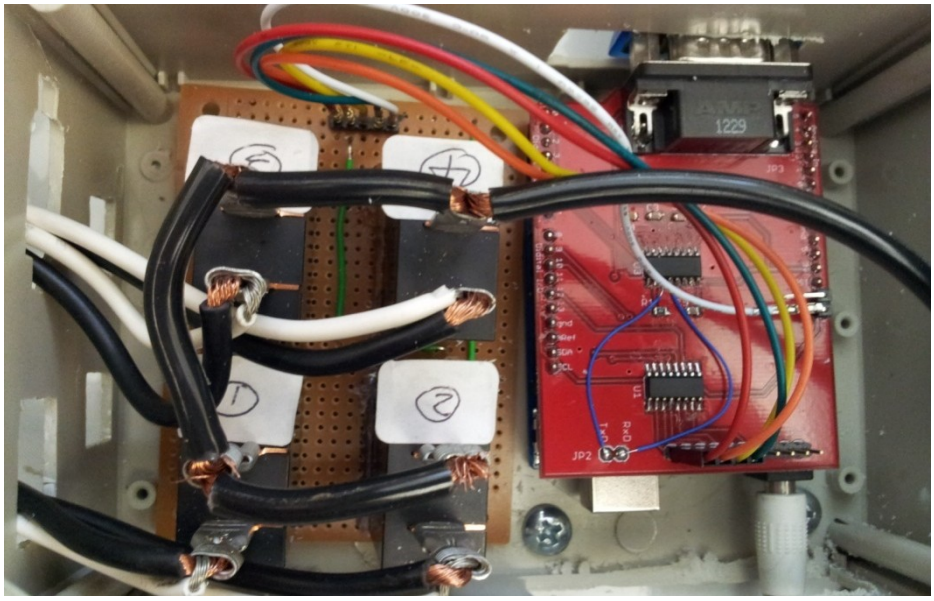

Figure 54. Local Controller of Level 1 EVSE with Controllability over Power to Outlets

The local controller is responsible for turning the outlet on/off, further reducing the round trips of commands and responses between the server and charging stations; thus, it accelerates the response time of the charging system.

In addition, the charging station's local controller has access to the power information of the meters, and so it can employ local charging algorithms to control charging. Regardless of where the charging algorithm resides, the algorithms involve two major operation flows at the server level: Enable Charging and Disable Charging. Each operation flow includes two sub-processes: Read Outlet On/Off Status and Read Power Information. Figure 55 shows the server operation flow for Level 1 EVSE.

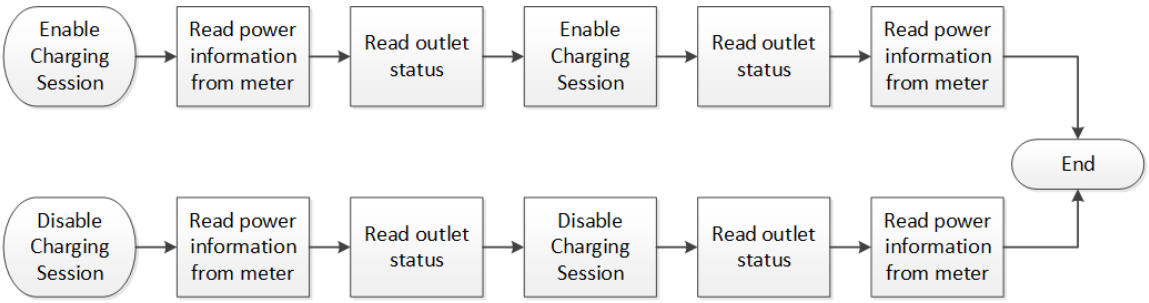

Figure 55. Server Operation Flow for Level 1 EVSE

With PIC embedded on the Level 1 EVSE, the control center can retrieve the power information and outlet status of four meters with a single command. For the new Level 1 EVSE, the server only needs three commands to finish the process to both Enable Charging and Disable Charging while it requires seventeen commands to finish the process in original system. The response time can be further reduced by pushing the power information and the outlet status to the database of the control center periodically; thus, a fast response Level 1 EVSE is achieved with a single command in both processes. Table 6 compares the required number of commands in the Enable/Disable charging process. The response times of the charging station in both processes are improved because the round trips of commands and responses between the server and the charging station are reduced.

TABLE 6. NUMBER OF COMMANDS COMPARISON

	Power Info.	Outlet Status	Enable/Disable Charging	Outlet Status	Power Infor.	Number of Commands
Original system	4	4	1	4	4	17
With PIC	1		1	1		3
With PIC & Pushing	0		1	0		1

By decreasing the number of communication transactions required for status reports and control operations, the PIC significantly decreases the delay time for switching PEV charging sessions.

3.5 Summary

In this chapter, a J1772 compatible one-circuit-to-four-outlet Level 2 EVSE and a 4-outlet Level 1 EVSE are designed to prevent underutilization of the power source. Both Level 2 and Level 1 controllers can be embedded with the local charging algorithm, which will be described in Chapter 4. As response time is further reduced by either collecting power information locally

or pushing the power information to the control center, a smart PEV charging infrastructure with a fast response is achieved to handle the shortage of energy in the local grid. This improvement leaves the control center with more computation power to serve a larger system, which enhances the capability of the existing WINSmartEV^{TM} framework.

CHAPTER 4 ELECTRIC VEHICLE CHARGING ALGORITHMS

The PEV charging infrastructure must take into account external factors – such as energy cost, grid conditions, user preference, local power capacity, etc – to deal with grid issues and reach target goals. In order for the system to work optimally, these specified issues and targets must be addressed using sophisticated charging algorithms which control the PEV charging automatically either by centralized or decentralized control schemes. These two design schemes guide the implementation of the algorithm: in a centralized control scheme, the control center controls the charging stations, while the controller in the charging station executes its embedded algorithm in the decentralized control scheme.

To maximize use of the available electrical grid and circuit capacity, based on the hardware developed in chapter 2 and chapter 3, charging algorithm either on the server or in the charging stations executes efficient control schemes to fulfill their objectives. In order for this PEV multiplexing charging scheme to become more appealing to users, the fair allocation of energy should be maximized by the charging algorithms by providing variable power to several PEVs from one circuit, either through multiplexing or variable current control. These charging algorithms, categorized as switching types and variable current types, are presented and analyzed in the following subsections.

4.1 Switching Type Charging Algorithms

The switching type charging algorithm is designed for the charging station where only one PEV can charge at a time on a given circuit. An example of this switching type algorithm is the Round-robin algorithm combined with First-Come-First-Served (FCFS) in WINSmartEV^{TM} as shown in Figure 56.

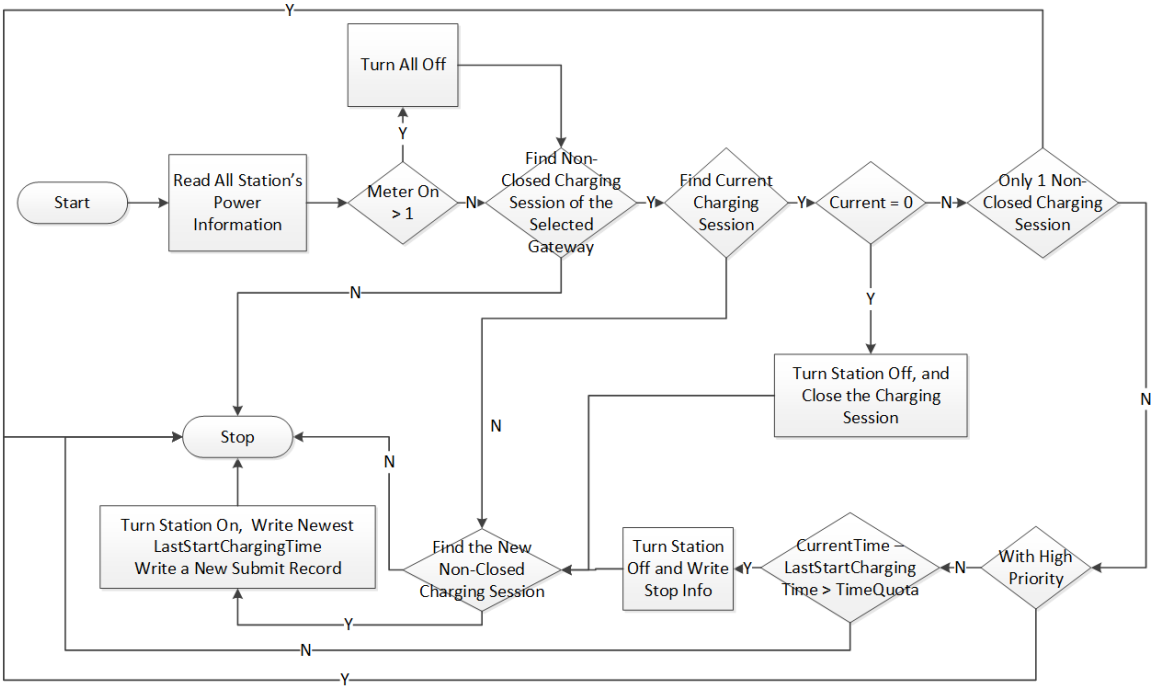

Figure 56. Round-robin Charging Algorithm [49]

In the WINSmartEV^{TM} system, the Station Controller in the control center has the flexibility and extensibility for the administrator to update the charging algorithm. In order to appeal to more users, a fair charging algorithm [19] is developed to maximize fairness in the allocation of charge time for the smart plug charger. In this case, each user's charge ratio τ is defined as the ratio of the charging time T_{Charge} and the stay time T_{Stay} in (4-1)

$$\tau \equiv T_{Charge} / T_{Stay} \tag{4-1}$$

For a "fair enough" charging system, each user's charge ratio τ should be close enough to be fair. To be more specific about the fairness system, for a given charging event, every user's mean charge ratio $\mu(\tau)$ should be close to the mean charge ratio of every user charging at time $\mu[\mu(\tau)]$. Therefore, both $\sigma[\mu(\tau)]$ and $\mu[\sigma(\tau)]$ must approach 0 when the system approaches a fair system. The normalized, non-dimensional fairness index α is defined in (4-2) to indicate

the fairness of the system.

$$\alpha \equiv 1 - \{\sigma[\mu(\tau)] + \mu[\sigma(\tau)]\}/2 \tag{4-2}$$

For a completely fair charging system, the charge ratio τ of each user should be the same. For a fair enough charging system, τ of each user should be close enough. The round-robin charging algorithm seems fair at first glance. However, the distributions of τ are not evenly distributed in four out of sixteen users' charging records, as shown in Figure 57.

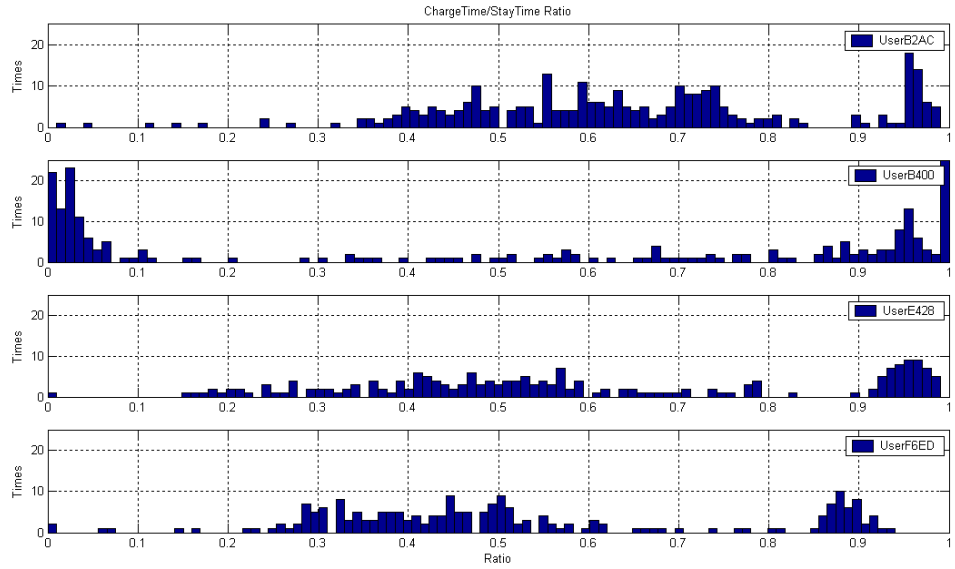

Figure 57. Charge Ratio Distribution of 4 Users [49]

The four users' means and standard deviations of the charge ratio, $\mu(\tau)$ and $\sigma(\tau)$, are summarized in Table 7.

TABLE 7. MEAN AND STANDARD DEVIATION OF CHARGE RATIO

UserID	Records	$\mu(\tau)$	$\sigma(\tau)$
B2AC	292	0.65	0.19
B400	227	0.53	0.45
E428	202	0.60	0.25
F6ED	208	0.52	0.23

From a statistical view point, $\mu(\tau)$ and $\sigma(\tau)$ can be used to describe more users' distributions. Figure 58 shows the distribution of 16 users' charge ratios by $\mu(\tau)$ and $\sigma(\tau)$.

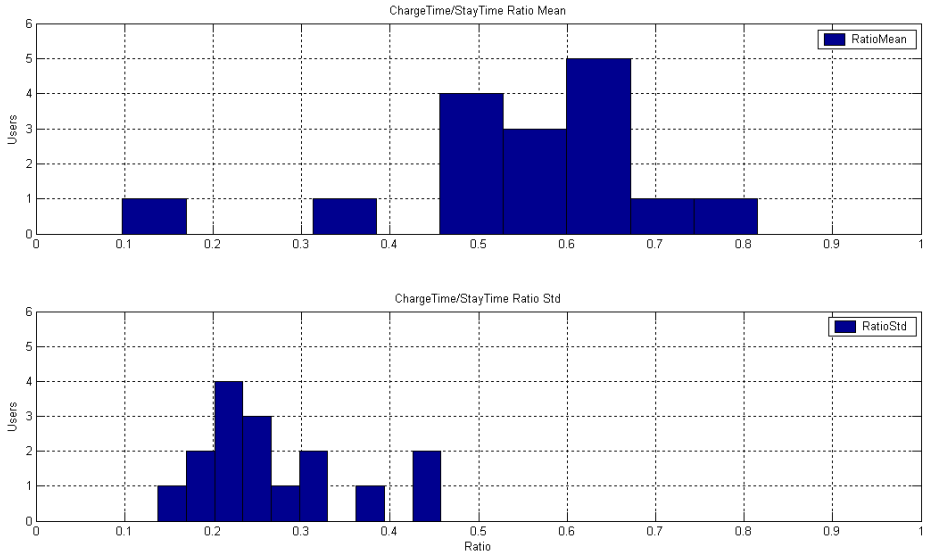

Figure 58. Charge Time Ratio Distribution of 16 Users [49]

Again, the distributions of $\mu(\tau)$ and $\sigma(\tau)$ can be described by four parameters: $\mu[\mu(\tau)]$, $\sigma[\mu(\tau)], \mu[\sigma(\tau)]$, and $\sigma[\sigma(\tau)]$ which are summarized in Table 8.

TABLE 8. MEAN AND STANDARD DEVIATION OF μ(τ) AND σ(τ)

Parameter	$\mu[\mu(\tau)]$	$\sigma[\mu(\tau)]$	$\mu[\sigma(\tau)]$	$\sigma[\sigma(\tau)]$
Value	0.56	0.16	0.27	0.09

When a system is fair, every user's $\mu(\tau)$ should be close to $\mu[\mu(\tau)]$. Therefore, both $\sigma[\mu(\tau)]$ and $\mu[\sigma(\tau)]$ must approach 0 as the system approaches complete fairness for each user. Only when both $\sigma[\mu(\tau)]$ and $\mu[\sigma(\tau)]$ approach 0, does the fairness index α approach 1; this is used to indicate the fairness of the system. The parameter $\sigma[\sigma(\tau)]$ can be viewed as the convergence of the system; when the system is fair, $\sigma[\sigma(\tau)]$ will converge to 0.

In the fair charging algorithm, when the second user's charging session overlaps that of the first user, the server predicts the second user's charge time T_{Charge} and the first user's stay time. After calculating the first user's remaining charge time, the server stops the first user's session and starts that of the second user. Before the first user leaves, the server switches back to finish the first user's session after finishing a certain portion of the second user's turn. The third user's session is treated as an overlap of the second user, the fourth user's turn is treated as overlap of the third user, and so on. Figure 59 shows the flow chart of the fair charging algorithm.

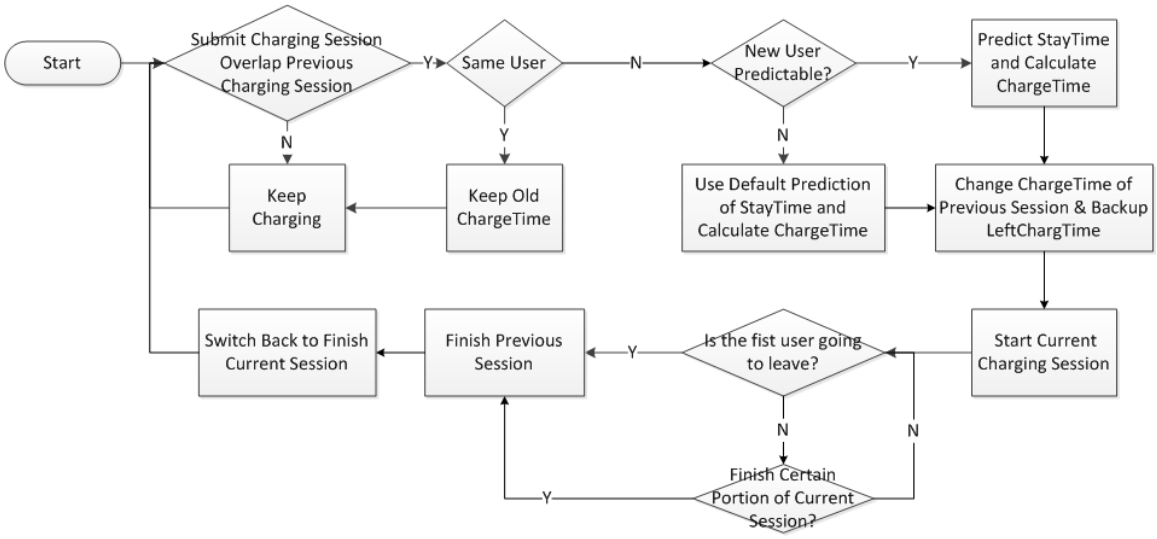

Figure 59. Flow Chart of Fair Charging Algorithm [49]

If the system switched multiple times between users, much charge time would be wasted in the switching process, causing all users to be worse off. Therefore, the Fair Charging Algorithm relies heavily on predicting a user's stay time. A forecast of users at a PEV charging station in [61] could be used for increasing accuracy in user's stay time; if the prediction of the user's stay time is accurate, the fairness maximization can be obtained while only switching charging once. A PEV's SOC status should not be considered for the purpose of predicting the owner's stay time, because an extra device, VMM [15], is needed for SOC data retrieval. Therefore, for predictable people, the stay time is predicted using either $u(T_{Stay})$ or a linear regression function based on a

user's historical charging records. For unpredictable people, the average stay time of all users $u\left[u\left(T_{Stay}\right)\right]$ is used for prediction. A number of switches may be required if the prediction of the stay time is not accurate enough. From the charging records, we found three types of people:

Type 1: Predictable - The distribution of T_{Stay} is independent of the Check-in time $T_{CheckIn}$. In this case, $u\left(T_{Stay}\right)$ should be larger than $\sigma\left(T_{Stay}\right)$, and the correlation $\gamma\left[T_{CheckIn}, T_{Stay}\right]$ should be close to 0. Figure 60 shows a sample of a type 1 predictable person where $u\left(T_{Stay}\right)=0.11$, $\sigma\left(T_{Stay}\right)=0.03$, and $\gamma\left[T_{CheckIn}, T_{Stay}\right]=0.067$.

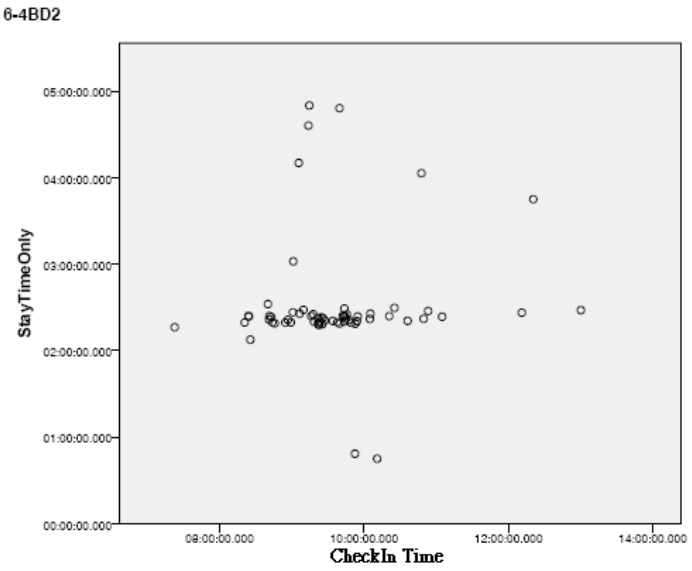

Figure 60. Sample of Type 1 Predictable Person [49]

Type 2: Predictable - In this case, T_{Stay} depends on $T_{CheckIn}$ and the correlation $\gamma\left[T_{CheckIn}, T_{Stay}\right]$ should be a negative value. A simple linear regression function is used to predict T_{Stay} according to the user's charging records. Figure 61 shows a sample type 2 predictable person with the correlation $\gamma\left[T_{CheckIn}, T_{Stay}\right]=-0.5984$

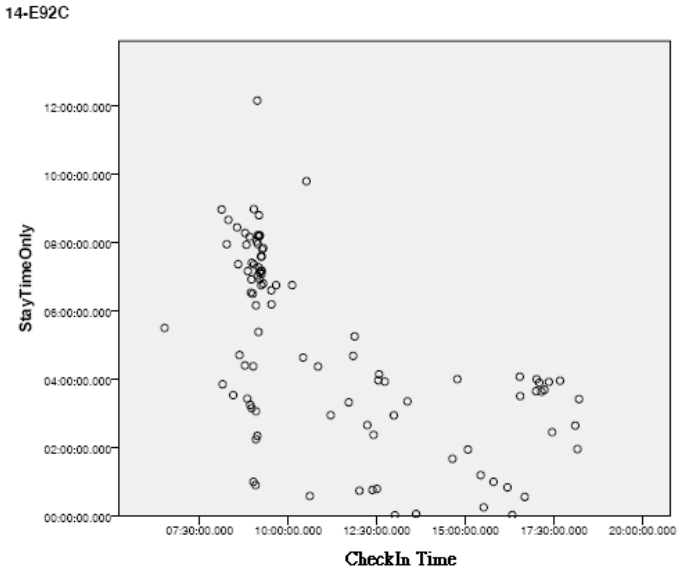

Figure 61. Sample of Type 2 Predictable Person [49]

Type 3: Unpredictable - For those who do not belong to type 1 or type 2, we use the average stay time of all users to predict T_{Stay}. Figure 62 shows a sample type 3 unpredictable person where $u(T_{Stay}) = 5.98$, $\sigma(T_{Stay}) = 13.38$, and $\gamma[T_{CheckIn}, T_{Stay}] = 0.0398$

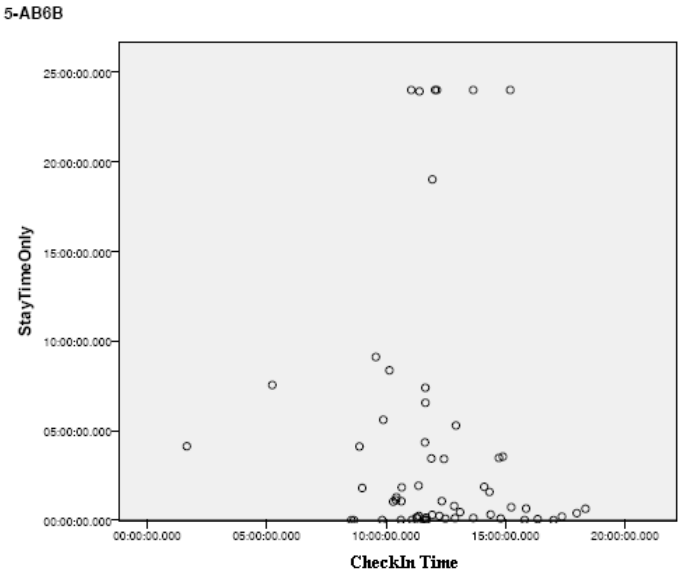

Figure 62. Sample of Type 3 Unpredictable Person [49]

TABLE 9 summarizes the characteristics of three types of predictable and unpredictable

people based on their charging records.

TABLE 9. MEAN AND STANDARD DEVIATION OF STAY TIME

Type	1	2	3
	Predictable		Unpredictable
Relation between T_{Stay} and $T_{CheckIn}$	Independent	Dependent	
Mean: $u(T_{Stay})$	0.11		5.98
STD: $\sigma(T_{Stay})$	0.03		13.38
Correlation: $\gamma[T_{CheckIn}, T_{Stay}]$	0.067	-0.5984	0.0398
Characteristics	$u(T_{Stay}) > \sigma(T_{Stay})$ $\gamma[T_{CheckIn}, T_{Stay}] \approx 0$	Negative Value of $\gamma[T_{CheckIn}, T_{Stay}]$	$u(T_{Stay}) < \sigma(T_{Stay})$ $\gamma[T_{CheckIn}, T_{Stay}] \approx 0$

For predictable people, $u(T_{Stay})$ is used to predict T_{Stay} of type 1 people while a simple linear regression function is used for type 2. For unpredictable people, the average stay time of all users $u[u(T_{Stay})]$ is used for prediction. A number of switches may be required if the prediction of the stay time is not accurate enough; in real world applications, the optimization of the fairness algorithm must account for the confidence of stay time and the time wasted in switching. Experimental results of User's Stay Time Prediction and Fair Charging Algorithm are presented as follows.

In order to show to the accuracy of prediction, we define the normalized, non-dimensional error rate of prediction $\varepsilon(T_{Predict})$ in (4-3)

$$\varepsilon(T_{Predict}) \equiv \frac{\sqrt{(T_{Stay} - T_{Predict})^2}}{Max(T_{Stay}, T_{Predict})} \tag{4-3}$$

According to the aforementioned prediction rule, the users' T_{stay} prediction error rate

distribution is shown in Figure 63. Note that the first and second charts represent $\mu[\varepsilon(T_{Predict})]$ and $\sigma[\varepsilon(T_{Predict})]$ for predictable people while the third and fourth represent $\mu[\varepsilon(T_{Predict})]$ and $\sigma[\varepsilon(T_{Predict})]$ for unpredictable people.

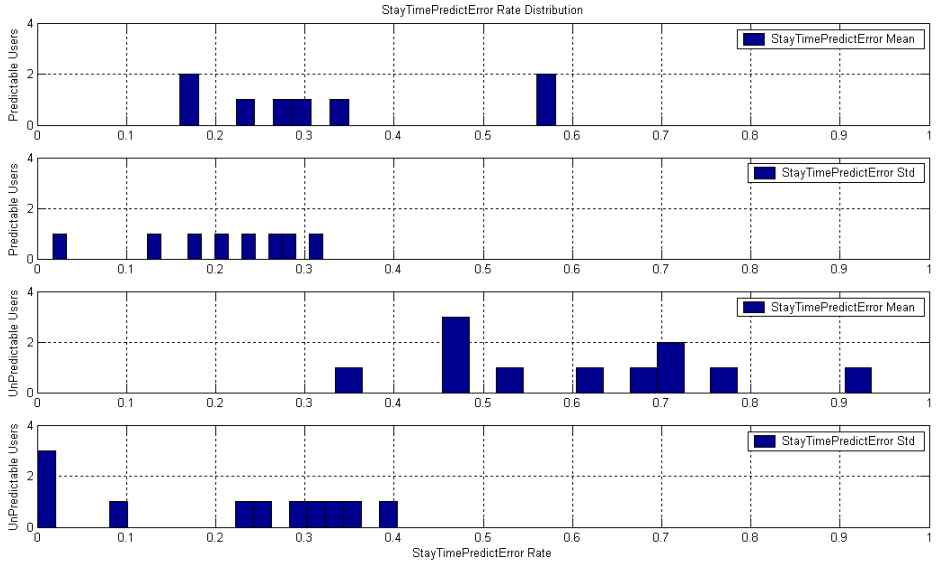

Figure 63. Prediction Error Rate Distribution [49]

The data shows that predictable people have better behavior in both $\mu[\varepsilon(T_{Predict})]$ and $\sigma[\varepsilon(T_{Predict})]$. In the simulation, we input the same Check-In Time in the charging records into the fair charging algorithm. After redistributing the power, the mean and the standard deviation of the ChargeTimeRatio τ are calculated in **TABLE** 10.

TABLE 10. COMPARISON BETWEEN $\tau_{RoundRobin}$ AND τ_{Fair}

Charging Algorithm	$\mu[\tau]$	$\sigma[\tau]$
RoundRobin	0.6014	0.5561
Fair	0.7281	0.2329

From the simulation results, the increase of $\mu[\tau]$ and the decrease of $\sigma[\tau]$ mean that users

more evenly receive energy from the charging station. To see how the system treats each user, the ChargeTimeRatio τ of each user are separately accumulated. The distribution of $\mu[\tau]$ and $\sigma[\tau]$ for each user is shown in Figure 64.

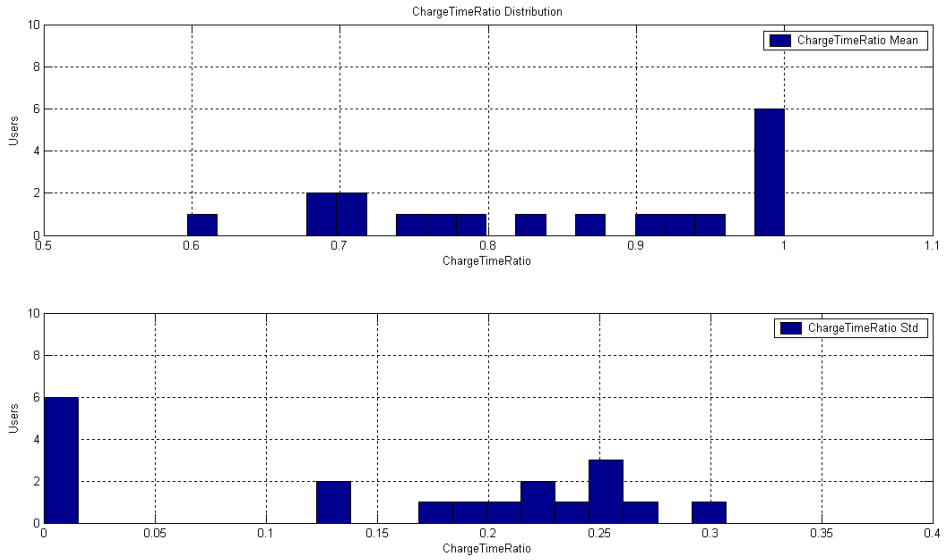

Figure 64. New ChargeTime Ratio Distribution [49]

The parameters of Fairness and Convergence are summarized in **TABLE** 11.

TABLE 11. FAIRNESS COMPARISON 1

Index	Parameter	Charging Algorithm	
		Round-Robin	*Fair*
Charge Ratio Average	$\mu[\mu(\tau)]$	0.5770	0.8492
Fairness Condiction 1	$\sigma[\mu(\tau)]$	0.2345	0.1374
Fairness Condiction 2	$\mu[\sigma(\tau)]$	0.2649	0.1509
Convergence	$\sigma[\sigma(\tau)]$	0.4018	0.1138
Fairness	α	0.7503	0.8558

The results show that the Fair Charging Algorithm is fairer to users compared to the round-robin algorithm. The round robin algorithm seems fair at first, but the fairness index shows that it favors the first user who starts charging. By defining charge time allocation fairness

and implementing an algorithm to maximize it, we can make multiplexing appeal to more users.

Fairness could technically be maximized by continuously switching charging power between PEVs. This process would only be feasible if the time to switch charging sessions between PEVs was close to zero. However, given hardware, network, and PEV constraints, the period of time to switch charging from one PEV to the next can be as high as minutes. If the system switched continuously between users, much charge time would be wasted in the switching process, causing all users to be worse off.

In real world applications, the switching time is significant and the stay times are predicted with more or less certainty. If the exact stay time of the PEVs is known, then fairness maximization can be obtained while only switching charging once, the minimum number of times required. However, if PEVs stay time is unknown, then fewer switching may often leave the charge time allocation for each PEV vary lopsided and unfair. Given these constraints, optimal execution of the fairness algorithm must account for charge switching time and the confidence of the stay time's prediction to find the best time between switching.

4.2 Variable Current Type Charging Algorithms

New charging algorithms must be designed and implemented to take advantage of the variable current sharing capability of the Level 2 stations. This section discusses the Simple Current Sharing algorithm, followed by the Fair Current Sharing algorithm.

Because the Station Controller on the server automatically controls the charging stations, the current sharing algorithm can be achieved within the server operation flow by setting up the duty cycle after enabling the charging session. However, in order to reduce the load on the server and accelerate the system's response time, the Simple Current Sharing algorithm can be embedded in

the firmware flow of the charging station. The state machine firmware flow of the local controller for the simple current sharing algorithm is shown in Figure 65.

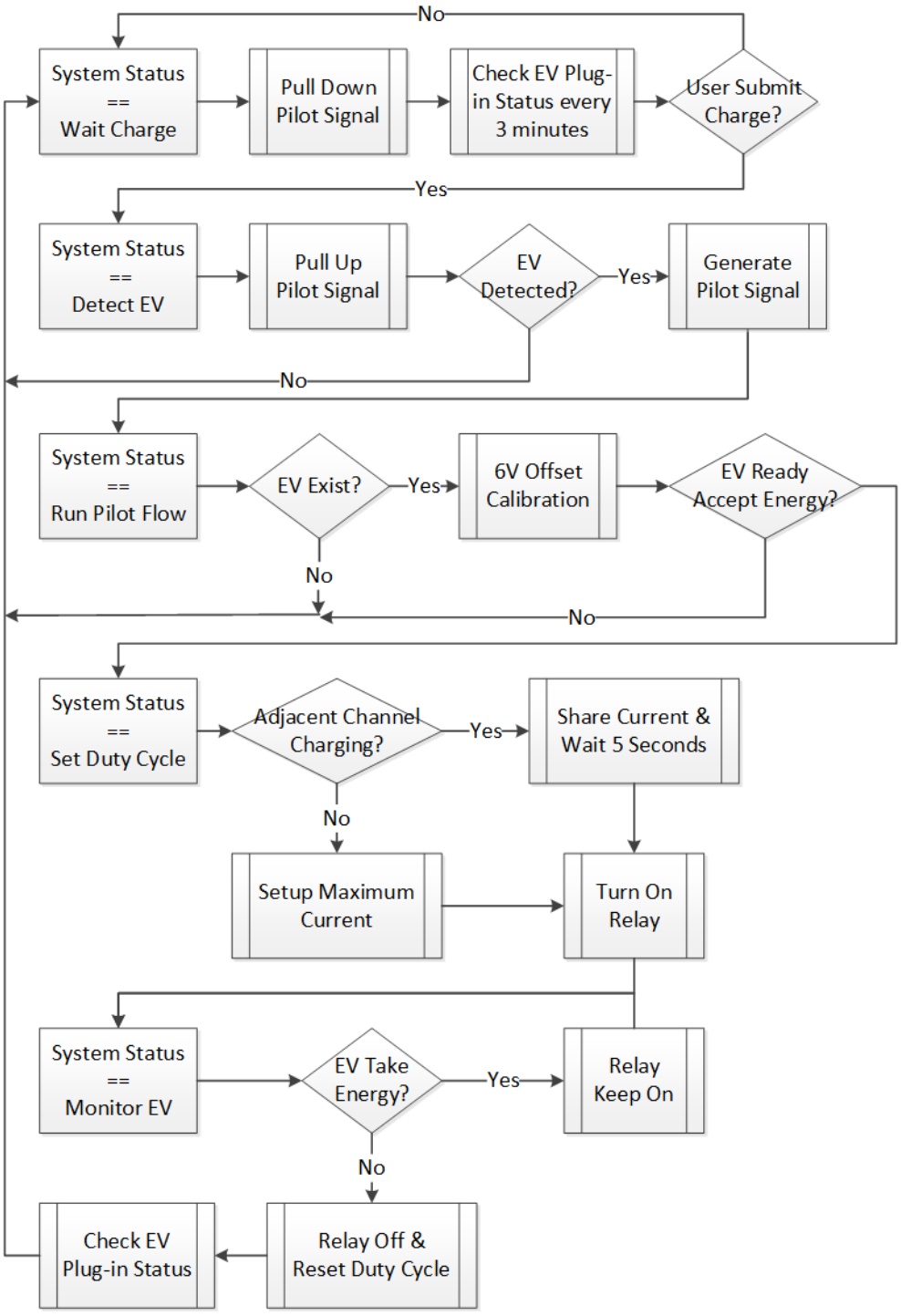

Figure 65. State Machine Firmware Flow of Current Sharing Algorithm

In the Simple Current Sharing algorithm, the local controller assigns the available power to the designated outlet by setting up the duty cycle of the pilot signal before the Monitor EV stage.

The process of setting up the duty cycle is inserted in between the processes of Run Pilot Flow and Monitor EV. The current sharing algorithm is based on the configuration of the EVSE and if there is no PEV charging in an adjacent channel, the firmware will set the maximum available current to this channel. Otherwise, the firmware will divide the current for the PEVs to share; note that there is a five second delay due to the experimental result of the PEV response time [56]. Once a PEV is unplugged, the local controller restores the power to other PEVs. The Monitor EV stage is handled periodically based on the timer interrupt flag. The J1772 standards require a faster PEV unplug detection so the Monitor EV stage is moved to the main loop for continuously checking unplug status. An experiment was conducted where 4 PEVs were plugged into the EVSE at once as shown in Figure 66. In the configuration of the experiment, four outlets share a single power line.

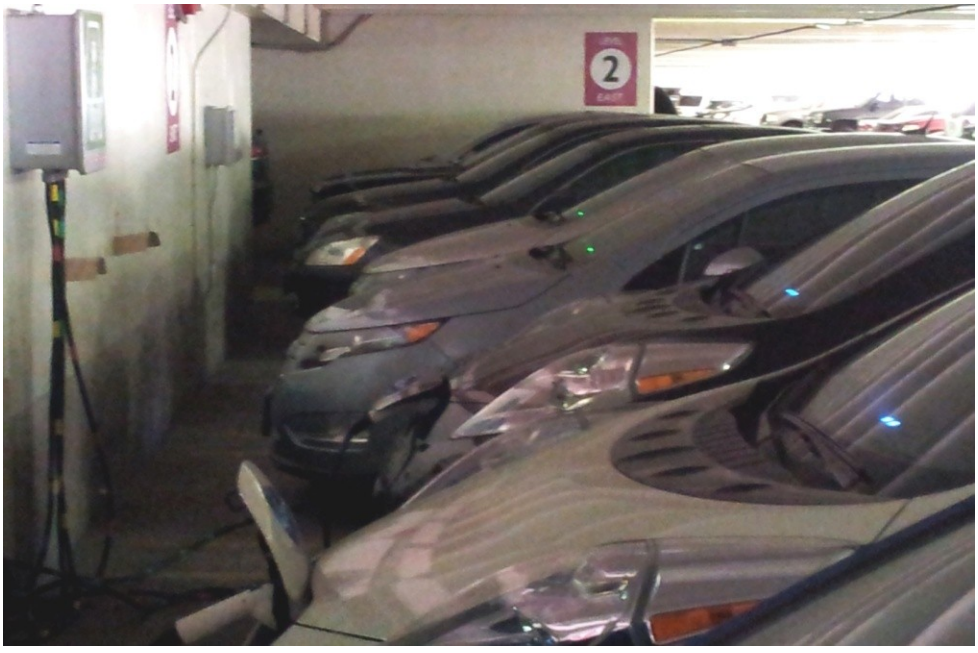

Figure 66. 4 PEVs Plugged into the EVSE

Figure 67 shows the experiment results of the Simple Current Sharing algorithm embedded in the charging station.

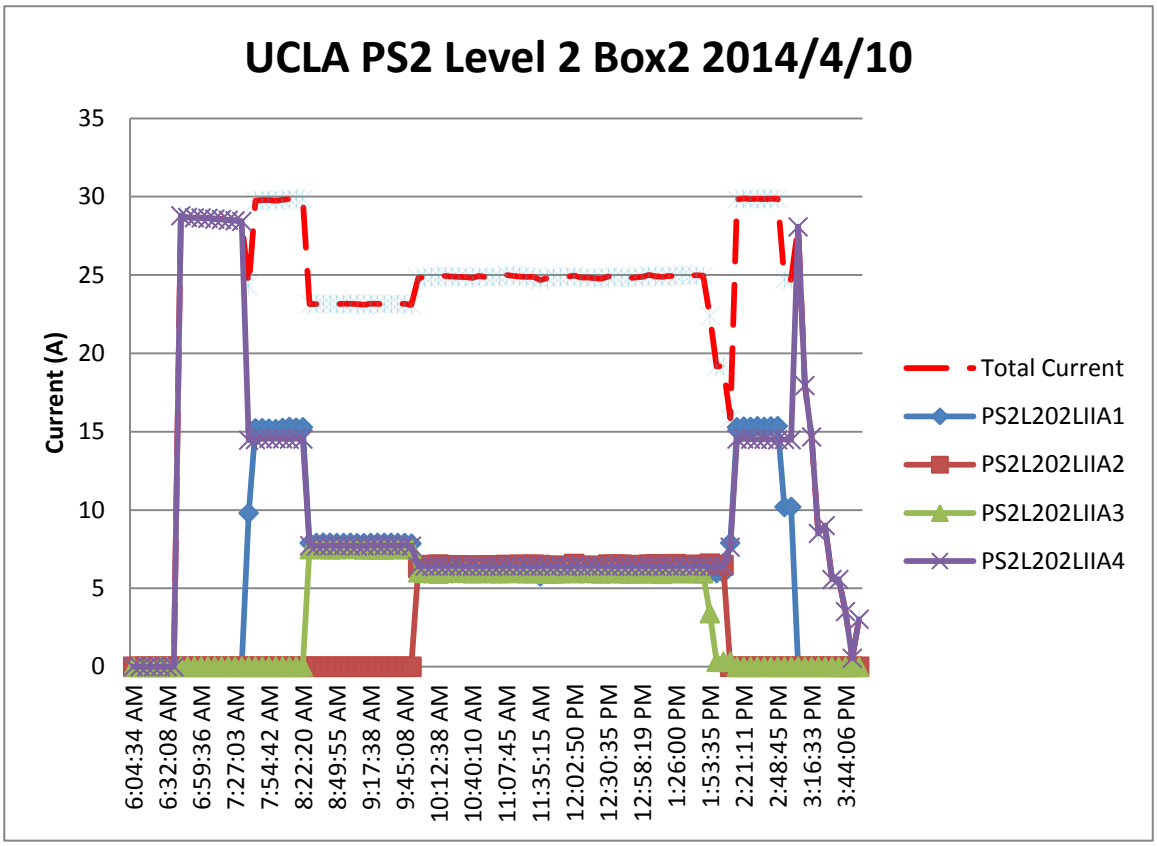

Figure 67. Results of Simple Current Sharing with 4 PEVs on a Single Circuit

In the experiment, the firmware initially set the maximum duty cycle to 50% (30A). When the first PEV connected, the charging station assigned its maximum capacity to it.; note that the first PEV did not draw 30A due to its on-board charging limitation. When the second PEV connected, the power capacity was divided by 2 for these two PEVs, providing 25% (15A) each. The PEVs were allotted 1/3 power capacity when the third PEV was connected, and a quarter of power capacity when four PEVs were plugged into the station. Note that in the cases of three and four PEVs, the current capacity dropped down to 24A due to the Ground Fault Circuit Interrupter (GFCI) tripping issue. As more and more PEVs connect to a single circuit, the imbalance

between two hot wires accumulates until it trips the GFCI. To avoid tripping the GFCI, the imbalance can be lowered to a safe range, by reducing the output current to the PEVs. Notice that when a PEV is unplugged or fully charged, the charging station restores capacity to the remaining charging PEVs in order to fully utilize the power capacity. The charging current's triangular curve is not seen in the measurement because the PEV's on-board charger takes care of charging the battery cells.

To more fairly distribute energy to PEVs based on historic charging records, we develop a Fair Current Sharing algorithm. The fairness index of a charging station with variable current control is related to the energy consumption E during the stay time T_{Stay}. The relationship between E, T_{Stay} and the average power P for the user is shown in equation (4-4).

$$P \equiv E / T_{Stay} = \int V(t) I(t) dt / T_{Stay} \tag{4-4}$$

For a completely fair system, the average power P of each user should be the same, which means each user's charge rate is also the same during the stay time. For a fair enough system, each user's charge rate should be close enough. If we assume V(t) to be a constant, a normalized, non-dimensional current share ratio ρ can be defined in (4-5)

$$\rho \equiv \frac{\int I(t) dt}{I_{MAX} \times T_{Stay}} \tag{4-5}$$

where I_{MAX} is the current capacity.

The switching type of fair charging algorithm can now be viewed as a special current sharing algorithm with a discrete current instead of a variable current. If the system is fair, every user's $\mu(\rho)$ should be close to $\mu[\mu(\rho)]$. Therefore, both $\sigma[\mu(\rho)]$ and $\mu[\mu(\rho)]$ approach 0 if and

only if the system approaches complete fairness for each user. We define a new normalized, non-dimensional fairness index β in (4-6)

$$\beta \equiv 1 - \{\sigma[\mu(\rho)] + \mu[\sigma(\rho)]\}/2 \tag{4-6}$$

The fairness index β approaches 1 if and only if both $\sigma[\mu(\rho)]$ and $\mu[\mu(\rho)]$ approach 0, which is used to indicate the fairness of the system. The parameter $\sigma[\sigma(\rho)]$ is viewed as the convergence of the system; $\sigma[\sigma(\rho)]$ converges to 0 when the system is fair. Figure 68 shows the flow of Fair Current Sharing algorithm.

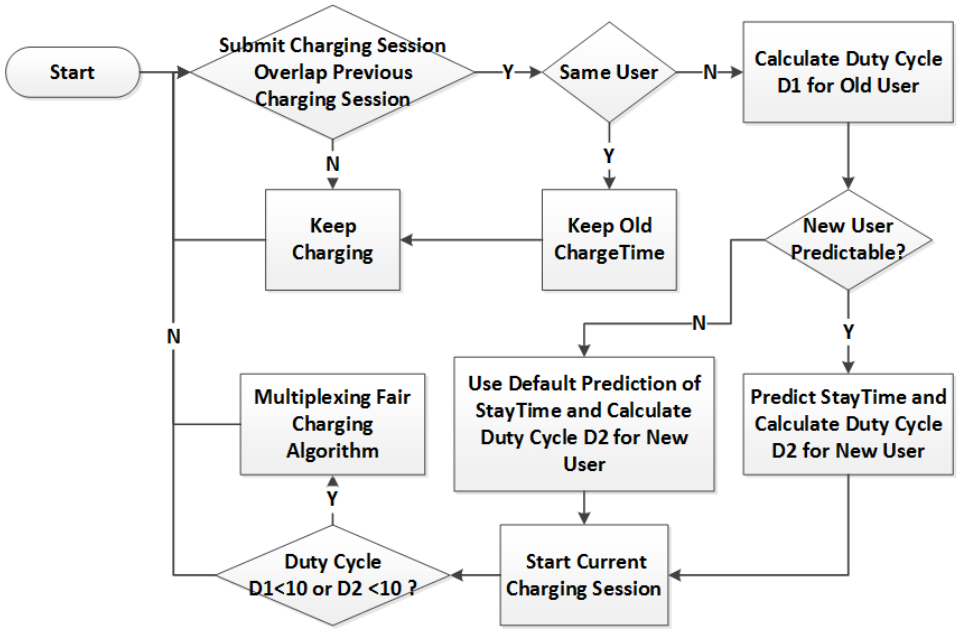

Figure 68. Fair Current Sharging Algorithm Flow Chart

When the second user's charging session overlaps that of the first user, the server still predicts the second user's charging time and the first user's stay time. However, instead of calculating charge time allocation for each PEV, the server calculates the maximum current each PEV is allowed to draw (I) based on the remaining energy consumption and the current share ratio ρ in (4-7). Instead of switching charging between the users' charging sessions, the server

allocates the current (I) that each PEV is allowed by changing the duty cycles (D) of the pilot signal.

$$\begin{cases} I_i = D_i \times 0.6 \\ I_{1,i} = \left(\rho_{T\arg et} \times I_{MAX} \times T_{1,Stay} - I_{1,i-1} \times t\right) / \left(T_{1,Stay} - t\right) \\ I_{2,i} = \rho_{T\arg et} \times I_{MAX} \end{cases} \tag{4-7}$$

$I_{1,I}$ represents the maximum allowed current for the first user and $I_{2,i}$ for the second user. The target value of the current share ratio of the system is $\rho_{T\arg et}$. The third user's session is treated as an overlap of the second user's session, and the forth user's turn is treated as an overlap of the third user's session. Note that in practical implementation, the maximum allowed current drawn is a discontinuous function of D_i based on J1772 standards (4-8).

$$\begin{cases} I_i = 0 & ,0 < D_i < 10 \\ I_i = 0.6 \times D_i & ,10 \le D_i < 85 \\ I_i = 2.5 \times \left(D_i - 64\right) & ,85 \le D_i < 96 \\ I_i = 0 & ,D_i \ge 96 \end{cases} \tag{4-8}$$

Because 240V with 30A is the most common installation, only the conditions in (4-9) are considered.

$$\begin{cases} I_i = 0 & ,0 < D_i < 10 \\ I_i = 0.6 \times D_i & ,10 \le D_i < 30 \end{cases} \tag{4-9}$$

If the result of maximum current drawn I_i is less than 6A, the Fair Charging algorithm with a 6A maximum will be used instead of the Current Sharing algorithm. Similar to the Fair Charging algorithm, the Fair Current Sharing algorithm also relies accurately predicting a user's stay time because the duty cycle calculation in (4-9) is based on the predicted stay time.

In the simulation of the Fair Current Sharing Algorithm, we use the same check-in time in the charging records as the input of the Fair Current Sharing Algorithm. After redistributing power, the mean and the standard deviation of the CurrentShareRatio ρ are calculated in **TABLE** 12.

TABLE 12. COMPARISON BETWEEN $\rho_{SimpleShare}$ **AND** $\rho_{FairShare}$

Charging Algorithm	$\mu[\rho]$	$\sigma[\rho]$
Simple Share	0.8333	0.2370
Fair Share	0.8878	0.1801

From the simulation results, the increase of $\mu[\rho]$ and the decrease of $\sigma[\rho]$mean that users more evenly share energy from the charging station. To see how the system treats each user, the CurrentShareRatios ρ of each user are separately accumulated. The distribution of $\mu[\rho]$and $\sigma[\rho]$ for each user is shown in Figure 69.

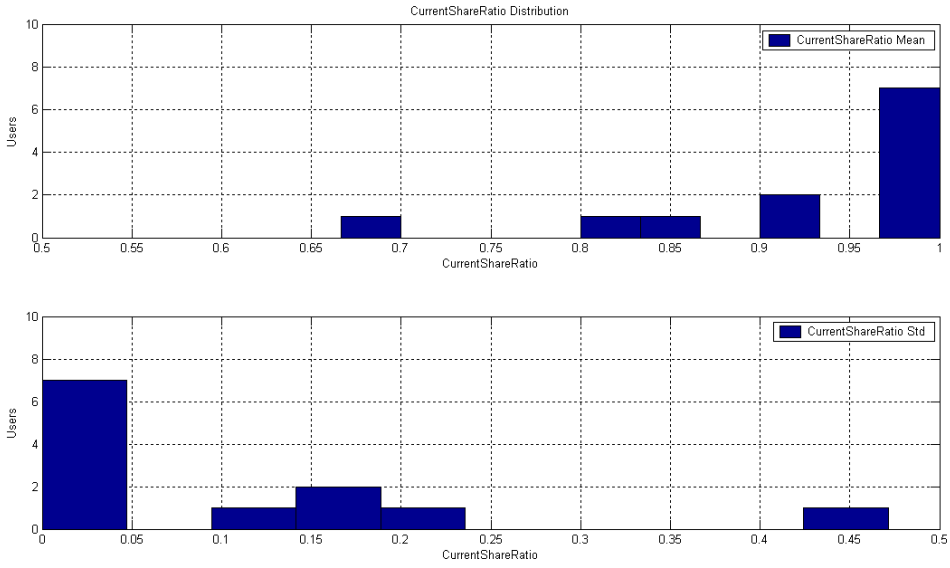

Figure 69. Current Share Ratio Distribution of 16 Users

The distributions of $\mu(\rho)$ and $\sigma(\rho)$ can be described by four parameters: $\mu[\mu(\rho)]$,

$\sigma[\mu(\rho)], \mu[\sigma(\rho)]$, and $\sigma[\sigma(\rho)]$. The parameters of Fairness and Convergence are summarized in **TABLE** 13.

TABLE 13. FAIRNESS COMPARISON 2

Index	Parameter	Charging Algorithm	
		Simple Share	*Fair Share*
Charge Ratio Average	$\mu[\mu(\rho)]$	0.9128	0.9301
Fairness index 1	$\sigma[\mu(\rho)]$	0.1168	0.1063
Fairness index 2	$\mu[\sigma(\rho)]$	0.1108	0.0953
Convergence	$\sigma[\sigma(\rho)]$	0.1402	0.1451
Fairness	β	0.8862	0.8992

The results show that the Fair Current Sharing algorithm is fairer to users compared with the Simple Sharing algorithm.

4.3 Discussion on Charging Algorithms

A server-based control system regulates stations based on remote charging algorithms that reside in the Station Controller. The algorithms can be developed based on user's time, energy price, or energy amount. Certain simple charging algorithms without power information or the PEV's SOC can be implemented on the local controller with no hardware change. A system with embedded charging algorithms reduces traffic between charging stations and the control center is reduced, and is faster and more efficient than a system with remote charging algorithms implemented on a server.

The authors in [60] conclude that the smart charging algorithms can be implemented locally in a charging station equipped with a PIC device. Because a PIC can retrieve and save power information locally in the smart charging station, the station can obtain the actual power consumption data of the PEV. To obtain a user's charge time, the local controller can use the

battery's SOC if the PEV is equipped with a VMM. With these data, it is possible to implement the Fair Current Sharing algorithm at the local level. In addition, the Fair Current Sharing algorithm becomes more practical when the charging stations are equipped with PICs set on data pushing mode, because the PIC improves the response time of the system.

The local controller inside a charging station is responsible for executing the charging schedule calculated by the server. After the server calculates the schedule according to the selected charging algorithm, it sends the schedule to the charging stations to control the charging sessions. When an event occurs that changes the charging session, the local controller requests the server to update the charging schedule; upon receipt, the server calculates a new schedule for the charging stations.

Nevertheless, only certain simple charging algorithms can be implemented locally, because the calculation power of the local microprocessor is limited. Thus, with local charging algorithms implemented at the station level, the server must only select the mode of the charging algorithms' modes for each charging station, saving significant computational resources on the server, which has more computing power. However, more complex charging and scheduling algorithms may still need to be implemented on the server. With local charging algorithms implemented, the control center can handle a larger smart charging system due to the reduction of traffic between the control center and the charging stations. Our experimental results still shows that the Fair Current Sharing algorithm performs better than the Simple Current Sharing algorithm.

4.4 Summary

In order to balance the requirements of PEV charging and the demands of the grid, the PEV charging infrastructure must account for external factors such as energy cost, grid conditions, user preference, local power capacity, etc; factors that can be treated as parameters of priority

when developing the charging algorithm. To fairly distribute the power source to every PEV, both switching and variable current types of fair charging algorithms treat every user with the same priority.

In order to have a faster and more efficient system with reduced traffic between the control center and stations, the local charging algorithm embedded in the EVSE should be considered. The control center will only need to choose the charging algorithm running on the EVSE, which significantly reduces server computing resources and leaves the control center with the capability to handle a larger charging system. The disadvantage is that only certain simple algorithms can be implemented locally due to the limited computational power of the local microprocessor. In addition, algorithms that require a user's historical charging records on the database are better suited to run on the server.

CHAPTER 5 SAFETY REQUIREMENT

Preventing electric hazards, such as electric shock and fire, is first priority in the design of PEV charging systems. Electric shock occurs upon contact of a human body part with electricity, which can cause injury or death. To prevent this scenario, the handle of the charging cable should have no voltage until it is plugged into a PEV. In addition, when there is an abnormal diversion of current from one of the hot wires, the charging station must shut off power immediately to prevent electric shock. To avoid starting fires, the charging station should stop charging when a PEV draws more current than its allotment. In case of emergency, PEV charging stations should also be turned off at every level, from the server to the station. To fulfill these objectives, relays inside the charging stations, which control power transfer to PEVs, should allow the server, local controller, and the Ground Fault Circuit Interrupter (GFCI) to turn on and off. The following subsections describe and examine the safety design at the control center level and station level.

5.1 Safety at Control Center Level

When exceptional conditions occur, the control center detects the abnormal status and automatically stops PEVs from charging. For example, if the PEV ignores the charging station's pilot signal, which stands for the current limitation of the outlet, and draws more electricity than the charging station allotted to it, the Station Controller in the control center will remotely stop the PEV from charging. In addition, the administrator can manually turn the relays of the charging stations on or off and check their status by sending commands through the server's Monitor and Control Center. As long as the connection between the server and charging stations exist, the charging stations can be reset manually or automatically on schedule. The charging station's local controller, upon receiving the system reset command from the server, resets the

station by turning off the switch on the station's power source. After the charging station loses power, the switch on the station's power source flips back to its normal position, turning on the charging station.. Furthermore, the authorized user can also stop charging via a mobile device that accesses the user control center.

Any emergency action taken at the top level will have a delay time that depends on the condition of the wireless communication including 3G, WiFi, ZigBee, and Cloud. Therefore, a fast acting local controller, described in section 5.2, is required to stop charging in case of an emergency.

5.2 Safety at Station Level

To prevent electrical hazards, PEV Plug-in Detection must ensure that the charging cable's handle has no voltage until it is plugged into a PEV. Also, when there is an abnormal diversion of current from a hot wire, the charging station must immediately shut off power to prevent electric shock. The GFCI in the charging station detects the difference of current between two hot wires and shuts off the safety relay when the difference has crossed the amperage threshold. To fulfill these safety requirements, both PEV Plug-in Detection and GFCI must be implemented at the station level. The details of the GFCI are described in section 5.2.1, and PEV Plug-in Detection in section 5.2.2.

5.2.1 Ground Fault Circuit Interrupter (GFCI)

For Level 1 charging stations (EVSmartPlug^{TM}), a single commercial breaker with GFCI at the power source fulfills the safety requirement set by Underwriters Laboratories (UL) because the PEV's trickle charge can automatically reset the GFCI.

The safety requirement for the Level 2 charging station requires that the charging stations handle the GFCI function in both the J1772 and UL standards. According to the J1772 standard [20], the control unit should handle both the pilot signal and the GFCI as shown in Figure 70.

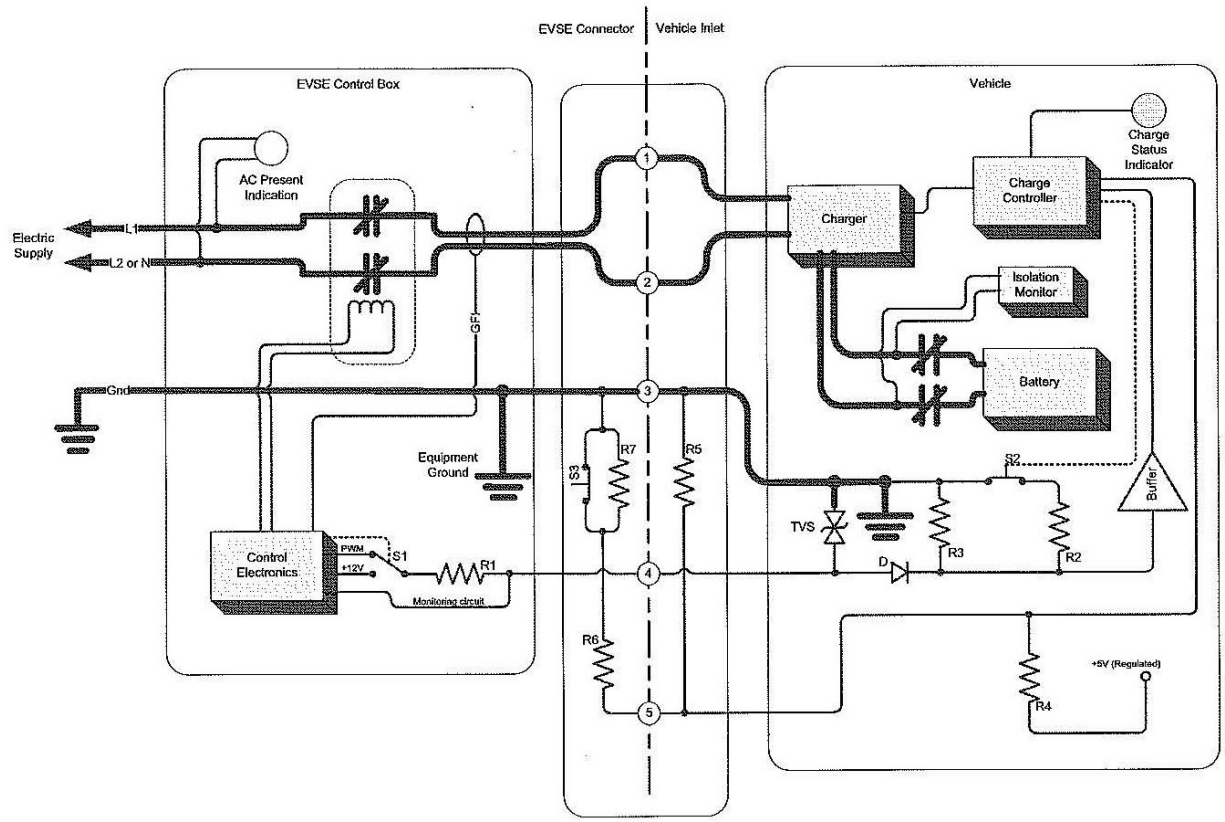

Figure 70. AC Level 2 System Configuration [20]

To integrate the GFCI function with the local controller, a station level safety control scheme is designed as shown in Figure 71. When the difference of current between two hot wires crosses amperage threshold, the GFCI circuit shuts off switch SW2, which turn off switch SW4, so that no power reaches the charging handle.

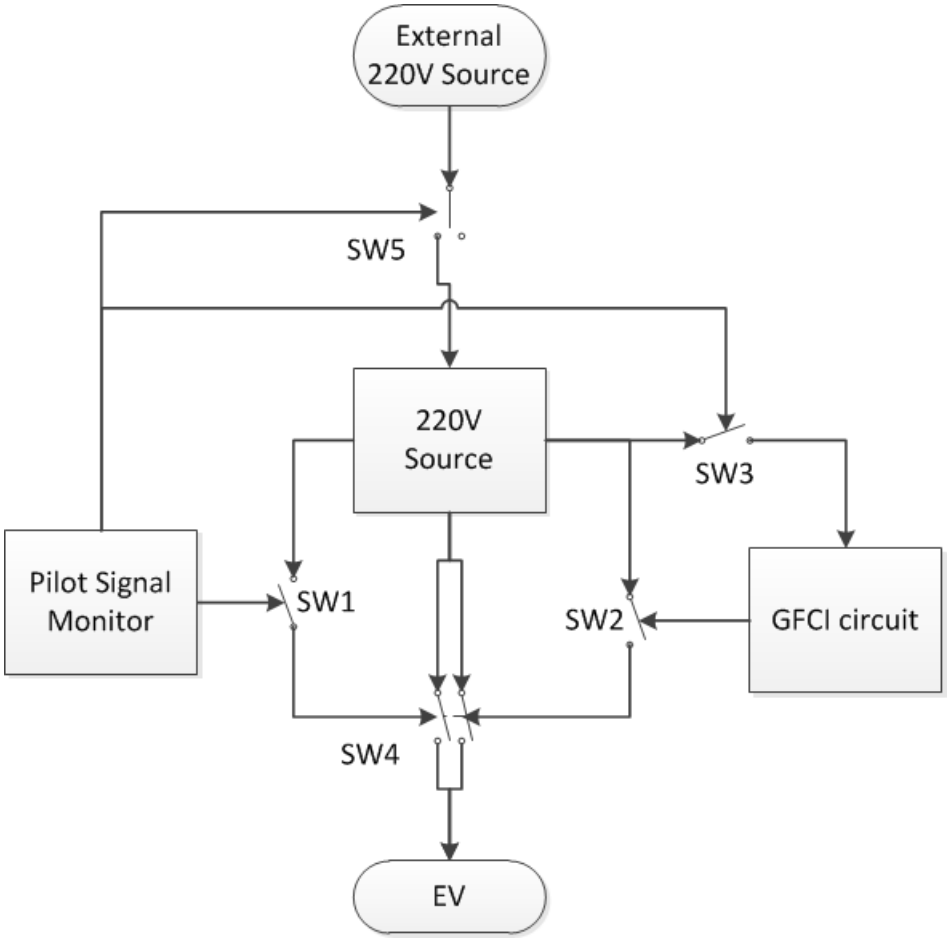

Figure 71. Schematic of Safety Control for the Relay [50]

In this control scheme, one leg of the contactor SW4 is controlled by the pilot signal monitor, while the other leg is controlled by the GFCI. The pilot signal monitor, upon receiving the command from the server, can reset the GFCI and the system by SW3 and SW5, which fulfills the objective of systematic safety integration.

Although the authors in [62] claim the GFCI of a networked charging station can be reset remotely, no details of control methods or schematics are presented. In [63], a GFCI is proposed with a microprocessor. In Figure 72, we propose a pure hardware GFCI with remote reset function to reduce material cost and increase the reliability.

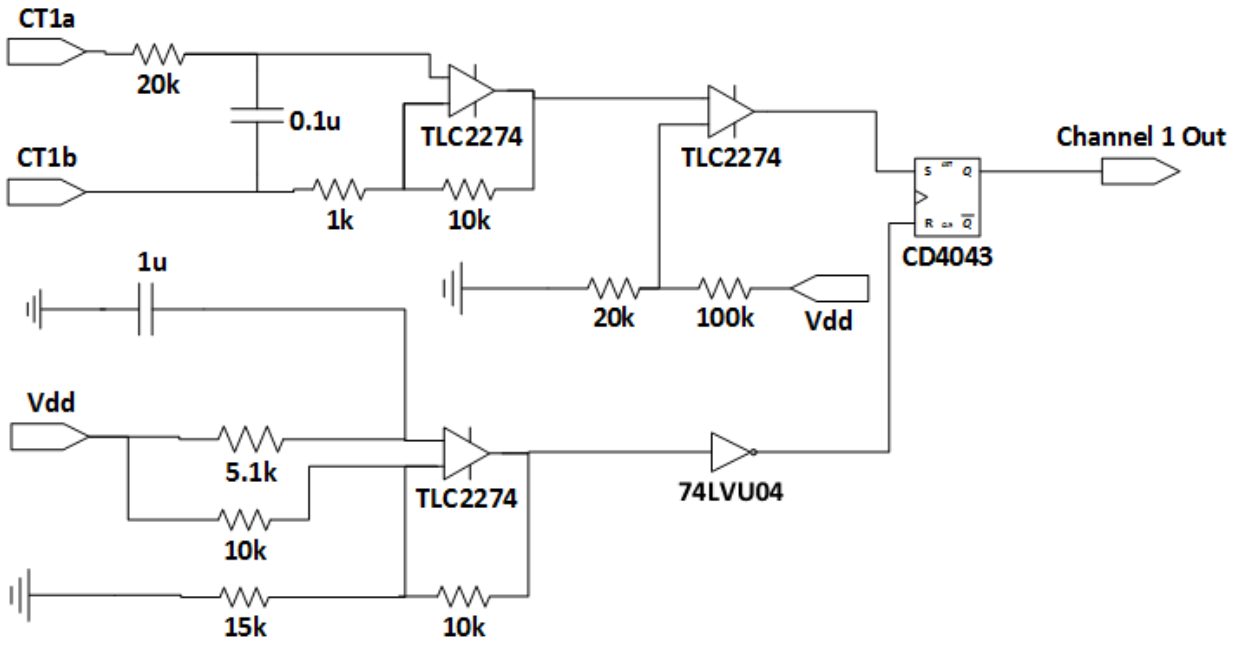

Figure 72. Pure Hardware GFCI Circuit [50]

Unlike a traditional GFCI, which requires manually pressing the reset button, a pure hardware GFCI with a remote reset function is used to increase reliability. The power to the PEV can be controlled by the server, the charging station's local controller, and the GFCI circuit.

This model features six major components: Current Transformer (CT), Low-pass Filter (LPF), non-inverting amplifier, voltage comparator, S-R latch, and Schmitt delay trigger circuit. The CT takes the difference between two hot wires and outputs a corresponding voltage. The LPF filters undesired noise from the mechanical relay. The non-inverting amplifier magnifies the signal from the CT. The voltage comparator functions as an A/D converter that converts the amplifier's sinusoidal signal into a digital signal. The S-R latch begins with an initial "Low" state and, upon receiving a "High' input signal is received, the latch also switches to a "High" state and maintains in that state until the GFCI circuit is reset. The Schmitt delay circuit generates a short pulse signal sent to the S-R latch's reset pin, which returns the latch to its initial "Low" state whenever the GFCI resets; unlike the traditional GFCI requires a manually pressing

the reset button, this GFCI simply needs its power source reset. Figure 73 shows the implementation of the GFCI circuit.

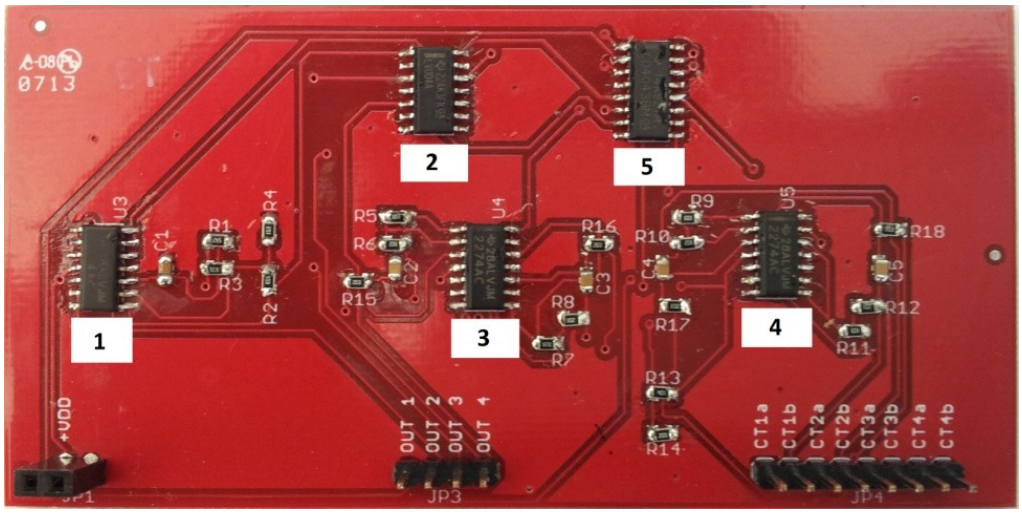

Figure 73. Implementation of 4-channel GFCI: (1) Schmitt Delay (2) Inverter (3) Voltage Comparator (4) Non-inverting Amplifier (5) SR Latch [50]

In order to have independent control over each GFCI channel in real-world applications, the microprocessor generates the reset signal (Reset) for the SR latch instead of controlling the GFCI board's power source, as shown in Figure 74.

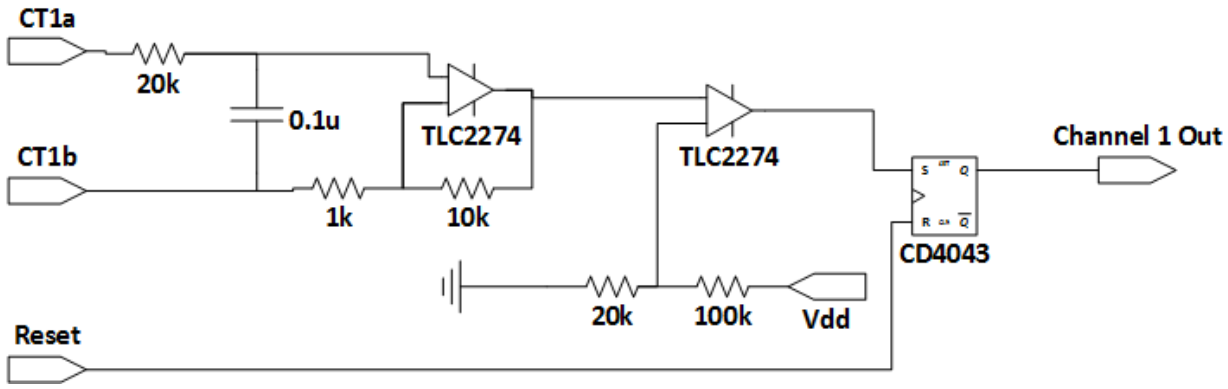

Figure 74. Schematic of GFCI

Whenever an outlet trips, the microprocessor can independently reset the GFCI without affecting other PEV charging session after the user unplugs the PEV.

Because the GFCI board is sensitive to the electromagnetic field generated by relays and contactors, false alarms can be easily triggered at the moment relays or contactors turn on due to glitches at the rising edge in the output signal of the GFCI. To prevent the false alarm, the local controller deglitches the output from GFCI board and shuts the contactor off. Figure 75 shows a new relay control method to avoid a GFCI false alarm.

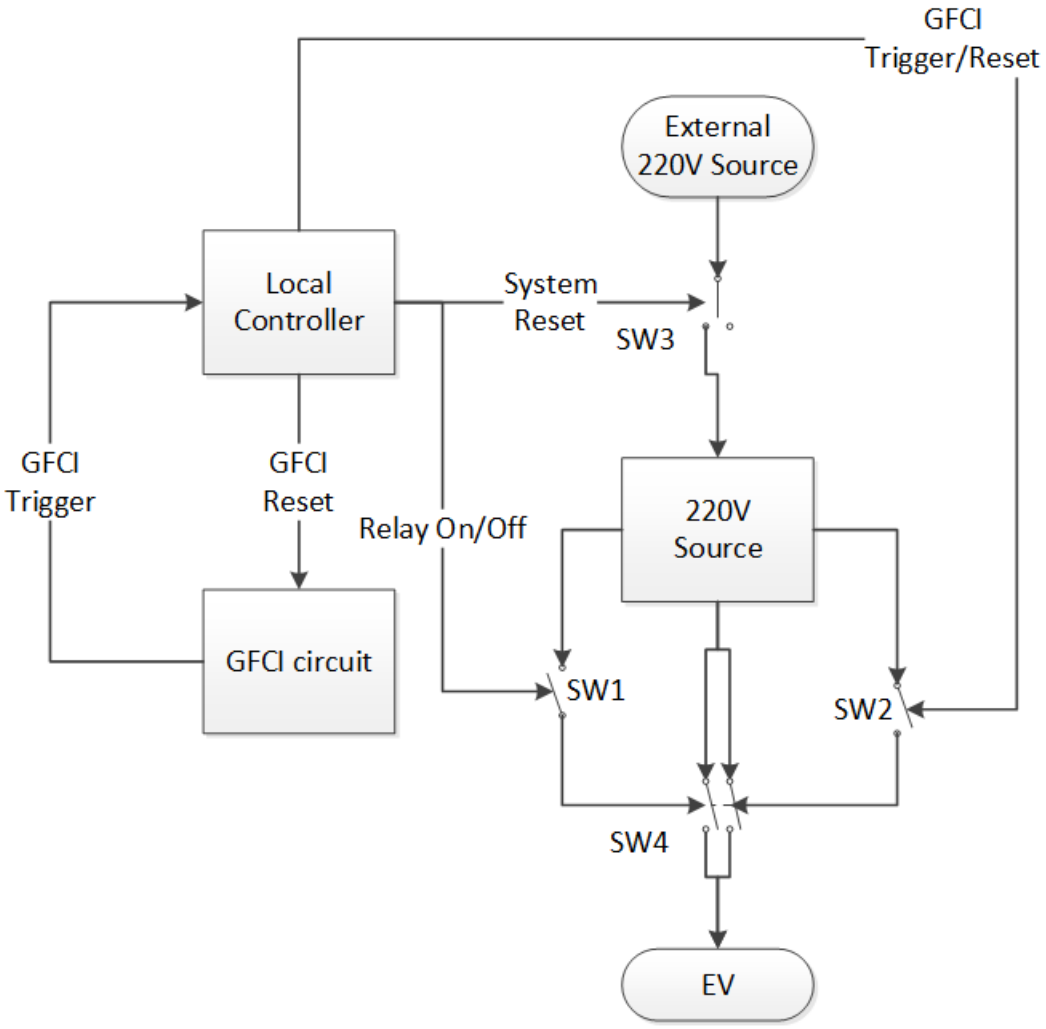

Figure 75. New Schematic of Safety Control for the Relay

In the new design, the GFCI board feeds its output to the local controller. Instead of controlling one leg of the contactor directly using the GFCI board, the local controller controls both legs of the

contactor for different conditions. The implementation of the Non-ZigBee Level 2 J1772 local controller with the GFCI function is shown in Figure 76.

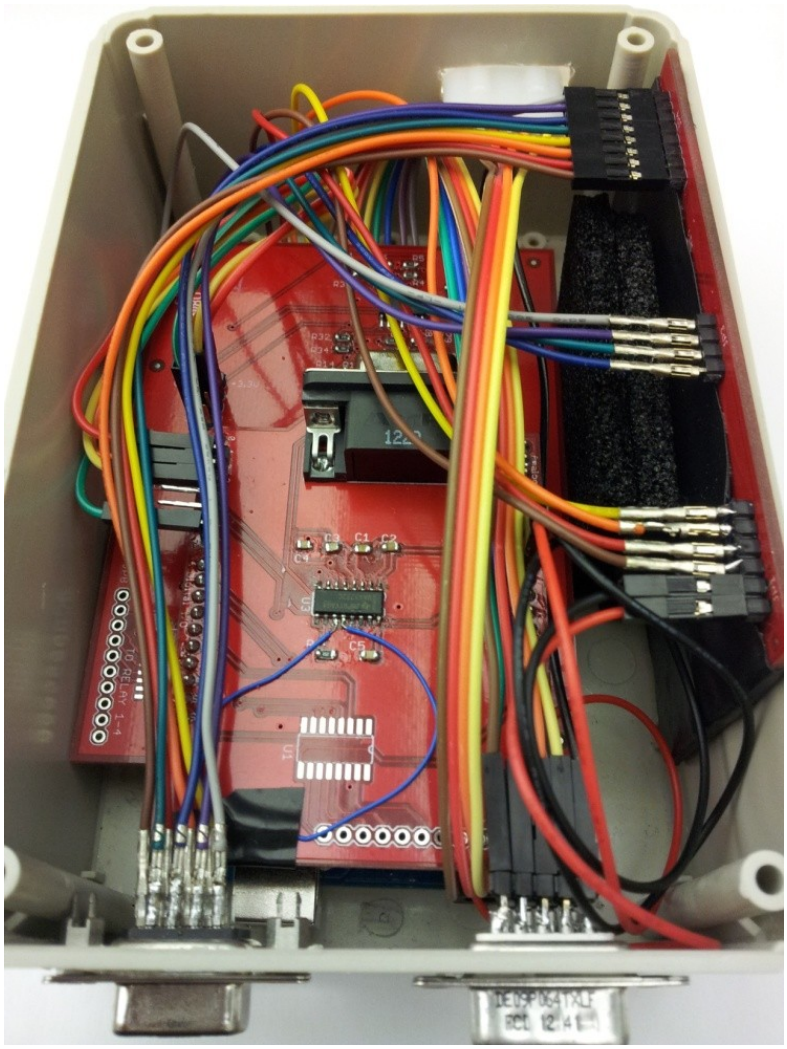

Figure 76. Local Controller for Level 2 Charging Station with GFCI

In order to have the fastest response time, the interaction between the GFCI board and the microprocessor is handled by the interrupt routine in the firmware as shown in Figure 77.

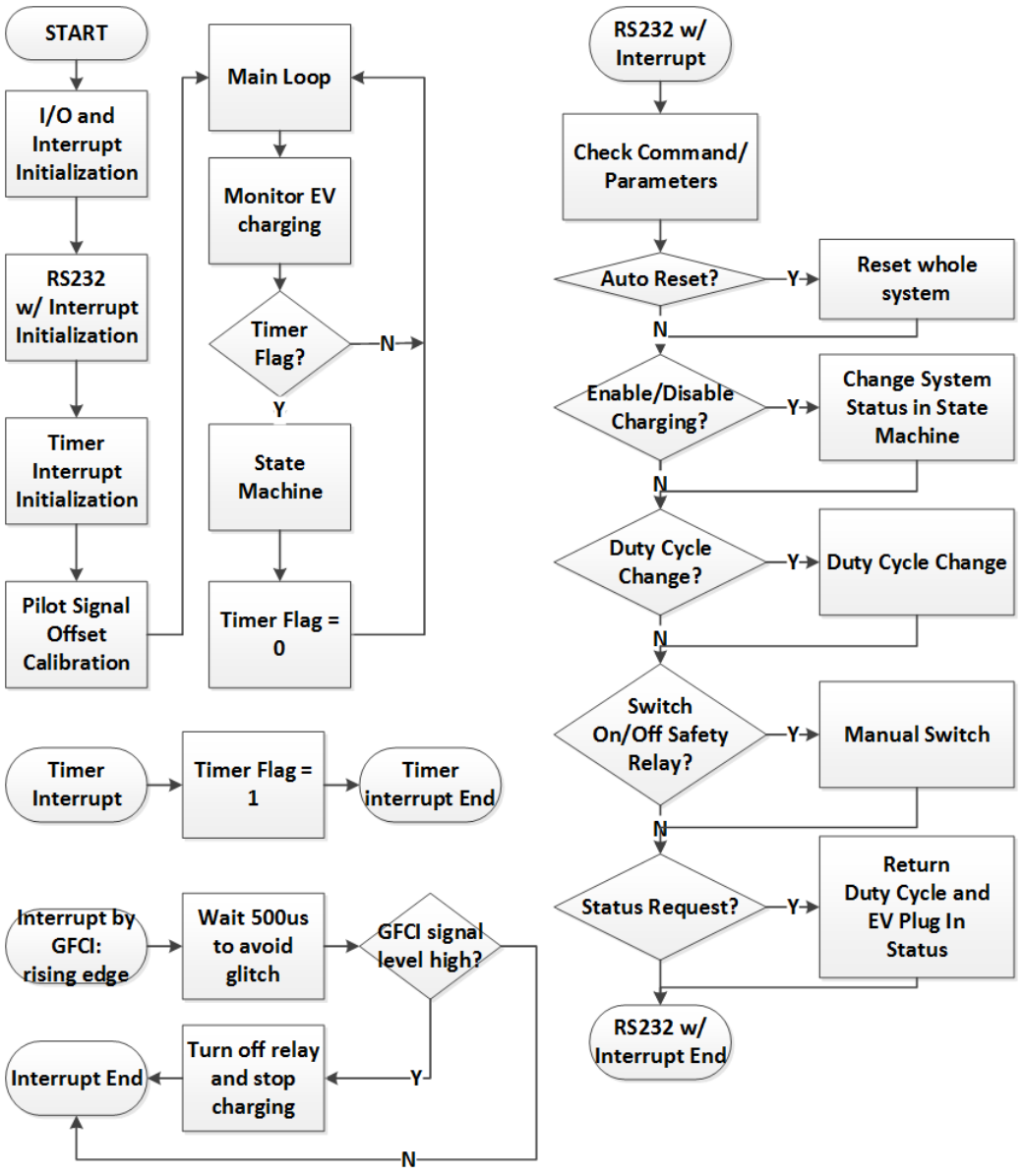

Figure 77. Local Controller Firmware Flow Chart

In the implementation of the GFCI function, four interrupt pins are used to monitor the outputs from the GFCI board with a rising edge trigger. In order to avoid a false alarm caused by the glitch at the rising edge, after an interrupt triggers, digital pins with a 500μs delay in the interrupt loop monitor the four outputs of the GFCI. If the controller detects the output pin is High, it terminates the power to the PEV by turning off the specific relays SW2, thus shutting off the contactor SW4 in Figure 75.

When the GFCI of the outlet is triggered, the system status of the state machine for the outlet will change to "Unplug Check"; the local controller keeps monitoring the plug-in status until the user unplugs the PEV. The GFCI of the outlet will be reset after the user unplugs the PEV.

The experiments on the detection of PEV plug-in status and the test of GFCI are performed and verified as follows. The trigger level and delay of the GFCI circuit are measured in this experiment with the circuit shown in Figure 78 and Figure 79.

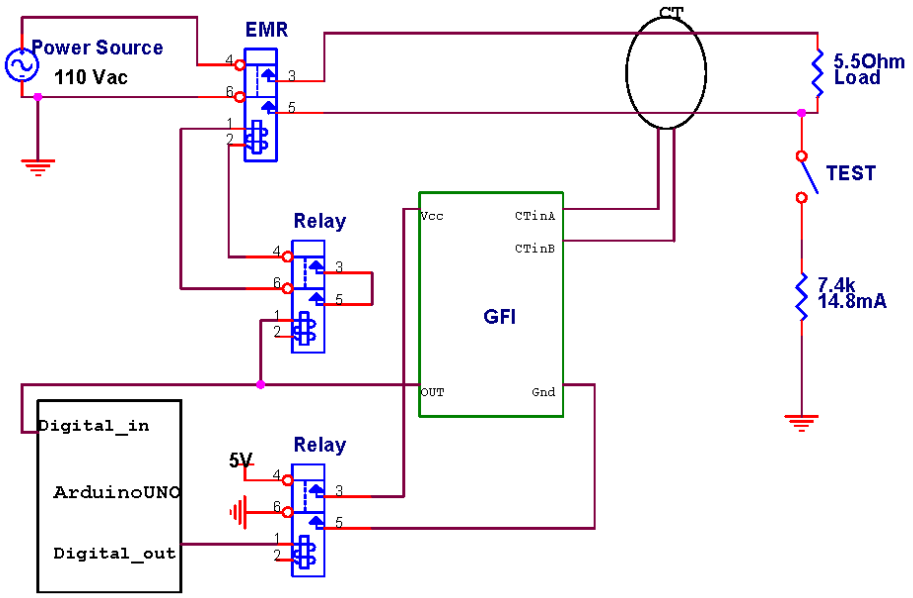

Figure 78. Schematics of GFCI Test [50]

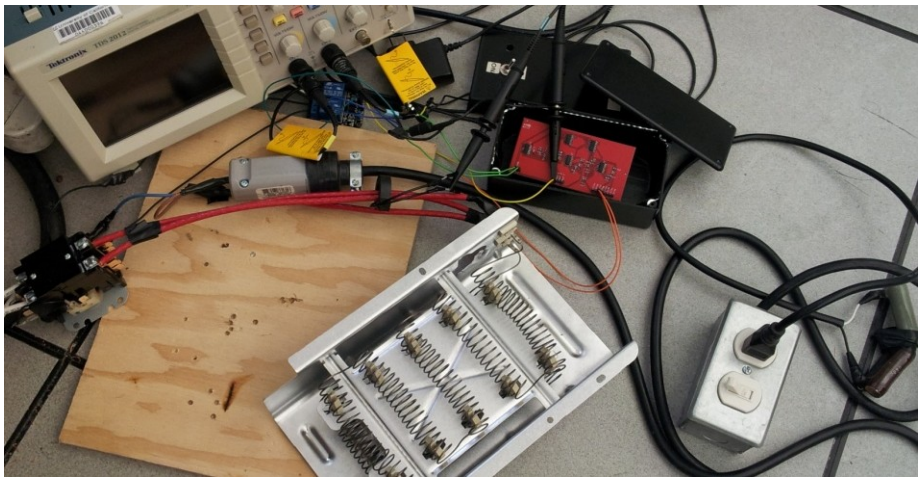

Figure 79. Setup for GFCI Experiments [50]

In order to see the trigger level and delay time, instead of flipping the TEST switch, which causes a larger signal to trigger the circuit, we use the following experimental procedure: (1) Test switch On; (2) GFCI is On; (3) Relay is On. Figure 80 shows the result of the experiment.

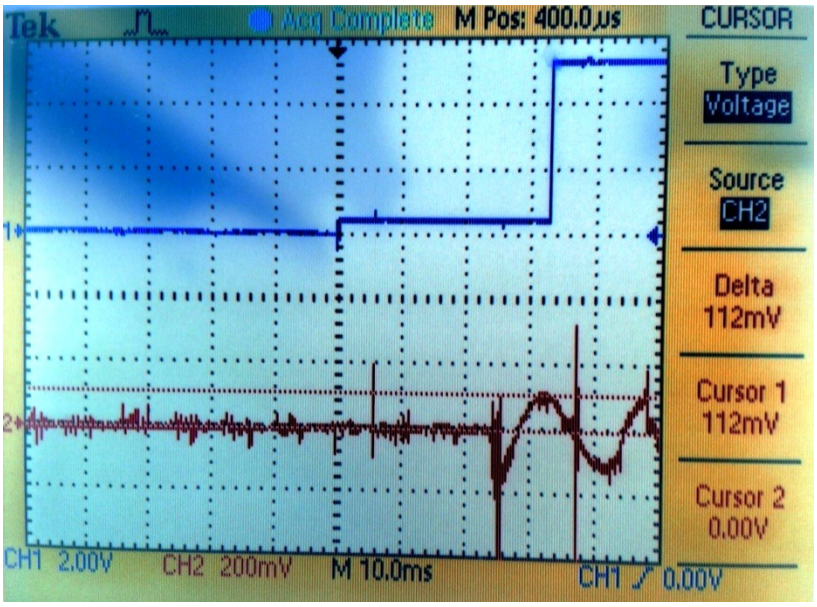

Figure 80. Results of GFCI Test [50]

Channel 1 (Blue) is the GFCI trigger signal, and channel 2 (Red) is the output of the CT. The result shows that the relay in Figure 78 has approximately 25ms delay after GFCI turns ON. When there is a 14mA difference between the hot wires, which is 110mV here according to the specification of CT, the GFCI becomes triggered on the positive cycle. The results also show that the GFCI circuits have approximately 1ms delay. The GFCI must be be enclosed in a grounded metal surface box to negate the electromagnetic disturbance from the electro-magnetic relay; the electromagnetic disturbance can also be mitigated by adding power and ground layer to the GFCI board. The GFCI was tested at least 300 times on each of the four channels, with a 21A load current on each channel, resulting in no failure.

As mentioned above, the GFCI becomes triggered by a 14mA difference between two hot wires on the positive cycle. If an abnormal diversion of current from a hot wire occurs on the

negative cycle, the GFCI trigger will be delayed by 8.3ms, a half cycle of 60Hz. In addition, the GFCI circuit itself has an approximate delay of 1ms. Compared to the maximum delay time of 8.3ms after the GFCI becomes triggered, a 500us delay time is acceptable in this GFCI design. To satisfy the safety requirement set by UL, the total delay of GFCI function should meet the maximum value of 24.9ms. The maximum delay in our proposed GFCI is 9.8ms, which satisfies this safety standard.

The UL safety standard also requires extra circuits such as a GFCI tester and voltage monitor on the contactors. The GFCI tester is the circuit to test the GFCI functionality before energizing the contactor. A solution for the GFCI tester is to add an extra wire in the current sensor from a 12V dc source; the local controller then turns on a specified small current on this wire using a digital output with a Darlington transistor and a power resistor. The voltage detector is a circuit that detects if the contactor is welding before enabling the contactor. When the contactor is welding, the charging station cannot stop power to the outlet. So there needs to be a way for the system to stop providing service. A possible solution is to use a voltage divider with power resistors to obtain a small AC voltage. In this case, a transformer is inserted in between to isolate the AC and DC voltage. Consequently, the local controller detects this DC voltage with a Schmitt trigger through its digital input pin to see if there is voltage on the charging station's outlet.

Once the safety feature is certified, the UL does not allow a firmware change by checking the firmware's CRC code. In order to have the flexibility to add new features to the firmware, the separation of a safety feature from the other functions is needed, since the safety function is not changing all the time. Therefore, one possible solution is to use an extra microprocessor to handle the safety features while the original one deals with the other functions. In this way, the charging station can keep up-to-date with new features while satisfying the UL certification.

5.2.2 PEV Plug-in Detection

According to J1772 specification [20], the PEV plug-in status is detected with the pilot signal generated in the charging station. When there is no PEV connected to the charging station, the voltage of the pilot signal pin on the handle should be +12V. After the user plugs in the PEV, the voltage of the pilot signal should be +9V or +6V depending on whether or not the PEV is ready to accept energy. The charging station initially generates the pilot signal with a duty cycle to indicate the charging station's allotted power. When the PEV is fully charged, the positive part of the pilot signal changes in range from +6V to +9V. When the user unplugs the PEV, the positive part of the pilot signal changes in range from +6V to +12V.

For the Level 1 charging station (EVSmartPlug^{TM}), PEV plug-in detection is handled by the trickle charge cable, where control of the pilot signal takes place.

For Level 2 charging station, the detection of the PEV plug-in status is implemented in the state machine of the firmware of the local controller in compliance with the J1772 standard. The Timer Flag is set to "1" in the timer interrupt loop. After the detection of PEV plug-in status process finishes, the Timer Flag is set to "0". Currently, the timer interrupt interval is set to 1 second in the firmware. This means the detection process is handled every 1 second. Note that the detection process' time needs to be less than the timer interrupt's interval so that the detection process can be handled correctly. Figure 81 shows the firmware flow of the pilot signal monitor.

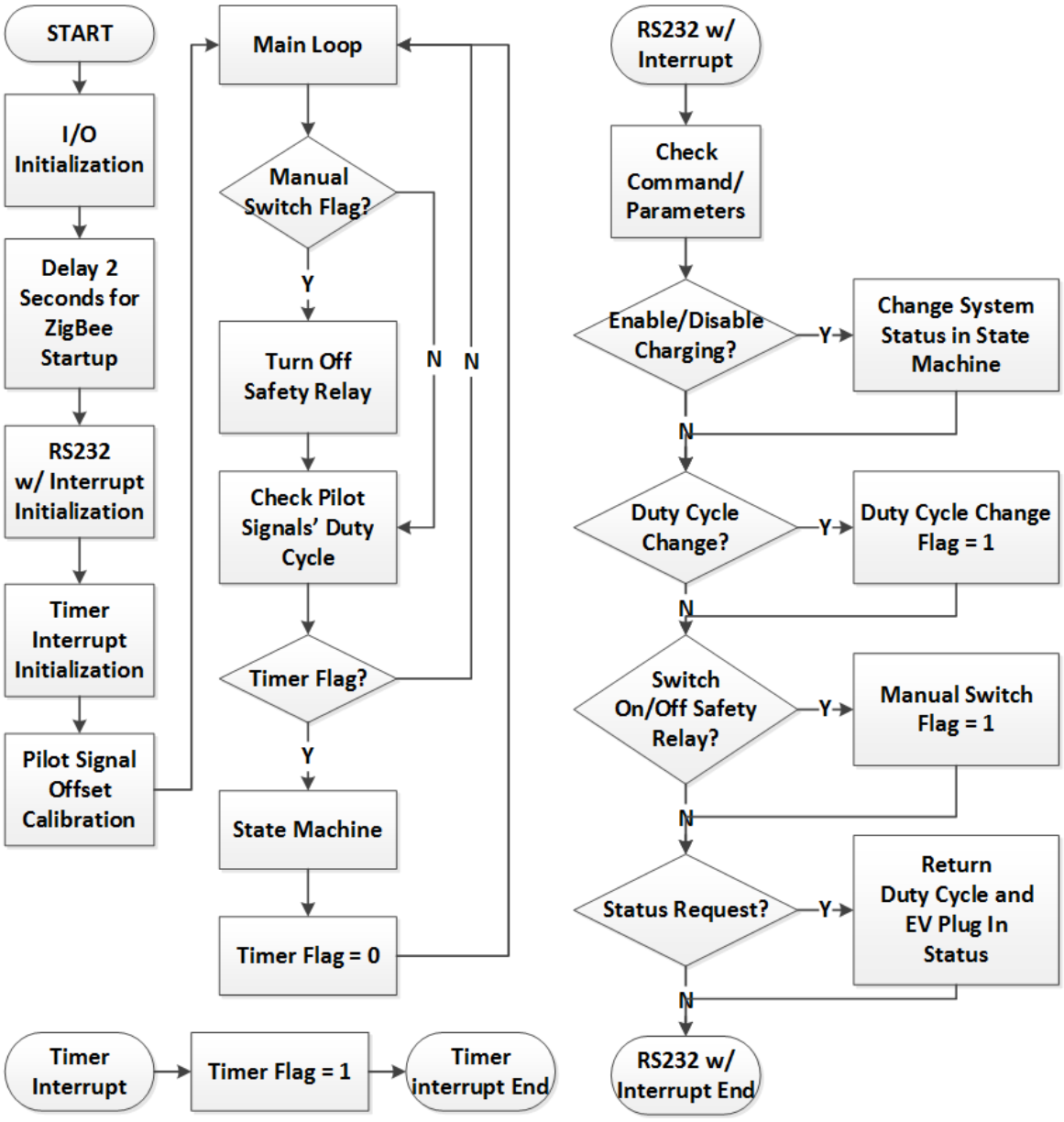

Figure 81. Firmware Flow of Pilot Signal Monitor [56]

Note that the PEV Plug-in Detection also serves as the trigger signal in the RFID authorization/authentication process in Chapter 2. The control center uses the PEV plug-in status to identify the presence of a PEV at a charging station and to associate the vehicle's ID with a particular charge outlet. The experiment's setup of PEV Plug-in Detection with different duty cycles is shown in Figure 82.

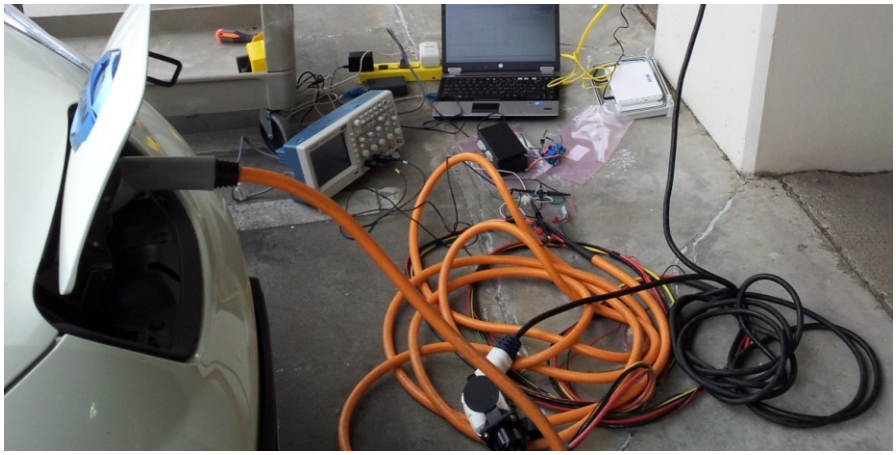

Figure 82. Experiment Setup for PEV Plug-in Detection [50]

In this experiment, the DC-converted pilot signal was measured at varying duty cycles for two distinct PEV states: PEV Disconnected and PEV Charging. The experimental results are shown in Figure 83.

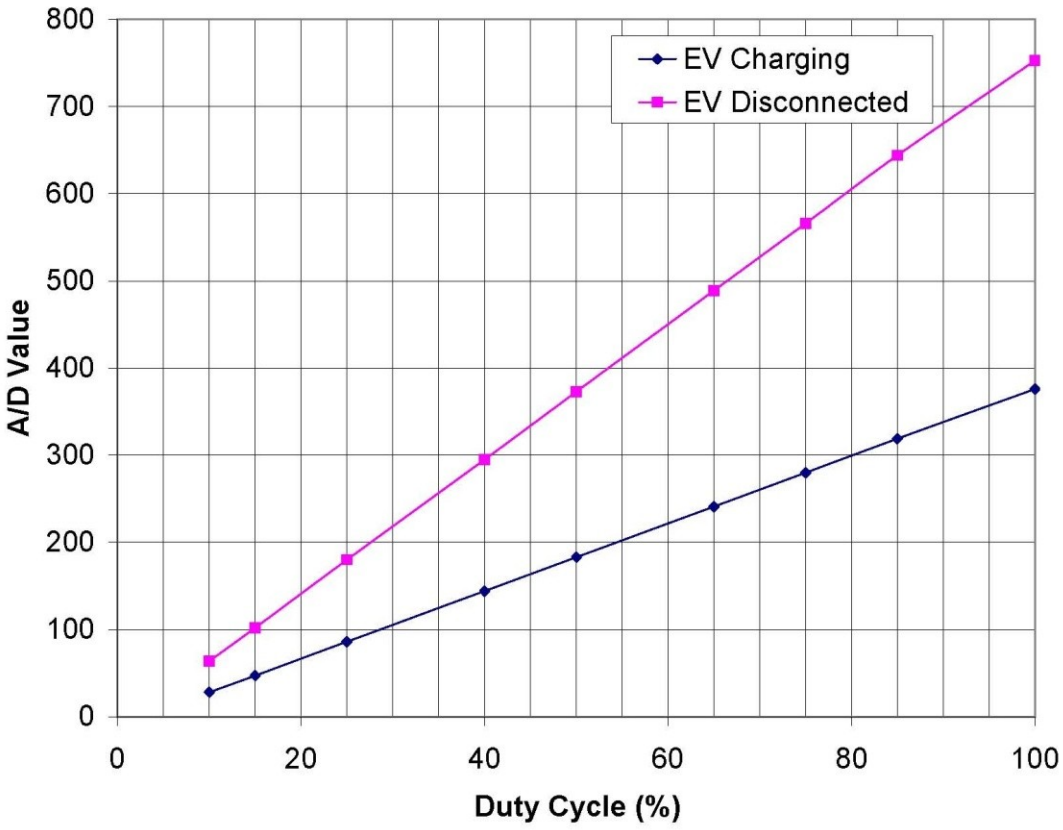

Figure 83. A/D Value vs. Pilot Signal Duty Cycle [50]

The results indicate that the DC values seen at the A/D converter are clearly distinguishable in these two states and have good linearity. Even when the duty cycle is around 10%, (or 6A – the minimum charging current set by the J1772 specification), the pilot signal monitor's resolution is sufficient to detect the PEV's plug-in status. The threshold value for detecting PEV plug-in status is set to be the average of these two states.

5.3 Summary

The prevention of electric hazards is first priority to PEV charging systems. When charging several PEVs from a single circuit, the total power consumption should fall within safety limits. When abnormal situations occur - for example, a PEV draws more current than the EVSE allocated to it - the control center should stop the PEV from charging to avoid causing a fire. In addition, the Plug-in Detection and GFCI at the station level protect the user from electrical shock. Thus, a safe and reliable charging infrastructure is achieved integrating safety mechanisms on all levels of control.

CHAPTER 6 SYSTEM RESPONSE TIME

As the PEV charging infrastructure increase in scale, the system response time becomes the key index of performance. In addition, the performance of the charging algorithms also counts heavily on the response time of the PEV charging infrastructure. In order to control the charging stations effectively, the system response time should be accelerated so that an efficient PEV charging infrastructure can be achieved. The system response time can be improved not only by the communication traffic between the control center and the charging stations but also the response time of the charging station. In section 6.1, the distribution of power information retrieval round trip time is measured and analyzed. As the communication traffic becomes the dominant factor in power information retrieval, reducing the number of round trips can be a solution to accelerate system performance. In section 6.2, the PEV's response time when changing the duty cycle of pilot signal is measured and formulated. When the response time of the charging station depends on the command type and parameters such as the pilot signal's duty cycle, the server waiting time should be a variable for faster system performance.

6.1 Response Time in Power Information Retrieval Case

In this section, the distributions of round trip time of power information retrieval are measured and presented. The round trip time of power information retrieval corresponds to the waiting time of the server for the response from the charging station after sending the command to retrieve power information. The round trip time, $T_{RoundTrip}$, is expressed in (6-1):

$$\begin{aligned} T_{RoundTrip} &= T_{Network} + T_{Metering} \\ &= \left(T_{Server\_Cloud} + T_{Cloud} + T_{Cloud\_Station}\right) + T_{Metering} \end{aligned} \tag{6-1}$$

$T_{Metering}$ stands for the time required by the meter to retrieve power information and it is

roughly estimated in the experiments. $T_{Network}$ includes the time required between the server and the charging station. The charging station can connect to the Internet through different networks including Ethernet, WiFi, and 3G, which makes $T_{Cloud\_Station}$ the dominant factor in the round trip time of power information between the server and the charging station, $T_{RoundTrip}$. Figure 84 shows the distribution of the round trip times. The round trip times were recorded every 5 minutes for one week under different network configurations. The upper chart corresponds to Ethernet while the lower chart to WiFi. In these two cases, we use $T_{Ethernet}$ and T_{WiFi} for $T_{Cloud\_Station.}$ Note that the server and the charging station use under the same default gateway in the experiment.

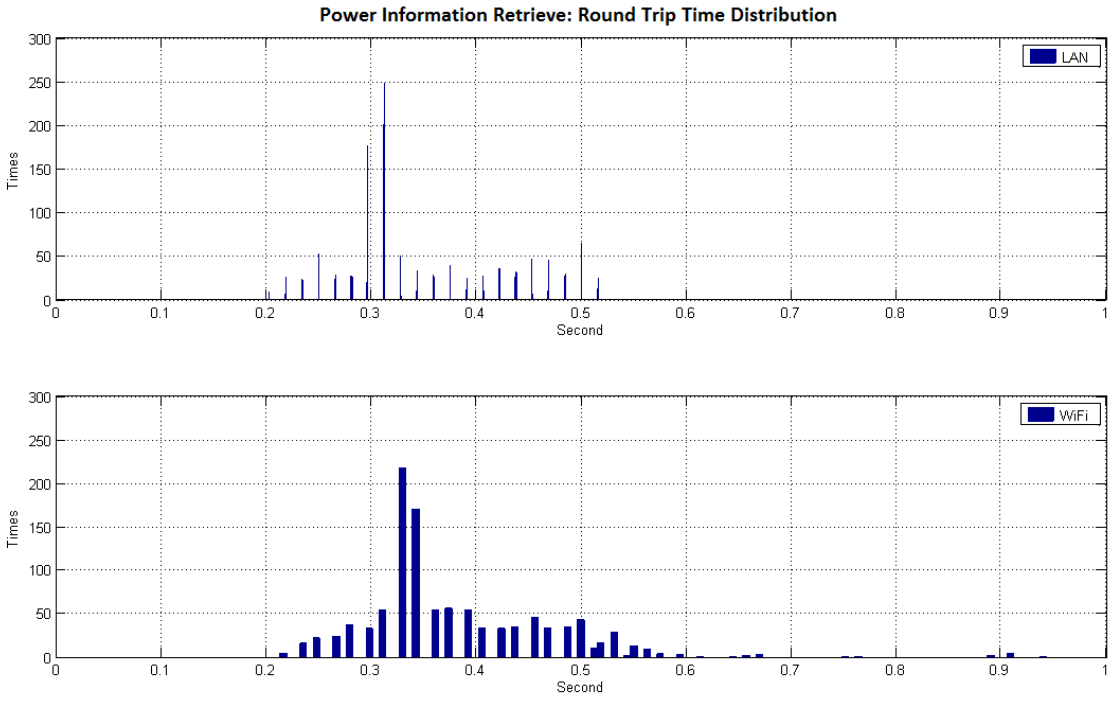

Figure 84. $T_{RoundTrip}$ with Ethernet (Upper) and WiFi (Lower) [60]

The experiment shows that the shortest $T_{RoundTrip}$ is around 0.2 seconds. Normally, when the server and the charging station are under the same default gateway with Ethernet, the $T_{Ethernet}$ is within the microsecond degree, which could be neglected in $T_{RoundTrip}$. T_{Cloud} is also approximate

to 0 in this case; therefore, $T_{RoundTrip}$ will be approximate to $T_{Meterging}$, which is expressed in (6-2):

$$T_{RoundTrip\_Ethernet} = (T_{Ethernet} + T_{Cloud}) + T_{Metering} \approx T_{Metering} \quad (6\text{-}2)$$

Here, $T_{Metering}$ is the dominant factor in the Ethernet case; therefore, the distribution of $T_{Metering}$ is approximate to $T_{RoundTrip}$. Compared to the Ethernet case, the lower chart of Figure 84 shows that T_{WiFi} is slightly slower than $T_{Ethernet}$. Note that $T_{Metering}$ is still the dominant factor in the WiFi case.

As for the 3G case, we measure $T_{RoundTrip}$ distributions of three charging stations in different locations - UCLA, LA downtown, and Santa Monica -in second, third, fourth charts in Figure 85. For purpose of comparison, the first chart of Figure 85 is the Ethernet case.

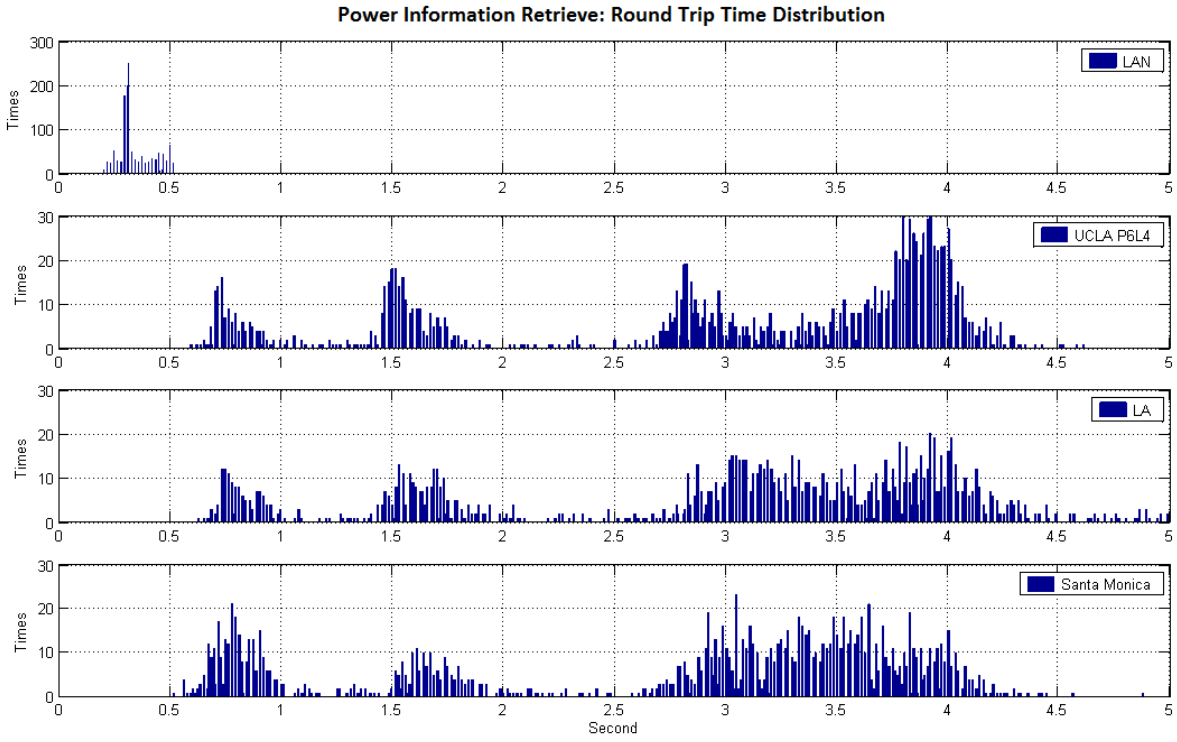

Figure 85. $T_{RoundTrip}$ with 3G in 3 Different Locations [60]

The round trip time $T_{RoundTrip}$ of 3G cases can be expressed in (6-3):

$$T_{RoundTrip\_3G} = \left(T_{Server\_Cloud} + T_{Cloud} + T_{3G}\right) + T_{Metering} \approx T_{3G} + T_{Metering} \quad (6\text{-}3)$$

The experiments show that T_{3G} is not a constant offset from the Ethernet case but a distribution probability with four peaks measured in its distribution. The distribution of round trip time in 3G cases, $T_{RoundTrip\_3G}$, shows no apparent difference in various locations; therefore, the round trip time model can be used in other places as long as they have the same configuration.

Because 3G connection quality is affected by people's usage in the cellular cell established by the base station, T_{3G} might vary during the day or the week. Figure 86 shows $T_{RoundTrip\_3G}$ for a charging station at UCLA during the week by day. The first chart of Figure 86 is $T_{RoundTrip\_3G}$ during a week and the x-axis of the first chart stands for seven days. (0 to 1 is Sunday, 1 to 2 is Monday, etc.) The second and third charts are the $T_{RoundTrip\_3G}$ on Sunday and Monday.

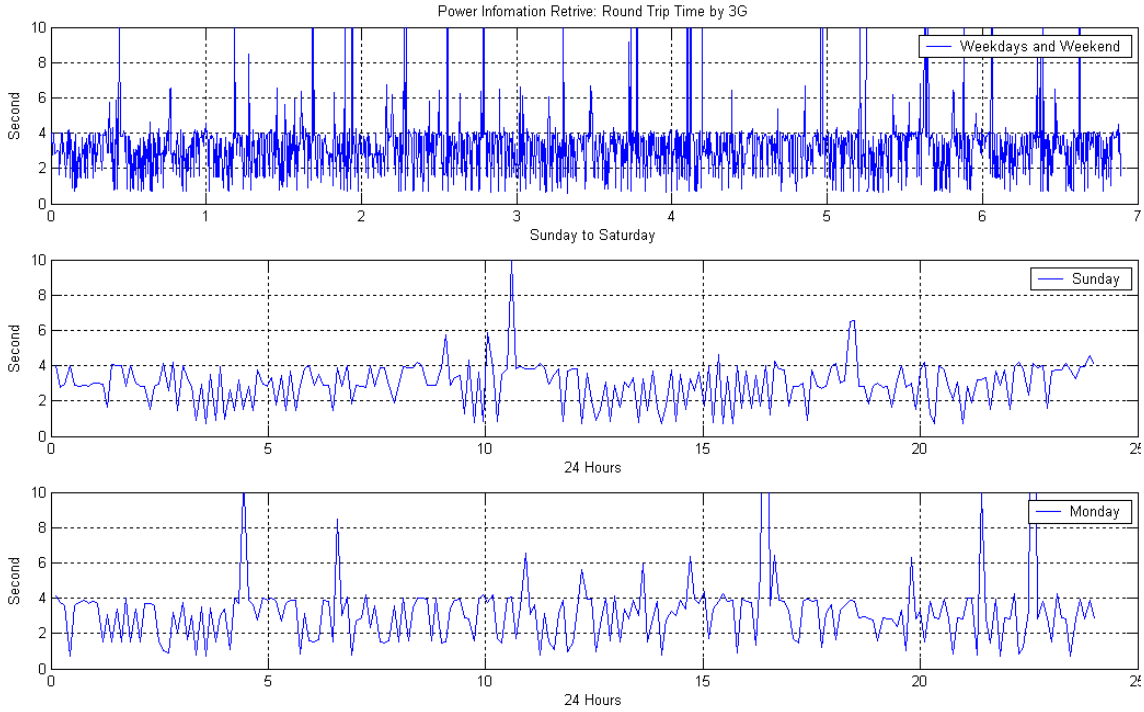

Figure 86. $T_{RoundTrip\_3G}$ during the Week and the Days [60]

The results show that $T_{RoundTrip\_3G}$ are faster during certain hours of Sunday and Monday, but the range of distribution is no different in these two cases. Therefore, the following analysis is not significantly affected by the variability between charging on week versus weekend days. The time required to retrieve power information $T_{Retrieval}$ of four meters in a single charging station is expressed in (6-4)

$$T_{Retrieval} = 4T_{RoundTrip\_3G} \approx 4\left(T_{3G} + T_{Metering}\right) \tag{6-4}$$

Equipped with the Power Information Collector (PIC) mentioned in Chapter 3, only one time request is required and $T_{Metering}$ is eliminated by its periodic retrievals. This leaves only T_{3G} for $T_{Retrieval}$, which makes the system 4.4 times faster than the original system. When taking the On/Off status retrieval into account, the PIC accelerates the whole system by 8.4 times. The system performance could be further accelerated by setting the PIC to be a data pushing device, which periodically sends power information to the server; the server can obtain the meters' information without waiting, which greatly improves the system's performance.

In order to retrieve data from a charging station's four meters in the 3G case of the data pull system, from (6-5), the control center needs to wait:

$$T_{Retrieval} = 4T_{RoundTrip\_3G} \approx 4\left(T_{3G} + T_{Metering}\right) \tag{6-5}$$

From the experiments, when we take the longest time into account, the control center needs to wait 20 seconds to finish power information retrievals. With PIC, only one time request is require and $T_{Metering}$ is eliminated by its periodic retrievals. This reduction in requests leaves only time T_{3G} for the server to retrieve power information. Because T_{3G} is 4.5 seconds in the longest case scenario, the new PIC system is 4.4 times faster than the original system. The new PIC

system is 8.4 times faster when taking the On/Off status retrieval into account.

The system performance can be further improved by setting the PIC to be a data pushing device, which means it periodically sends the power information from the meters to the control center. The control center can have the meters' power information without waiting, which greatly improves the performance of the system. One concern is that the power information is not real time data. From the experiments, the PIC can retrieve the power information of one meter locally within ($T_{Ethernet}$+$T_{Metering}$), which is less than 1 second. To finish the power information retrieval of four meters and report these data to the control center, it will take

$$T_{\mathrm{R}etrieval\_PIC} = 4T_{Ethernet} + 4T_{Metering} + 0.5T_{3G} \tag{6-6}$$

Subtract (6-6) from (6-5), we get

$$\begin{aligned} & T_{save} \\ & = T_{\mathrm{R}etrieval} - T_{\mathrm{R}etrieval\_PIC} \\ & = 4\left(T_{3G} + T_{Metering}\right) - \left(4T_{Ethernet} + 4T_{Metering} + 0.5T_{3G}\right) \\ & = 3.5T_{3G} - 4T_{Ethernet} \\ & \approx 3.5T_{3G} \end{aligned} \tag{6-7}$$

Compared to the power information retrieval time of the original system, the control center could save $3.5T_{3G}$ in power information retrieval, which is 17.5 seconds in the worst case. Therefore, the data pushing system is much faster than the original system.

From the comparison of the required number of commands in the Enable/Disable charging process in Chapter 3, the response time of the charging station in both processes is improved because the number of round trips for commands and responses between the server and the charging station is reduced. **TABLE** 14 summarizes the total time required in the Enable/Disable charging processes of three systems

TABLE 14. COMPARISON OF TIME REQUIRED FOR CHARGING PROCESS

Time Required	Original System	System with PIC	System with PIC plus Pushing Data
Power Information	$4T_{Retrieve}$	$T_{Retrieve}$	$0.5T_{3G}$
Outlet Status	$4T_{Retrieve}$		
Enable/Disable Charging	T_{3G}	T_{3G}	T_{3G}
Outlet Status	$4T_{Retrieve}$	$T_{Retrieve}$	$0.5T_{3G}$
Power Information	$4T_{Retrieve}$		
Total Time	$16T_{Retrieve} + T_{3G}$	$2T_{Retrieve} + T_{3G}$	$2T_{3G}$
Total Time, Slowest Case (sec)	84.5	14.5	9
Times Faster Compared to Original System	1	5.83	9.39

The results show that the PIC dramatically accelerates the Enable/Disable process by 5.83 times in the slowest case. By setting the PIC to be a data pushing device, the system response time is further shortened by 9.39 times of the original system in the slowest case, compared to the original system.

6.2 Server Waiting Time for Duty Cycle Change

In the experiment, we measure the PEV's response time with the pilot signal change command. The testbed is a Nissan Leaf with a 110V charging cable. Figure 87 shows the setup for the experiment.

Figure 87. Experiment Setup for Changing Pilot Signal Duty Cycle [56]

To insert and swap our pilot signal with the original signal from the charging cable, a J1772 adaptor is made as shown in Figure 88.

Figure 88. J1772 Adaptor [56]

Figure 89 shows the comparison between the original pilot signal (yellow) and our pilot signal (blue).

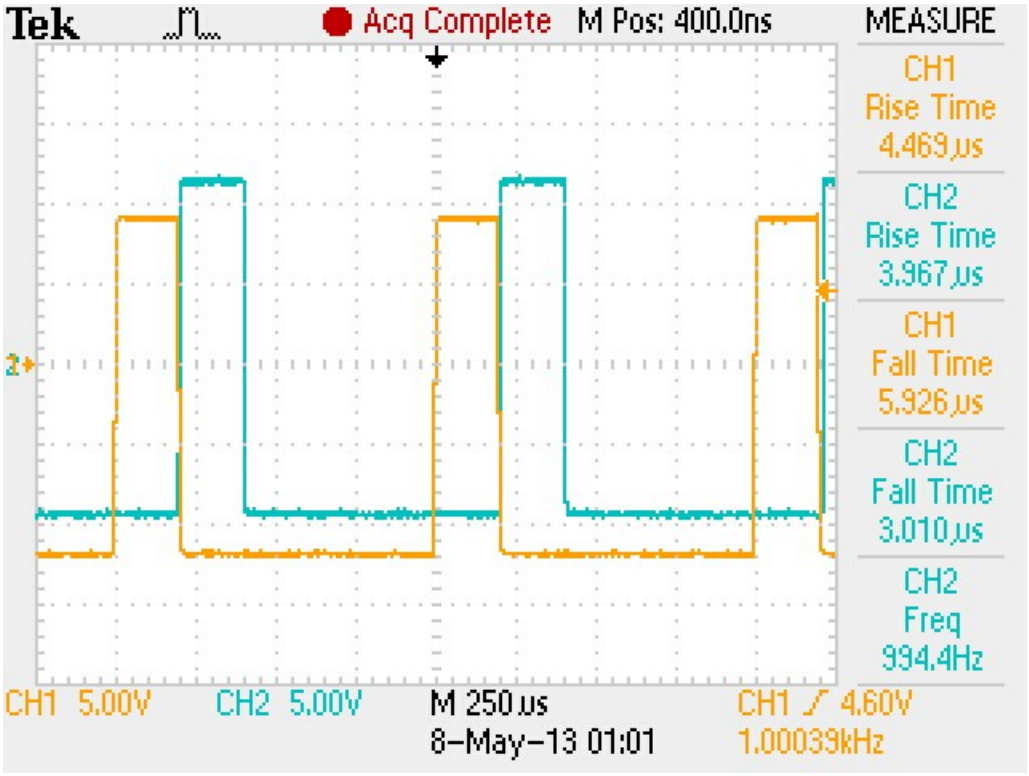

Figure 89. Comparison between 2 Pilot Signals [56]

The frequency of our pilot signal (994 Hz) is in the range of the J1772 specification (980~1020 Hz). The rise time (3.9 µs) and the fall time (3 µs) of our pilot signal are slightly over the values specified in J1772 (2 µs). However, compared with the pilot signal of the commercial charging cable (yellow), our pilot signal (blue) is better in both cases of rise time and fall time, which means our signal would work with commercial PEV.

Four cases were tested in the experiments including: (1) 0A to 12A, (2) 12A to 0A, (3) 8A to 12A, and (4) 12A to 8A, which covers the cases of switching between high and low current. The results are show in Figure 90, Figure 91, Figure 92, and Figure 93. Channel 1 (yellow) is the current taken by the PEV while channel 2 (blue) is the pilot signal.

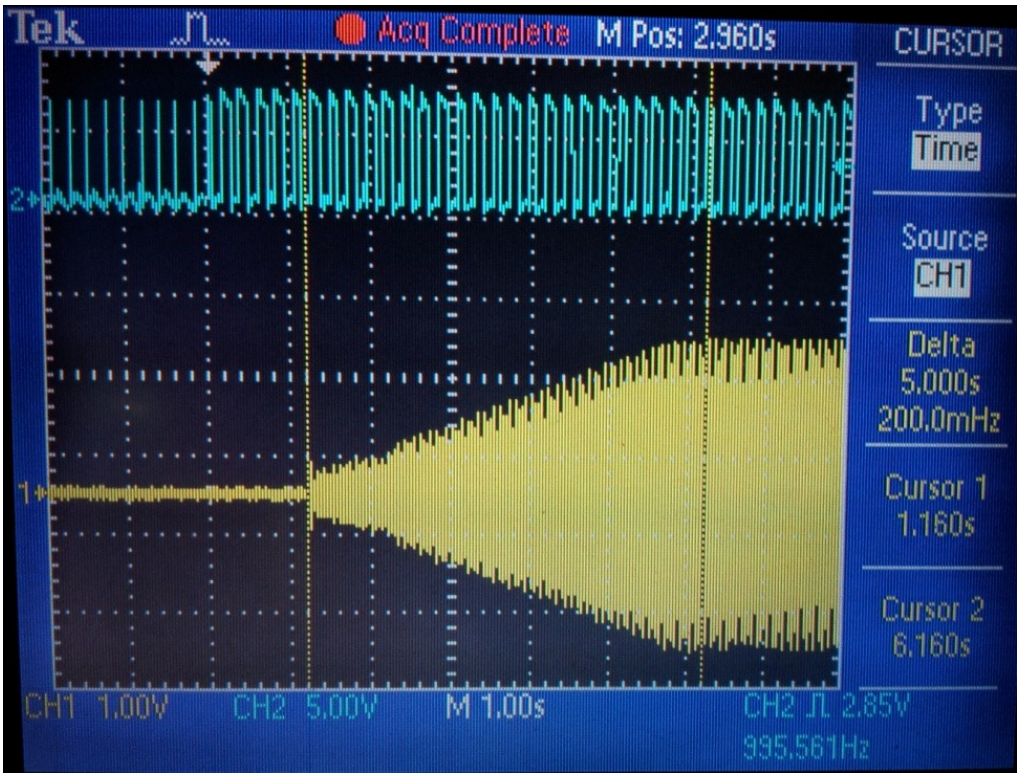

Figure 90. From 0A to 12A [56]

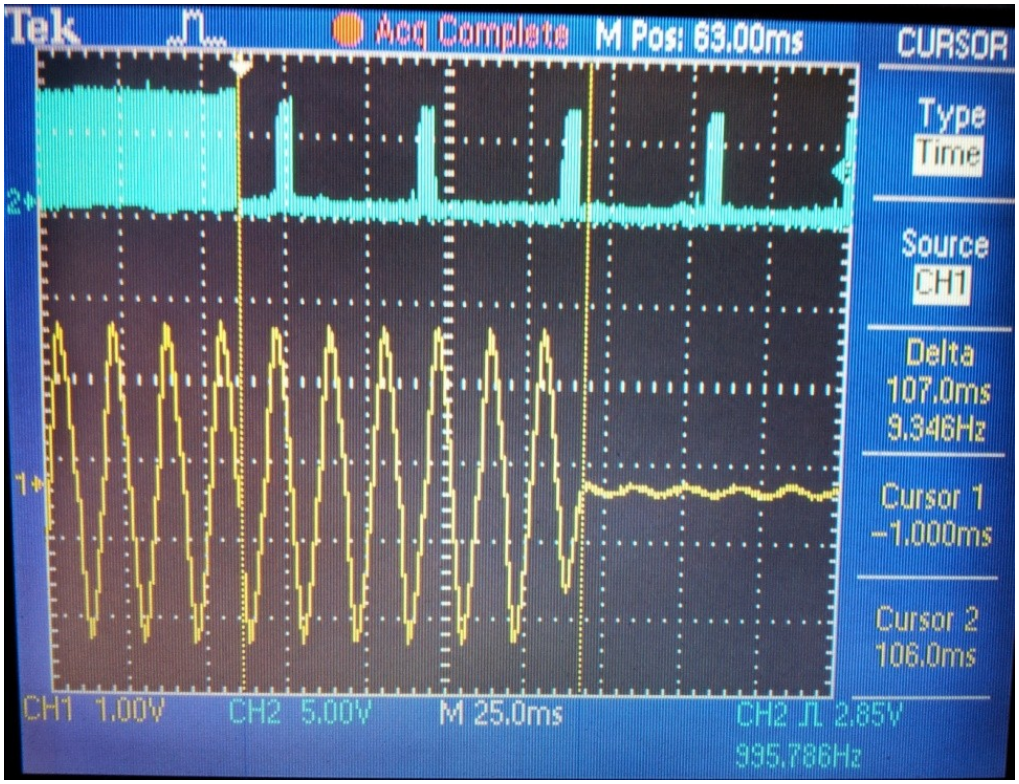

Figure 91. From 12A to 0A [56]

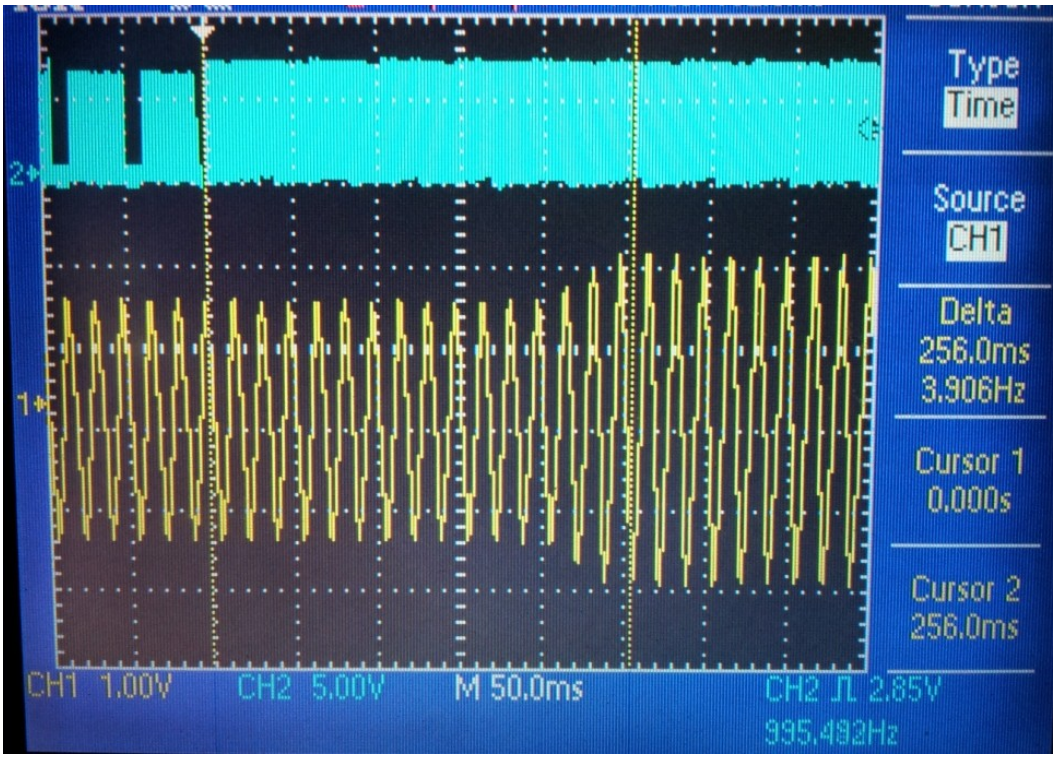

Figure 92. From 8A to 12A [56]

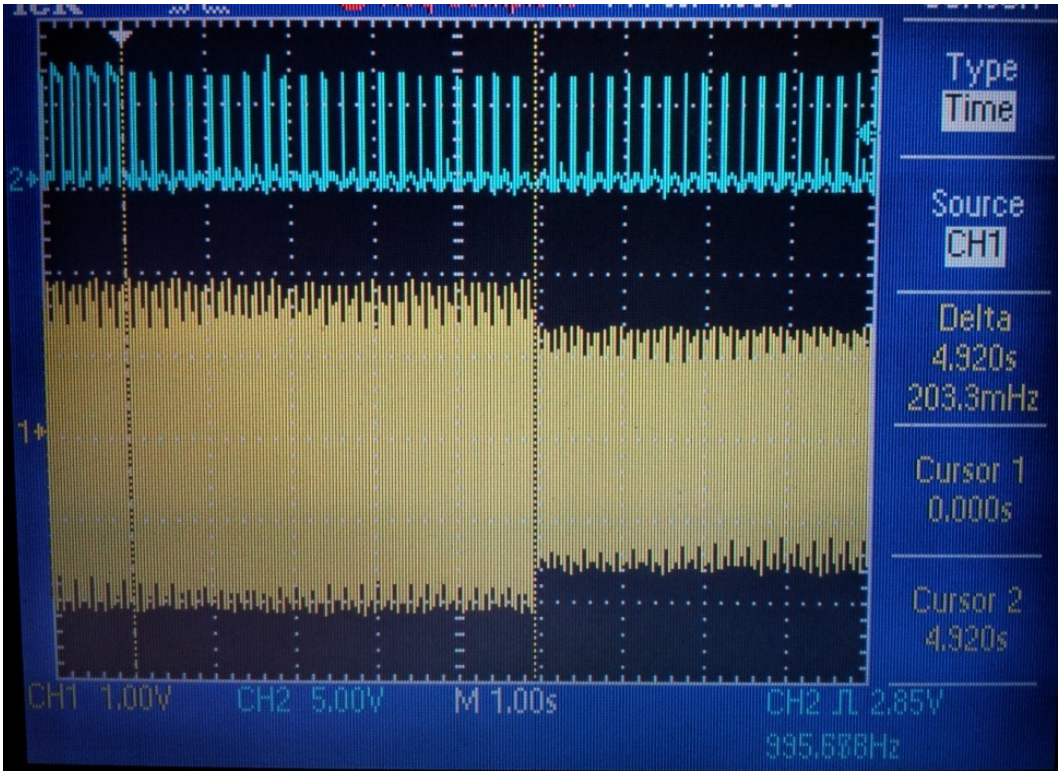

Figure 93. From 12A to 8A [56]

Note that in Level 1 (110V) charging, even though the server sets the duty cycle larger than 20%, which makes the maximum current capable of being larger than 12A, the Nissan leaf will only take 12A. Here we define T_{EvExe} to be the time between the PEV receiving the command and it starting to change the current; T_{EvResp} is the time between the PEV starting to change the current and when it is settling down. T_{EV} is the summation of T_{EvExe} and T_{EvResp} which can be expressed in (6-8).

$$T_{EV} = T_{EvExe}(I_{init}, I_{final}) + T_{Ev\,Resp}(I_{init}, I_{final}) \tag{6-8}$$

The experiments are summarized in **TABLE** 15. Notice from the experiments, the T_{EvExe} and T_{EvResp} are related to both the initial current I_{init} and final current I_{final}.

TABLE 15. PEV RESPONSE TIME (NISSAN LEAF)

	I_{init} (A)	I_{final} (A)		
		0	8	12
T_{EvExe} (ms)	0		1000	1000
	8	100		250
	12	100	5000	
T_{EvResp}(ms)	0		3000	5000
	8	10		60
	12	10	60	
T_{EV} (ms) = T_{EvExe} + T_{EvResp}	0		4000	6000
	8	110		310
	12	110	5060	

In the case of I_{final}=0A, T_{EvExe} is 100 ms and T_{EvResp} is 10 ms, which are relatively faster than other cases. It is possible that the PEV could turn off its switch in 100 ms without changing its load and 10 ms would be the transient response to 0A. In the case of I_{init}=0A, T_{EvExe} is 1000 ms and T_{EvResp} is proportional to the final current. It is possible that the PEV turns on its switch in 1000 ms and starts to consume a current proportional to the final current. In the case of I_{init}=12A and I_{final}=8A, T_{EvExe} is 5000 ms. It is because the PEV's battery management system needs to balance the battery cells and then change its load.

The timing analysis of the whole system can be further analyzed to improve the performance. The time for returning of changing duty cycle T_{Return} can be expressed as (6-9):

$$\begin{aligned} T_{\mathrm{Return}} &= T_{ControlUnit} + T_{GatewayServer} \\ &= T_{ZigBee} + T_{3gUplink} + T_{Cloud} \end{aligned} \tag{6-9}$$

Let $T_{waiting}$ be the waiting time after receiving the successful return of the pilot signal duty cycle change and before sending the power information request. The waiting time $T_{waiting}$ at server side plug T_{Return} is required to be greater than T_{EV}, which can be expressed in (6-10).

$$\begin{aligned} & T_{\mathrm{Return}} + T_{waiting} \\ & \approx \left(T_{ZigBee} + T_{3gUplink} + T_{Cloud}\right) + T_{waiting} \\ & \approx T_{3gUplink} + T_{Cloud} + T_{waiting} \\ & > T_{EV} = T_{EvExe}(I_{init}, I_{final}) + T_{Ev\,\mathrm{Re}sp}(I_{init}, I_{final}) \end{aligned} \tag{6-10}$$

We can rewrite (6-10) to be (6-11).

$$\begin{aligned} & T_{waiting} > T_{EV} - T_{\mathrm{Return}} \\ & \approx T_{EvExe}(I_{init}, I_{final}) + T_{Ev\,\mathrm{Re}sp}(I_{init}, I_{final}) - \left(T_{3gUplink} + T_{Cloud}\right) \end{aligned} \tag{6-11}$$

From (6-11), we can see $T_{waiting}$ depends on I_{init}, I_{final}, and the communication traffic. To speed up the system performance, $T_{waiting}$ can be set to be various values depending on I_{init} and I_{final}, rather than a fixed value.

The experimental data in [57] can be represented by (6-12) and (6-13).

$$T_{EvExe}(I_{init}, I_{final}) = \begin{cases} 1000 & , I_{init} = 0 \\ 100 & , I_{final} = 0 \\ 250 & , I_{init} < I_{final} \\ 5000 & , I_{init} > I_{final} \end{cases} \tag{6-12}$$

$$T_{Ev\,\mathrm{Re}sp}(I_{init}, I_{final}) = \begin{cases} 400 \times I_{final} & , I_{init} = 0 \\ 10 & , I_{final} = 0 \\ 60 & , otherwise \end{cases} \tag{6-13}$$

Therefore,

$$
\begin{aligned}
T_{EV} &= T_{EvExe}(I_{init}, I_{final}) + T_{Ev\,Resp}(I_{init}, I_{final}) \\
&= \begin{cases} 1000 + 400 \times I_{final} & , I_{init} = 0 \\ 110 & , I_{final} = 0 \\ 310 & , I_{init} < I_{final} \\ 5060 & , I_{init} > I_{final} \end{cases}
\end{aligned} \tag{6-14}
$$

The time of returning the duty cycle T_{Return} is expressed in (6-15)

$$
\begin{aligned}
T_{Return} &= T_{ControlUnit} + T_{GatewayServer} \\
&= T_{ZigBee} + T_{3gUplink} + T_{Cloud}
\end{aligned} \tag{6-15}
$$

Set $T_{waiting}$ to be the waiting time between the successful return from the change in the pilot signal duty cycle and the power information request, which is expressed in (6-16)

$$
\begin{aligned}
& T_{Return} + T_{waiting} \\
& \approx \left(T_{ZigBee} + T_{3gUplink} + T_{Cloud}\right) + T_{waiting} \\
& \approx T_{3gUplink} + T_{Cloud} + T_{waiting} \\
& > T_{EV} = T_{EvExe}(I_{init}, I_{final}) + T_{Ev\,Resp}(I_{init}, I_{final})
\end{aligned} \tag{6-16}
$$

Rewrite (6-16), $T_{waiting}$ is expressed in (6-17)

$$
\begin{aligned}
& T_{waiting} > T_{EV} - T_{Return} \\
& \approx T_{EvExe}(I_{init}, I_{final}) + T_{Ev\,Resp}(I_{init}, I_{final}) - \left(T_{3gUplink} + T_{Cloud}\right) \\
& = \begin{cases} 1000 + 400 \times I_{final} - \left(T_{3gUplink} + T_{Cloud}\right) & , I_{init} = 0 \\ 110 - \left(T_{3gUplink} + T_{Cloud}\right) & , I_{final} = 0 \\ 310 - \left(T_{3gUplink} + T_{Cloud}\right) & , I_{init} < I_{final} \\ 5060 - \left(T_{3gUplink} + T_{Cloud}\right) & , I_{init} > I_{final} \end{cases}
\end{aligned} \tag{6-17}
$$

From (6-17), $T_{waiting}$ depends on I_{init} and I_{final}. In [60], T_{Cloud} can be ignored compared with T_{3G}. Assume that $T_{3gUplink}$ is approximately half of T_{3G}, which is the round trip time between the cloud and the charging station. Therefore, (6-17) can be rewritten as (6-18)

$$T_{Waiting} > \begin{cases} 1000 + 400 \times I_{final} - 0.5 \times T_{3G} & , I_{init} = 0 \\ 110 - 0.5 \times T_{3G} & , I_{final} = 0 \\ 310 - 0.5 \times T_{3G} & , I_{init} < I_{final} \\ 5060 - 0.5 \times T_{3G} & , I_{init} > I_{final} \end{cases} \quad (6\text{-}18)$$

With further information from I_{init} and I_{final}, $T_{waiting}$ can be set to be variable values based on I_{init} and I_{final} rather than a fixed value in order to accelerate the performance of the system.

The system performance can be improved by adjusting the waiting time of the server, $T_{waiting}$. $T_{waiting}$ starts after the server receives the successful return of the change in the pilot signal's duty cycle and ends before sending the power information request. $T_{waiting}$ can be expressed in (6-19),

$$T_{Waiting} > T_{EV} - \left(T_{3gUplink} + T_{Cloud}\right) \quad (6\text{-}19)$$

where T_{Ev} stands for the time between the PEV receiving the command to change the current and settling down the current change. Note that T_{EV} depends on the initial current I_{init} and final current I_{final}. From the experiment T_{Cloud} can be neglected compared to T_{3G}. Let's assume that $T_{3gUplink}$ is approximately half of T_{3G}, which is the round trip time between the cloud and the charging station; therefore, we can rewrite (6-19) into (6-20):

$$T_{Waiting} > T_{EV} - 0.5T_{3G} \quad (6\text{-}20)$$

The maximum value of the T_{EV} is 6 seconds and T_{3G} falls in the range of 5 seconds in most cases in the experiments. Therefore, the maximum value of $T_{waiting}$ could be 3.5 seconds on the server for the 3G case to cover most of cases. With information from I_{init} and I_{final}, $T_{waiting}$ can be set to a lower value rather than a fixed value to speed the system's performance.

The command sets for the server and return values from the charging station is summarized as follows. Based on the experiments the server waiting time for the command sets are formulized and summarized in Table 16.

TABLE 16. WAITING TIME OF COMMAND SETS

Command	Description	Waiting Time
atrs	Auto-reset the charging station	$T_{Waiting} > 0.5T_{3G} + T_{GatewayStartUp}$
duty	Change the duty cycle of pilot signal	$T_{Waiting} > \begin{cases} 1000 + 400 \times I_{final} - 0.5 \times T_{3G} & , I_{init} = 0 \\ 110 - 0.5 \times T_{3G} & , I_{final} = 0 \\ 310 - 0.5 \times T_{3G} & , I_{init} < I_{final} \\ 5060 - 0.5 \times T_{3G} & , I_{init} > I_{final} \end{cases}$
enab	Enable EV charging	$T_{Waiting} > T_{3G} + T_{EnableCharging\,Process} + T_{Ev\,Resp}$
rely	Turn on/off relay manually	$T_{Waiting} > T_{3G}$
rest	Disable EV charging	$T_{Waiting} > T_{3G}$
resp	ZigBee handshake response	$T_{Waiting} = 0$
rgst	Return all registered ZigBee MAC address	$T_{Waiting} > T_{3G} + T_{GatewayUSB\_timeout}$
stat	Charging station status request	$T_{Waiting} > T_{3G} + T_{GatewayUSB\_timeout}$
test	ZigBee handshake request	$T_{Waiting} = 0$

In order to accelerate the server's performance, the server's waiting time should be set to different values according to the command set from Table 16. In the case of duty cycle change, to shorten the server's waiting time $T_{waiting}$, it can be set to variable values based on I_{init} and I_{final} rather than a fixed value to satisfy all conditions. Moreover, the simulation of the change in the pilot signal's duty cycle in chapter 3 shows it takes 30ms to reach a steady state; this value must be handled in the firmware of the local controller.

6.3 Summary

In this chapter, the system response time is evaluated in two cases: the response time of power retrieval and the server waiting for the duty cycle change. In section 6.1, the results show the EVSE with PIC is 5.83 times faster than the original system. The system response time can be accelerated by 9.39 times by setting the PIC to be a data pushing device. In section 6.2, the system response time can be improved by setting the server's wait time to variable values according to commands and parameters rather than a fixed value. By applying the technologies developed in this chapter, an efficient PEV charging infrastructure can be achieved with a faster system response time.

CHAPTER 7 CONTRIBUTION AND FUTURE WORK

The major contribution in this thesis is devising a smart charging system with current sharing technology to solve the problem of circuit underutilization, which occurs when a charger remains connected to a PEV for much longer than necessary. Furthermore, this system is able to serve demand response purposes. When demand response signals from the grid operator enter the system, either as an interrupt signal or price curve signal, the control center takes actions to satisfy the operator's demand. In addition, current sharing technology may also be applied to other appliances once they begin accepting current throttle signals similar to the pilot signal set by SAE J1772.

The charging algorithms developed in this thesis are based on a premise of free energy. In the case of non-free energy – i.e. the parking lot starts collecting money for charging – we must account for the price curve and user preference. There are many published charging algorithms based on price curve, energy availability, demand response, or user preference. For example, there is a simulation for a priority based PEV charging algorithm [35], which takes into account SOC, stay time and power constraints, for balancing grid limitations and user satisfaction. A discrete-time scheduling algorithm [34] attempts to satisfy more consumers by giving priority to consumers with the highest unevenness, defined by the difference between the current charge profile and residual charge profile.

In order to simplify the control scheme, these parameters, conditions, and constraints in a sense can be translated into priority handling problems. For example, price curve and user preference can be treated as parameters of priority while the types of Electric Vehicle (Plug-in Hybrid EV, PHEV or pure Battery EV, BEV), the size of the internal onboard charger, and the capacity of the PEV's battery can also provide the conditions when handling priority. When the

price curve meets the user's demanded price, the control center will arrange the charging sessions based on either the user's bidding or PEV's conditions to avoid energy surges on the power grid. With dynamic priority handling, the energy management of smart charging stations can be simplified to a single factor. Overall, the priority can be defined as a function with multiple parameters depending on real applications.

To handle a user's priority, we must account for many factors including the charging time ratio, the energy consumption ratio, and the start time of a charging session. A switching type of fair charging algorithm has been developed to fairly manage a user's charging time ratio. In this case, the charging station can only switch charging sessions between user sessions. In order to treat users fairly, each user has the same weight factor for the charging time ratio to fulfill an equal priority. In addition to handle the priority in the switching type of fixed current multiplexing algorithm, the priority will be treated as the combination of charge time ratio and charge start time. As for the variable current type of current sharing algorithm, instead of equal weight factor for charging time ratio, every user has the same weight factor of energy consumption ratio. In this case, the charging station can share a current among many users by using either a local or a remote current sharing algorithm. In the current sharing algorithm, the priority will be treated as the combination of the energy consumption ratio and the charging start time. Overall, the fair charging algorithm, either a switching type or variable current type, can be viewed as special cases of priority handling problem and every user has the same priority.

To dynamically handle the priority in the charging algorithm, either the control center or local controller must sample the energy consumption and set the priority periodically; the priority is the weight factor of either the charging time ratio or the energy consumption ratio in the charging algorithm. The priority can be simply scaled from 1 to 10 or with higher resolution

depending on the service requirement. A simple priority treatment can be handled as a normalized weight factor divided by the summation of all users' priorities. Similarly to the fairness index defined in the fair charging algorithm, the convergence index of the dynamic priority handling can be examined from the convergence of the users' charging time ratios or energy consumption ratios. Nevertheless, the performance of dynamic priority handling depends on the prediction of available energy in the near future, which is based on accurately predicting the arrival of upcoming PEVs to a charging station. Consequently, the prediction of a station's power availability in the near future can be handled using the prediction of PEV arrivals. Based on historical data there are many existing methods to predict PEV arrival in the near future including recursive curve fitting and machine-learning. This dynamic priority handling method should encourage the acceptance of electrical power sharing technology by PEV users.

CONCLUSION

We can move away from fossil fuel vehicles in the direction of energy independence and lower greenhouse gas emissions by purchasing PEVs. As more PEVs hit the road and become proliferate in the car market, a sufficient charging infrastructure becomes imperative. The lack of infrastructure investment, which is one of the issues facing PEV adoption, could be due to underutilization because a single dedicated PEV charger may be connected to a single PEV for much longer than necessary to charge its battery. This wasteful and costly use can be alleviated by an economical, smart PEV charging system.

This smart PEV charging system should not only enhance the stability and reliability of the local power grid, but also provide an energy efficient, cost-effective, and user friendly technology. WINSmartEV^{TM} uses variable current controlling and multiplexing capabilities to allocate scare power resources to the maximum number of PEVs. However, to integrate PEV charging into the existing infrastructure, a control system is required to manage charging sessions and the current supplied to the PEVs, accounting for all available and relevant information, including user requirements and the demands of the electrical grid. To track this information and electricity consumption across the grid, we leverage the software on the server used to monitor and control charging stations. In addition, the smart charging infrastructure allows for scalable and customized solutions for interoperability with standards because of its modular design. The design's difficulty and novelty lie in the hardware and firmware development of the charging station. Collaboration between the server and charging stations requires a master-slave control scheme to enhance the performance of smart features including charging algorithms, RFID authentication and authorization, and safety requirements. The design of this architecture and related components are the contribution of the research.

The charging algorithm functions, depending on issues and targets, as a key component in the charging infrastructure. To make a decentralized control scheme possible, charging stations must be controlled by embedded, charging algorithms. These algorithms can be enhanced by adding a Power Information Collector (PIC) to EVSE to retrieve power information and the relay status of the meters. This centralized retrieval of information allows the server to control the charger as a slave, making the network structure more robust and scalable. The network traffic is further reduced between the charging station and the control center because the charging algorithm already resides in the charging station. As a consequence, the system can respond faster. Aside from this benefit, charging algorithms can help consumer acceptance of multiplexing by ensuring that electrical circuits are shared fairly during charging. Allocation fairness of charge time is provided by a charging algorithm for Level 1 chargers. The concept of current sharing for Level 2 chargers goes beyond fairness in charge time to the fair distribution of power. The Simple Current Sharing algorithm is significantly fairer than a switching round robin algorithm and fully utilizes the power resource of the circuit without forecasting users' stay time. On the other hand, the Fair Current Sharing Algorithm, based on users' charging records, is calculated on the server side and executed with minimal instructions on the EVSE side.

Another primary component of the charging infrastructure requires a convenient method for a user to enable charging at a smart station. This convenience is achieved using a Zigbee-based RFID charging authorization and authentication system. The system provides ease in forming a large wireless network and allows automatic and seamless charging authorization and authentication at the moment of the PEV's arrival without need for user involvement, The approach allows authorization/identification capabilities to be added to the WINSmartEV^{TM} charging infrastructure without excessive modifications in the underlying structure using a

remote identification tag and a charging station-based reader. PEVs are equipped with remote tags for charge-state monitoring, so adding authorization/identification capabilities is a matter of writing new firmware and software for existing hardware. In addition, the use of a mesh network helps maintain a robust connection between PEVs and charging stations in a real world environment that is subject to signal blocking conditions.

The last component comprises a systematic safety design for WINSmartEV^{TM} that is implemented on all levels of the control system. The enhancements to the GFCI system run a system check to ensure that the system is operating properly and will shut off power when required in order to prevent electric hazards.

The enhancements bring SMERC research one step closer to a safe, energy efficient, economical, and user friendly smart charging technology that enhances the stability and reliability of the local grid while meeting the convenience needs of PEV drivers. With the aforementioned enhanced functionalities, the WINSmartEV^{TM} smart charging infrastructure is poised to serve, not only as one of the key components in the nationwide smart grid application, but as part of the larger push for PEV proliferation.

BIBLIOGRAPHY

[1] R. Gadh et al., “Smart Electric Vehicle (EV) Charging and Grid Integration Apparatus and Methods”, US Patent, PCT International Patent, Ser. No. US20130179061A1, WO2011156776A2, WO2011156776A3, PCT/US2011/040077, US13/693, Jun. 10, 2010.

[2] R. Gadh et al., ”Intelligent electric vehicle charging system”, US Patent, PCT International Patent, Ser. No. WO2013019989A2, WO2013019989A3, PCT/US2012/049393, Aug. 2, 2011.

[3] R. Gadh et al., ”Network based management for multiplexed electric vehicle charging”, US Patent, PCT International Patent, Ser. No. US20130154561A1, US13/691,709, Nov. 30, 2011.

[4] R. Gadh et al., ”Power Control Apparatus and Methods for Electric Vehicles”, US20140062401A1, US2013/975313, Aug. 24, 2013.

[5] R. Lowenthal, D. Baxter, H. Bhade, and P. Mandal, "Network-controlled charging system for electric vehicles," US Patent US7956570B2, Jun. 7, 2011.

[6] D. Baxter, H. Bhade, R. Lowenthal, and P. Mandal, "Network-controlled charging system for electric vehicles through use of a remote server," US Patent US8138715B2, Mar. 20, 2012.

[7] D. Baxter, C. F. Hagenmaier, Jr., M. T. Tormey, and R. Lowenthal, "Electrical circuit sharing for electric vehicle charging stations," US Patent US8013570B2, Sep. 6, 2011.

[8] S. Mal, A. Chattopadhyay, A. Yang, and R. Gadh, "Electric vehicle smart charging and vehicle-to-grid operation,” *International Journal of Parallel, Emergent and Distributed Systems,* vol. 27, no. 3. Mar. 2012.

[9] S. Lee, J. Lee, and H. Sohn, “Classfication of Charging Systems according to the Intelligence and Roles of the Charging Equipment”, *International Conference on ICT Convergence 2013*, Jeju, Korea, Oct. 14-16, 2013

[10] S. Hadley and A. Tsvetkova, “Potential impacts of plug-in hybrid electric vehicles on regional power generation,” *Oak Ridge National Laboratory, Tech. Rep.*, 2008.

[11] G. A. Putrus et al., "Impact of electric vehicles on power distribution networks", *Vehicle Power and Propulsion Conference, 2009. VPPC'09. IEEE*. IEEE, 2009.

[12] E. Akhavan-Rezai et al. "Uncoordinated charging impacts of electric vehicles on electric distribution grids: Normal and fast charging comparison", *Power and Energy Society General Meeting, 2012 IEEE*. IEEE, 2012.

[13] C. R. Green II, L. Wang, and M. Alam, “The impact of plug-in hybrid electric vehicles on distribution networks: A review and outlook", *Renewable and Sustainable Energy Reviews* 15.1 (2011): 544-553.

[14] M. Kintner-Meyer et al. "Impact Assessment of Plug-in Hybrid Vehicles on the US Power Grid." *The 25th World Battery, Hybrid and Fuel Cell Electric Vehicle Symposium & Exhibition*, Shenzhen, China. 2010.

[15] K. Clement-Nyns, E. Haesen, and J. Driesen, "The impact of charging plug-in hybrid electric vehicles on a residential distribution grid." *Power Systems, IEEE Transactions on* 25.1 (2010): 371-380.

[16] A. Masoum, A. Abu-Siada, and S. Islam, “Impact of uncoordinated and coordinated charging of plug-in electric vehicles on substation transformer in smart grid with charging stations”, *Innovative Smart Grid Technologies Asia (ISGT),* 2011 IEEE PES, Nov. 13-16, 2011.

[17] J. Liu, "Electric vehicle charging infrastructure assignment and power grid impacts assessment in Beijing", *Energy Policy,* Vol. 51, Dec. 2012, p544-p557.

[18] G. Mauri, P. Gramatica, E. Frasciolo, and S. Fratti, "Recharging of EV in a typical Italian urban area: Evaluation of the hosting capacity", *2011 IEEE PowerTech, Trondheim*, Jun. 19-23, 2011.

[19] S. Deilami, A. Masoum, P. Moses, and M. Masoum, "Real-time coordination of plug-in electric vehicle charging in smart grids to minimize power losses and improve voltage profile*," IEEE Trans. Smart Grid,* vol. 2, no. 3, pp. 456-467, Sep. 2011.

[20] "SAE Electric Vehicle and Plug in Hybrid Electric Vehicle Conductive Charge Coupler," *SAE International Surface Vehicle Recommended Practice.* (http://standards.sae.org/j1772_201210//) [03/11/2014]

[21] J. Rezgui, S. Cherkaoui, and D. Said, "A two-way communication scheme for vehicles charging control in the smart grid", *2012 8th International Wireless Communication and Mobile Computing Conference (IWCMC)*, Limassol, Aug. 27-31, 2012.

[22] M. Singh, P. Kumar, and I. Kar, "Implementation of Vehicle to Grid Infrastructure Using Fuzzy Logic Controller", *IEEE Transactions on Smart Grid*, Volume 3 Issue 1, March 2012.

[23] SAE International Standards for Electric Vehicle (http://topics.sae.org/electric-vehicles/standards/) [03/11/2014]

[24] W. Su, W. Zeng, and M. Chow, "A digital testbed for a PHEV/PEV enabled parking lot in a Smart Grid environment", *2012 IEEE PES Innovative Smart Grid Technologies (ISGT)*, Washington, DC, Jan. 16-20, 2012.

[25] L. Herrera, R. Murawski, G. Feng, E. Inoa, E. Ekici, and J. Wang, "PHEVs charging stations, communications, and control simulation in real time", *2011 IEEE Vehicle Power and Propulsion Conference (VPPC)*, Chicago, IL, Sept. 6-9, 2011.

[26] Powertech EV Service (http://www.powertechlabs.com/areas-of-focus/clean-transportation/electric-vehicle-engineering-services/) [04/16/2014]

[27] My Electric Avenue (http://myelectricavenue.info) [04/16/2014]

[28] X. Su, C. Chu, B.S. Prabhu, and R. Gadh "On the Identification Device Management and Data Capture via WinRFID Edge-Server", *IEEE Systems Journal,* 1(2), 95-104, Dec. 2007.

[29] Y. He, B. Venkatesh, and L. Guan, "Optimal scheduling for charging and discharging of electric vehicles," *IEEE Trans. Smart Grid*, vol. 3, no. 3, Sep. 2012.

[30] A. Shepelev, C. Chung, C. Chu, R. Gadh, "Mesh Network Design for Smart Charging Infrastructure and Electric Vehicle Remote Monitoring *", International Conference on ICT Convergence 2013,* Jeju, Korea, Oct. 14-16, 2013.

[31] J. Bae, B. Zhiguo, "The CAN Communication Application on the BMS", *International Conference on ICT Convergence 2013*, Jeju, Korea, Oct. 14-16, 2013

[32] C. Ahn, C. Li, and H. Peng, "Decentralized charging algorithm for electrified vehicles connected to smart grid", *2011 American Control Conference (ACC),* San Francisco, Jun. 29-Jul.1, 2011.

[33] S. Vandael, N. Boucke, T. Holvoet, and G. Deconinck, "Decentralized demand side management of plug-in hybrid vehicles in a smart grid", *Proceedings of the First International Workshop on Agent Technologies for Energy Systems (ATES 2010)*, Toronto, May 10-14, 2010.

[34] H. Lu, G. Pang, and G. Kesidis, “Automated Scheduling of Deferrable PEV/PHEV Load by Power-Profile Unevenness”, *2013 IEEE International Conference on Smart Grid Communications,* Vancouver, Canada, Oct. 21-24, 2013.

[35] P. Mahat, M. Handl, K. R. Kanstrup, and A. P. Lozano, "Price based electric vehicle charging", *2012 IEEE Power and Energy Society General Meeting*, San Diego, CA, Jul. 22-26, 2012.

[36] E. S. Rigas, S. D. Ramchurn, N. Bassiliades, and G. Koutitas, “Congestion Management for Urban EV Charging Systems”, *2013 IEEE International Conference on Smart Grid Communications,* Vancouver, Canada, Oct. 21-24, 2013.

[37] J. A. P. Lopes, F. J. Soares, and P. M. R. Almeida, “Integration of electric vehicles in the electric power system”, *Proceedings of the IEEE,* Vol. 99, Issue 1, p168–p183, Jan. 2011.

[38] J. de Hoog, D. A. Thomas, V. Muenzel, D. C. Jayasuriya, T. Alpcan, M. Brazil, and I. Mareels, Julian, "Electric vehicle charging and grid constraints: Comparing distributed and centralized approaches", *2013 IEEE Power and Energy Society General Meeting (PES)*, Vancouver, BC, Jul. 21-25, 2013.

[39] S. Bayram, G. Michailidis, and M. Devestikiotis, “Electric Power Resource Provisioning for Large Scale Public EV Charging Facilities”, *2013 IEEE International Conference on Smart Grid Communications*, Vancouver, Canada, Oct. 21-24, 2013.

[40] T. Logenthiran and D. Srinivasan, "Multi-agent system for managing a power distribution system with plug-in hybrid electrical vehicles in smart grid", *2011 IEEE PES Innovative Smart Grid Technologies-India (ISGT India),* Lollan, Kerala, Dec. 1-3, 2011.

[41] S. Sun, M. Dong, B. Liang, "Distributed Regulation Allocation with Aggregator Coordinated Electric Vehicles", *2013 IEEE International Conference on Smart Grid Communications*, Vancouver, Canada, Oct. 21-24, 2013.

[42] J. Lin, K, Leung, and V. Li, "Online Scheduling for Vehicle-to-Grid Regulation Service", *2013 IEEE International Conference on Smart Grid Communications,* Vancouver, Canada, Oct. 21-24, 2013.

[43] R. Wang, Y. Li, P. Wang, and D. Niyato, " Design of a V2G Aggregator to Optimize PHEV Charging and Frequency Regulation", *2013 IEEE International Conference on Smart Grid Communications,* Vancouver, Canada, Oct. 21-24, 2013.

[44] P. Kulshrestha, L. Wang, M. Chow, and S. Lukic, "Intelligent energy management system simulator for PHEVs at municipal parking deck in a smart grid environment," Power & Energy Society General Meeting, *PES '09. IEEE*, Calgary, Alberta, Canada, Ju. 26-30, 2009.

[45] W. Su, and M. Chow, "Computational intelligence-based energy management for a large-scale PHEV/PEV enabled municipal parking deck," *Applied Energy*, Volume 96, p.171-182, Aug. 2012.

[46] Q. Dong, D. Niyato, P. Wang, and Z. Han, "An Adaptive Scheduling of PHEV Charging: Analysis under Imperfect Data Communication," *2013 IEEE International Conference on Smart Grid Communications*, Vancouver, Canada, Oct. 21-24, 2013.

[47] W. Tang, S. Bi, and Y. Zhang, "Online Speeding Optimal Charging Algorithm for Electric Vehicles without Future Information", *2013 IEEE International Conference on Smart Grid Communications*, Vancouver, Canada, Oct. 21-24, 2013.

[48] T. Raviv, "The battery switching station scheduling problem", *Operations Research Letters*, Volume 40, Issue 6, p.546-550, Nov. 2012.

[49] C. Chung, J. Chynoweth, C. Qiu, C. Chu, and R. Gadh, "Design of Fair Charging Algorithm for Smart Electrical Vehicle Charging Infrastructure", *International Conference on ICT Convergence 2013*, Jeju, Korea, Oct. 14-16, 2013

[50] C. Chung, E. Youn, J. Chynoweth, C. Qiu, C. Chu, and R. Gadh, "Safety Design for Smart Electric Vehicle Charging with Current and Multiplexing Control", *2013 IEEE International Conference on Smart Grid Communications*, Vancouver, Canada, Oct. 21-24, 2013.

[51] C. Chung, A. Shepelev, C. Qiu, C. Chu, and R. Gadh, "Design of RFID Mesh Network for Electric Vehicle Smart Charging Infrastructure" *2013 IEEE International Conference on RFID Technologies and Applications*, Johor Bahru, Malaysia, Sep. 4 – 5, 2013.

[52] "NIST Framework and Roadmap for Smart Grid Interoperability Standards Release 2.0", Office of the National Coordinator for Smart Grid Interoperability, National Institute of Standards and Technology, U.S. Department of Commerce, Feb. 2012

[53] "ZigBee Specification", ZigBee Alliance, 043474r17, Jan. 17, 2008.

[54] "IEEE Std 802.15.4", IEEE Computer Society, Oct. 1, 2003.

[55] "Smart Energy Profile 2.0 Technical Requirements Document", ZigBee Alliance, Apr. 24, 2010.

[56] C. Chung, P. Chu, and R. Gadh, "Design of Smart Charging Infrastructure Hardware And Firmware Design of The Variable Current Multiplexing Charging System," *Seventh Global Conference on Power Control and Optimization, PCO2013*, Aug. 25-27, 2013.

[57] "A True System-on-Chip Solution for 2.4-GHz IEEE 802.15.4 and ZigBee Applications," Texas Instruments, SWRS081A, Apr. 2009.

[58] "CC253x System-on-Chip Solution for 2.4 GHz IEEE 802.15.4 and ZigBee Applications," Texas Instruments, SWRU191, Apr. 2009.

[59] B. Vaidya, D. Makrakis, and H. T. Mouftah, “Efficient Authentication Mechanism for PEV Charging Infrastructure”, *2011 IEEE International Conference on Communications (ICC)*, Kyoto, Jun. 5-9, 2011.

[60] C. Chung, J. Chynoweth, C. Qiu, C. Chu, and R. Gadh, "Design of Fast Response Smart Electric Vehicle Charging Infrastructure," *IEEE Green Energy and Systems Conference, IGESC 2013*, Long Beach, U.S.A., Nov. 25, 2013.

[61] M. Majidpour, C. Qiu, C. Chung, P. Chu, R. Gadh, and H. R. Pota,“ Fast Demand Forecast of Electric Vehicle Charging Stations for Cell Phone Application”, *2014 IEEE Power & Energy Society General Meeting*, National Harbor, MD (Washington, DC Metro Area), Jul. 27-31, 2014.

[62] H. Bhade, M. Tormey, D. Baxter, R. Lowenthal, and P. Mandal, "Overcurrent and ground fault protection in a networked charging station for electric vehicles," US Patent US8072184B2, December 6, 2011

[63] Open Electric Vehicle Supply Equipment (OPEN EVSE) (https://code.google.com/p/open-evse/) [2014/04/13]

[64] User’s Manual Model CS-40, ClipperCreek Inc., p.16. (http://www.clippercreek.com/pdf/CS-40%20User%20Manual%20DLP%20IP%20081205%20v03.pdf) [2014/02/10]

[65] E. Akhavan-Rezai, M. F. Shaaban, E. F. El-Saadany, and F. Karray. “Priority-based Charging Coordination of Plug-in Electric Vehicles in Smart Parking Lots”, *2014 IEEE PES Innovative Smart Grid Technologies (ISGT)*, Washinton, DC, Feb. 2014.

[66] “Production of 100% Electric, Zero Emission Nissan Leaf begins at Oppama, Japan (”http://www.nissan-global.com/EN/NEWS/2010/_STORY/101022-01-e.html) [5/10/2014]

[67] J. Chynoweth, C. Chung, C. Qiu, P. Chu, and R. Gadh, "Smart Electric Vehicle Charging Infrastructure Overview", *The Innovative Smart Grid Technologies (ISGT) Conference*, Washington, DC , USA., Feb. 19-22, 2014.